MODULATION OF TUMOUR BURDEN IN MOUSE LUNGS BY ONCOSTATIN M

MODULATION OF TUMOUR BURDEN IN MOUSE LUNGS BY ONCOSTATIN M

By LAURA IZAKELIAN, B.Sc. Honours (McMaster University)

A Thesis Submitted to the School of Graduate Studies in Partial Fulfillment of the Requirements for the Degree Masters of Science

MASTERS OF SCIENCE (2014) McMaster University, Hamilton Ontario

(Medical Sciences: Infection and Immunology)

TITLE: Modulation of Tumour Burden in Mouse Lungs by Oncostatin M

AUTHOR: Laura Izakelian, B.Sc. Hons. (McMaster University)

SUPERVISOR: Dr. Carl Richards, BSc., MSc., Ph.D.

NUMBER OF PAGES: 142

ABSTRACT

Lung cancer is the leading cause of cancer-related mortality, resulting in more deaths than breast, colorectal, and pancreatic cancers combined in North America. As such, research regarding the underlying mechanisms and pathogenesis of the disease is critical. Inflammation induced by inflammatory cytokines, such as gp130 cytokines, has been implicated in chronic lung diseases, and more recently in the development of lung cancer. The roles of gp130 cytokines IL-6 and Oncostatin M (OSM) in lung cancer has yet to be fully elucidated, although these cytokines have been noted to contribute to the pro-tumour cytokine environment as well as the growth and survival of certain tumour cells. Based on previous findings that overexpression of OSM increased tumour burden in a mouse model of lung cancer, it is hypothesized that OSM is a key player in the establishment and progression of pulmonary tumours in mice, and depletion or elevation of OSM activity modulates tumour burden in the B16F10 mouse melanoma model, as well as the induced mutant K-ras mouse model of lung cancer, independently of direct action on tumour cells.

Findings presented in this thesis demonstrate that pulmonary OSM overexpression enhances tumour burden in the B16 pulmonary melanoma metastases mouse model of lung cancer, whereas pulmonary overexpression of IL-6 did not. In addition, although OSM overexpression resulted in increased lung IL-6 and eosinophil recruitment in this model, neither IL-6 nor eosinophils were required in the induction of increased tumour burden, as assessed in IL-6 deficient (IL-6 -/-) or eosinophil deficient (GATA-1 -/-) mice. While preliminary experiments suggested accelerated tumour burden due to OSM

overexpression in the inducible oncogenic K-ras mouse model, experiments in mutant K-ras +/- transgenic OSMRβ -/- mice determined that OSMRβ was not required for the development of tumours in this model.

In studies completed to examine the mechanisms underlying the effects of OSM on tumour burden, direct stimulation of K-ras tumour cell lines LLC and LKR-13 with OSM *in vitro* did not alter tumour cell proliferation. Furthermore, conditioned media from mouse lung fibroblasts (MLFs) treated with OSM, as well as co-cultures with MLFs treated with OSM, did not alter LLC or B16F10 cell proliferation. This suggests that direct stimulation of tumour cells or indirect stimulation through fibroblasts may not contribute to mechanisms by which OSM stimulates increased tumour burden *in vivo*. Co-cultures of tumour cells and cells collected in bronchoalveolar lavage (BAL) fluid from mice treated with AdDel70 or AdOSM *in vivo* caused an increase in tumour cell proliferation, however adherent macrophage populations did not. The *in vitro* work suggests other mechanisms or multiple cell types are required in addition to macrophages or fibroblasts. Collectively, the work presented in this thesis supports a pro-tumorigenic role of Oncostatin M in mouse models of tumour growth in lungs, through an IL-6 and eosinophil independent mechanism.

ACKNOWLEDGEMENTS

With the completion of this thesis, I'd like to extend my greatest gratitude to the individuals who provided support and encouragement throughout the past two years. Firstly, I'd like to thank my supervisor Dr. Carl Richards, whose continuous passion and dedication to his research fueled my curiosity and created a wonderful learning environment. I'd also like to thank my committee members Dr. Brian Lichty and Dr. Karen Mossman, who challenged my knowledge and offered guidance while also helping me think critically of my work throughout my studies.

To past lab members (Sean Lauber, David Schnittker, Tamanna Chibber) and present, thank you for making this experience enjoyable. Sean Lauber, thanks for all your guidance during the first year of my studies, and for your expertise and support with *in vivo* experiments. To Steven Wong and Karen Kwofie, I'm glad we've become good friends over the past two years, and wish you all the best in future endeavors. In addition, I'd like to thank members of the Xing Lab, as well as the Bramson Lab, for all the laughs and jokes that made some stressful periods bearable. I'd also like to thank Jane-Ann Smyth from the Ask Laboratory and Kyle Stephenson from the Lichty Laboratory for their expertise and assistance with animal experimental techniques.

I'd like to express my sincere appreciation to my parents and sister Lilit for their unconditional love and motivation to succeed in all of life's challenges, as well as my friends, for their unequaled support and encouragement throughout all my endeavors. Lastly, I'd like to thank Ryan Frederiks, for his unfaltering positivity, love, and support during both the good and stressful times throughout these years.

TABLE OF CONTENTS

LIST OF FIGURES

LIST OF ABBREVIATIONS

AdDel70 – Empty adenovirus vector

AdOSM – Adenovirus vector encoding Oncostatin M

αSMA – Alpha smooth muscle actin

BAL – Bronchoalveolar lavage

BALF – Bronchoalveolar lavage fluid

CAF – Cancer-associated fibroblast

CT – Computed tomography

ECM – Extracellular Matrix

ELISA – Enzyme-linked immunosorbent assay

EMT – Epithelial-mesenchymal transition

EoMT – Endothelial-mesenchymal transition

FBS – Fetal bovine serum

GATA-1 -/- - mice with knockout mutation of double GATA binding site

Gp130 – Glycoprotein 130

GTP – Guanosine Triphosphate

H&E – Hematoxylin and Eosin

IL - Interleukin

IL-6 -/- - mice with knockout mutation of IL-6

JAK – Janus kinase

K-RAS – Kristen rat sarcoma

LLC – Lewis lung carcinoma

MAPK – Mitogen-activated protein kinase

MLF – Mouse lung fibroblast

MMP – Matrix metalloproteinase

MYC – Myelocytomatosis viral oncogene homolog

NSCLC – Non-small cell lung cancer

OSM – Oncostatin M

OSMRβ – Oncostatin M Receptor beta

OSMRβ -/- - mice with homozygous knockout of Oncostatin M receptor beta

PBS – Phosphate-buffered saline

PI3K – Phosphoinositide-3 kinase

qRT-PCR – Quantitative reverse transcriptase polymerase chain reaction

RAS – Rat sarcoma viral oncogene homolog

SCLC – Small cell lung cancer

SPARC - Secreted protein acidic and rich in cysteine

STAT – Signal transducer an activator of transcription

TAM – Tumour-associated macrophage

TAN – Tumour-associated neutrophil

TGFβ – Transforming growth factor beta

TNFα – Tumour necrosis factor alpha

VEGF – Vascular endothelial growth factor

CHAPTER 1: Introduction

1.1 - Lung Cancer

Lung cancer remains the leading cause of cancer death among both men and women[1]accounting for approximately 27% of cancer deaths[2]. An estimated 14% of all new cancer cases are lung cancer diagnoses, which have been categorized into 2 main types: small cell lung cancer (SCLC) and non-small cell lung cancer (NSCLC)[2]. NSCLC accounts for approximately 85% of cases, and is subcategorized into 3 main groups: squamous cell carcinoma, adenocarcinoma (which is the most common manifestation), and large-cell carcinoma[1,3]. Of these subtypes, adenocarcinomas, characterized by neoplasia of epithelial tissue, accounts for 40% of NSCLC patients[4]. One of the primary causes of lung cancer is tobacco smoking, and the incidence rate among men has been decreasing in association with the steady decline of smoking in North America[2]. There are 4 stages of NSCLC, with the fourth known as the advanced stage and indicates presence of tumour metastasis[1,4].

There are 4 main courses of treatment for patients with NSCLC: surgery, radiation therapy, chemotherapy, and targeted therapy[1]. Surgery may include removal of either the lobe with the tumour (lobectomy) or an entire lung (pneumonectomy). Radiation therapy is used if size or location of the tumour renders surgical removal non-feasible[5,4]. Chemotherapy is often used in combination with the options described above. Platinum-based chemotherapy drugs, such as cisplatin and carboplatin, can be used to treat a broad range of cancers[6]. Unfortunately, toxicity profiles remain a significant issue, as these chemotherapeutic drugs are associated with severe side effects including neurotoxicity

and nephrotoxicity among others[6]. Thus, one of the main goals in the development of cancer treatments, aside from eliminating cancerous cells and achieving longer-term survival rates, is decreasing toxicities associated with the drugs prescribed. In patients with advanced stage disease, targeted therapies are used in combination with chemotherapeutic drugs to target mutations causing uncontrolled cell proliferation.

1.2 – Common Mutations in Lung Cancer

Mutations in oncogenes such as EGFR, HER2, BRAF, RAS, MEK1, PIK3CA, and MET, are commonly found in NSCLC cases[3,7]. These mutations are considered "driver" mutations due to two properties: they cause constitutive activation of the signaling protein involved[7], and multiple driver mutations are generally not present concurrently in the same tumour[3]. Epidermal Growth Factor Receptor (EGFR) is one of the families of tyrosine kinases, including EGFR and HER2, that regulate RAS-MAPK and PI3K/AKT signal transduction pathways involved in cell survival, metastasis, and proliferation[8]. EGFR mutations are more common in never-smokers[7] and account for 27% of all NSCLC cases (according to COSMIC database at www.sanger.ac.uk). Interestingly, the most common targeted therapies used to treat NSCLC target the EGFR and VEGF signaling pathways. As EGFR signaling upregulates VEGF expression, and VEGF plays a pro-angiogenic role in tumour development, current clinical trials are testing a combination of EGFR tyrosine kinase inhibitors (TKIs) such as geftinib and erlotinib, and VEGF-targeting drugs such as bevacizumab, with successful results in phase II trials[9,10,11]. Though these treatments are promising, the primary concern with the use of EGFR TKIs remains the development of resistance to these drugs through genetic

alterations in proteins downstream of the EGF receptors[3]. These genetic alterations, including mutations in K-ras and PIK3CA genes, provide acquired resistance of the tumour to EGFR TKIs[3,12]. Thus, further studies must be completed to overcome the development of resistance to these therapies. Study of the mechanisms underlying lung cancer initiation and progression will allow for the establishment of other targeted therapies.

1.3 - Inflammation and Cancer

Although mutations are necessary for tumour initiation, both intrinsic mutations and extrinsic factors, such as infections and the environment, contribute to the pathogenesis of cancer[13]. Additionally, many environmental causes contributing to tumour initiation are associated with chronic inflammation, such as tobacco smoking[14]. The first link between inflammation and cancer was noted with the observation of presence of leukocytes in tumours[13]. Many cases of inflammation associated tumour progression have since been studied. One example is in the case of *Helicobacter pylori* infection, where persistent infection with this type of bacteria has been associated with the development of gastric cancer[15]. Infections with hepatitis B or C have also been found to increase the risk of hepatocellular carcinoma development[16] and ageing-associated senescence in cells and consequent accumulation of DNA damage can also result in tumour-promoting chronic inflammation[17]. Apart from associations of infections with tumour promotion, the heterogenous cell population of tumours reveals involvement of the inflammatory response. Tumour-associated macrophages (TAMs), tumour-infiltrating lymphocytes (TILs), and a number of innate immune cells including neutrophils,

eosinophils, mast cells and myeloid-derived suppressor cells are frequently found in the tumour microenvironment[13].

TAMs show similar phenotype to alternatively activated macrophages, which are macrophages that have assumed an M2 phenotype, contrasting the classically activated (or M1) phenotype of inflammatory macrophages. M1 macrophages function in immune defense and anti-tumour immunity, secreting pro-inflammatory mediators including tissue necrosis factor (TNF), IL-1, and nitric oxide[18]. M2 macrophages, on the other hand, play a role in wound repair and fibrosis, secreting regulatory cytokines such as transforming growth factor- β1 (TGFβ1) and platelet-derived growth factor (PDGF)[19]. TAMs as well as tumour cells also release IL-10, which suppresses T cell effector functions, and induce a number of angiogenic growth factors[15]. Increased TAMs in tumour tissue is generally associated with poor prognosis as they are thought to promote tumour growth and aid tumour invasion and angiogenesis[20].

Interestingly, macrophage populations can be skewed to an M1 or M2 phenotype *in vitro* using selective cocktails such as IFNγ and LPS (M1) or IL-4 and IL-13 (M2)[21]. In a recent report by Komori *et al* (2013) the gp130 cytokine Oncostatin M was demonstrated to manipulate macrophages into an M2 phenotype in adipose tissue, where OSMRβ -/- mice presenting with mature-onset obesity and adipose tissue inflammation initially had increased expression of inflammatory cytokines and a higher percentage of M1-marker positive macrophages than M2-marker positive macrophages among total adipose tissue macrophages (ATMs)[22]. Upon OSM stimulation of peritoneal macrophages removed from WT and OSMRβ -/- mice, the investigators found elevated levels of

macrophage galactose-type C-type lectin 1 (MGL1) and IL-10 in WT compared to OSMRβ -/- mice, characteristic of an M2 phenotype[22]. These studies strongly suggest a relationship between overexpression of Oncostatin M and the skewing of macrophages into the M2 phenotype.

The tumour stroma has often been compared to a wound that does not heal[23]. In both the wound and cancer microenvironment, active angiogenesis is accompanied by proliferating fibroblasts that secrete various extracellular matrix constituents, such as fibronectin and collagen type I[24]. While these activated fibroblasts are eventually removed via apoptosis from the granulation tissue when the wound has healed[24], fibroblasts in the tumour stroma, termed cancer-associated fibroblasts (CAFs), continue to expand and secrete proteins of the extracellular matrix, a process termed desmoplastic reaction[25]. CAFs is a term used to describe the population of fibroblasts in the tumour stroma that have been most commonly recognized by their acquired expression of αSMA, much like myofibroblasts in tissue repair[26]. However, due to the heterogeneity of the population, the expression of this protein does not fully define CAFs with tumour promoting properties. Thus, additional markers characteristic of CAFs may include expression of Secreted Protein Acidic and Rich in Cysteine (SPARC)[27], fibroblast activation protein (FAP) and platelet-derived growth factor receptor[26,28]. These CAFs may derive from local fibroblasts, as well as pericytes and smooth muscle cells from nearby vasculature, and by epithelial-mesenchymal transition (EMT) or endothelial-mesenchymal transition (EoMT)[24,28]. CAFs grafted with immortalized human prostatic epithelial cells resulted in significantly larger tumours, compared to normal

fibroblasts/immortalized epithelial cells or compared to CAF/normal prostatic epithelial cell grafts[29]. In examining stromal-tumour cell interaction, Akashi *et al* (2001) showed that using both lung adenocarcinoma and squamous cell carcinoma cells, laminin α3 and α5, main components of the basement membrane, were found to be fragmented or completely absent in areas of fibroblastic proliferation within the tumours[30]. Expression of laminin protein was also significantly reduced in eleven of twelve cancer cell lines *in vitro*, compared to normal lung epithelial cells[30]. Due to these results, it was suggested that during the early stages of tumour development, the basement membrane that separates lung cancer cells and stromal fibroblasts undergoes fragmentation. This results in cancer cell-induced alterations to the stroma and has been linked to lymph node metastasis and poor prognosis[24,30]. As the basement membrane also acted as a regulator of cytokine diffusion, in its absence, cytokines released by tumour cells, including TGFβ, platelet-derived growth factor (PDGF) and fibroblast growth factor-2 (FGF2), stimulate local fibroblast activation and fibrosis, which are involved in immune surveillance suppression, as well as fibroblast growth and activation[31]. A recent study by Depner *et al* (2012) examined the role of IL-6 in tumour cell-fibroblast interactions using IL-6 overexpressing HaCaT ras squamous cell carcinomas (SCCs) that exhibited invasive growth into the collagen gel in a 3-dimensional co-culture model with stromal fibroblasts[32]. This invasive property was abolished upon absence of fibroblasts, or with the use of IL-6 neutralizing antibody, thus demonstrating the requirement of IL-6 and stromal fibroblasts for altered tumour cell activity in that model[32].

1.4 - Cytokines and Inflammation

Among the numerous cytokines involved in inflammatory processes, including TNFα and IL-1β, a strong relationship has been established between gp130 cytokines and modulation of inflammation[33,34]. The gp130 family, consisting of IL-6, Oncostatin M, LIF, IL-11, IL-27, IL-31, cardiotrophin, and CNTF, refers to a group of cytokines that all require binding to a receptor complex consisting of at least one gp130 receptor subunit[35]. Though gp130 is ubiquitously expressed in a wide range of cells and tissues, cytokine-specific receptor chains can be more confined to certain cell types[36]. Despite different cytokine-specific receptors, all gp130 cytokines induce JAK-STAT, MAPK, and PI3K signaling pathways upon binding to the receptor complex[35,36]. Recent studies have implicated IL-6 in contrasting roles during acute and chronic inflammation, where it contributes to beneficial protective immunity in the acute phase, but contributes to adverse effects in chronic inflammation. IL-6 has been determined to be a requirement for resistance to multiple pathogens, as the absence of IL-6 increases susceptibility to pathogens such as *Toxoplasma gondii,* and *Candida albicans*[33]. In addition, in a study using intratracheal administration of an adenovirus encoding IL-6 (AdIL-6), results demonstrated significant lymphocytic recruitment and hyperplasia in the parenchyma, as well as increased bronchial-associated lymphoid aggregate, and bronchial and alveolar epithelial cell hyperplasia[37]. Inflammatory properties of IL-6 were also observed in a mouse model of RA, where IL-6 was detected in the synovial fluid of RA patients, and was found to induce the development of osteoclasts, contributing to the progression of the

disease[38]. Indeed targeting IL-6 signaling has been successfully developed as an alternative to TNFα blockade in rheumatoid arthritis[39,40].

1.5 – Gp130 Cytokines and Cancer

In addition to their involvement in inflammatory processes, gp130 cytokines IL-11, LIF, IL-6, and OSM have been noted to play a variety of roles in tumour development. Studies have implicated IL-11 in progression of gastric adenocarcinoma, where elevated IL-11 expression is found in these tumours, and complete abrogation of tumours in IL-11R α1 knockout mice[41]. A possible role in colorectal cancer has also been identified, as studies have shown IL-11 secretion by TGFβ-stimulated fibroblasts conferred increased metastatic capacity upon implantation of genetically altered colorectal cancer cells constitutively producing IL-11 in mice, compared to control cancer cells[42]. In a similar fashion, TGFβ stimulation of dermal fibroblasts was found to increase contractility and pro-invasive properties in an IL-11-dependent manner, as the effects of TGFβ stimulation were lost upon use of anti-LIF antibody[43]. Interestingly, secreted IL-11 protein levels were found to be significantly higher in highly metastatic breast cancer cell lines, compared to less metastatic cell lines, and conditioned media from IL-11 secreting breast cancer cells induced matrix remodeling, as well as STATs phosphorylation in dermal fibroblasts[43]. These results suggest that IL-11 stimulation of fibroblasts by squamous carcinoma cells may induce the acquisition of pro-invasive properties, dependent upon STAT3 activation. In addition to IL-11 and LIF, IL-6 and OSM have been implicated in the pathogenesis of some cancers.

1.5.1 - IL-6

IL-6 acts by binding to either the IL-6 receptor, which then induces homodimerization of gp130 signal transducing protein[35], or to soluble IL-6 receptor (sIL-6R), which enables trans-signaling, and increases the number of cells responsive to IL-6 signaling. IL-6 is an important mediator of fever and induces the expression of various acute-phase proteins[13]. It is known to act on B cells, T cells, and hematopoietic progenitor cells. In B cells, it induces maturation into antibody-secreting plasma cells, whereas in murine hematopoietic progenitor cells, it stimulates cell entry into the G1 phase of the cell cycle[35]. IL-6, along with other inflammatory cytokines TNF and IL-1, has been reported to stimulate the production of angiogenic factors such as VEGF[14]. Interestingly, IL-6 has also been found to play a role in human multiple myeloma, where tumour cells stimulated IL-6 release by stromal cells, which promoted myeloma cell growth, as well as resistance to therapy[44].

Some studies have reported the involvement of IL-6 specifically in lung cancer. An interesting study examined IL-6 promotion of lung cancer stem cell (CSC) growth[45]. It was shown that there was upregulation of IL-6 receptor in CSCs compared to non-CSCs, and that growth of these cells was significantly inhibited after transfection with IL-6 siRNA or use of IL-6R monoclonal antibody[45]. IL-6 may thus be an autocrine factor in lung cancer stem cell proliferation.

1.5.2 - Oncostatin M

Oncostatin M is a multifunctional cytokine originally named as such due to its inhibitory effects on A375 melanoma cells[36]. In the human system, OSM can bind

directly to either leukemia inhibitory factor receptor (LIFR) or Oncostatin M receptor (OSMR), which causes either receptor to heterodimerize with gp130 and induce signal transduction[46]. Similar to IL-6, OSM is produced by activated T cells and macrophages in response to inflammatory signals generated by pathogens or TLR ligands, and signaling via the gp130 receptor induces the JAK/STAT pathway, as well as the MAPK pathway[46]. Oncostatin M is involved in inflammatory responses by stimulating the synthesis of acute phase proteins by liver cells, chemokines by fibroblasts, and IL-6 production by endothelial cells[35]. It also modulates extracellular matrix (ECM) remodeling, as it induces increased expression of ECM-modifying proteins such as tissue inhibitors of metalloproteinases (TIMPs), which balance the degradation of the matrix by MMPs[46].

The receptor for OSM (OSMR) has been reported to be expressed on many cell types including epithelial cells, fibroblasts, endothelial cells, hepatocytes, chondrocytes, and smooth muscle cells[36,46] in addition to a number of tumour cell types, including breast and prostate carcinoma cells, as well as melanoma, and sarcoma cells[46]. In human breast cancer cell lines, OSM has been found to down-regulate estrogen receptor-α (ER-α) and progesterone receptor expression associated with a worse prognosis, as ER and PR negative tumours are more aggressive and less responsive to therapy[47]. Higher OSM levels were also associated with a shorter survival period, suggesting that increased levels of Oncostatin M was associated with breast cancer progression[47]. It has recently been postulated that c-Myc, mediated by OSM induced STAT3 signaling, may act as a molecular switch to alter the response of mammary epithelial cells to OSM[48]. In this paper, Kan *et al*., reported that when c-Myc was suppressed in human mammary

epithelial cells via STAT3 activation, OSM treatment inhibited cell growth. Suppression of growth was arrested, however, with constitutive c-Myc overexpression[48]. A paradoxical role of OSM has also been observed in normal and preneoplastic bronchial epithelial cells, where OSM inhibited cell growth of normal cells, but increased proliferation of some pre-neoplastic cells[49]. Oncostatin M and IL-6 cytokines have also been correlated with an increase in VEGF in prostate cancer cell lines (DU-145), and are hypothesized to modulate prostate tumour progression[50].

Precise functions of IL-6 and Oncostatin M cytokines in the inflammatory processes in lung cancer have yet to be elucidated. This study aims to examine the link between these inflammatory cytokines and lung cancer using animal models.

1.6 - K-ras Oncogenes and Lung Cancer

Ras mutations occur in approximately 15-25% of all lung adenocarcinoma cases[51], and 90% of those mutations are specifically found in K-ras[52], making oncogenic K-ras one of the most common genetic alterations in human lung cancer[53]. K-ras mutations drive constitutive *Ras* signaling[52]. Driver mutations such as those in K-ras do not overlap with other driver mutations, such as those in BRAF or EGFR, but is frequently associated with mutations in the *p53* pathway. Interestingly, 97% of these mutations involve codons 12 or 13, at the Walker A motif. This domain interacts with GAP, and with a single amino acid mutation, hinders the ability of the enzyme to catalyze the hydrolysis of GTP to GDP[54].

There is compelling evidence that inhibition of K-ras mutations function in tumour cells to decrease tumorigenesis. In a study by Rachagani *et al* (2011) the effects of

silenced oncogenic K-ras^{G12D} alleles in pancreatic cancer cells were examined *in vivo* and *in vitro*[55]. Upon expression of shRNA specific for K-ras^{G12D} alleles, pancreatic cancer cells demonstrated decreased proliferation, invasion, motility, and increased doubling time *in vitro,* as well as decreased metastases upon implantation *in vivo*[55]. In addition, silencing of the oncogenic K-ras allele resulted in decreased expression of cyclins D and E, decreased downstream signaling pathways shown by decreased phospho ERK1/2, phospho AKT, and NFκB, as well as increased expression of E-cadherin[55]. These results suggested that the oncogenic K-ras allele enhances invasive and metastatic properties in pancreatic cancer cells by inhibition of E-cadherin and cell-cycle checkpoints. This trend was also observed by Sunaga, et al., where knockdown of oncogenic K-ras using retrovirus-mediated shRNA resulted in suppression in proliferation but not complete inhibition of various NSCLC cell lines *in vitro*, as well as tumour growth *in vivo*[56]. Instead, it was reported that although the MAPK pathway was suppressed in these cells, there was an upregulation of phosphorylated EGFR and STAT3[56]. Knockdown of the mutant K-ras allele did, however, sensitize tumour cells to other therapeutics, including EGFR and p38 inhibitors[56]. There are a number of inhibitors generated to target function of K-ras mutations currently in trials, including farnesyl transferase inhibitors, which inhibit farnesylation required for plasma membrane localization of K-ras[57]. Unfortunately, K-ras is alternatively modified and localized to the plasma membrane, leading to unsuccessful inhibition[57]. As such, alternate methods of blocking localization of K-ras are being studied, however there are currently no successful K-ras-targeted therapies[58].

Activation of oncogenic K-ras mutation, using a conditional mutant mouse with both clara cell secretory protein (CC10)-Cre recombinase and lox-stop-lox K-ras ^{G12D} alleles, resulted in a profound inflammatory response in the lungs, consisting of an increase in macrophage and neutrophil infiltration, in addition to increased TNFα, VEGF, KC, and MCP-1 levels[53]. Using immunohistochemistry, it appeared that macrophages localized more in alveolar spaces, but neutrophils were predominantly co-localized near tumours[53]. Thus, oncogenic K-ras activation generates an inflammatory response while acting as a driving force in tumour development. This response is also apparent in the oncogenic K-ras mouse model of lung cancer, developed by Tyler Jacks[59].

1.7 - *RAS* Signaling

Ras genes encode three, highly homologous, Ras proteins: K-ras, H-ras, and N-ras. These are small GTPase proteins that are involved in the induction of multiple signal transduction pathways, including Mitogen-activated Protein Kinase (MAPK), and the Phosphoinositide 3-Kinase (PI3K)/AkT pathways[60]. Normally, binding of growth factors to cell-surface receptors, such as epidermal growth factor receptors (EGFRs), result in activation of adaptor protein complexes and guanine-nucleotide exchange factors (GEFs)[52]. GEFs catalyze the dissociation of GDP from *RAS* proteins to permit *Ras* binding to GTP and activation of *Ras,* subsequently activating downstream signaling[60]. After *Ras* has been activated, GTPase activating proteins, or GAPs, catalyze the hydrolysis of bound GTP to GDP. Thus, *Ras* cycles between activated GTP-bound and inactivated GDP-bound states, the latter eliminating *Ras*-induced signaling. Activated *Ras* regulates cell growth and proliferation via mediating expression of proteins such as JUN

and FOS through the MAPK/ERK pathway[61], and promotes cell survival, by inactivating several pro-apoptotic proteins including BAD and Bax via the PI3K/AKR pathway[62]. *Ras* signaling has also exhibited mediatory functions of angiogenesis by induction of increased expression of Vascular Endothelial Growth Factor (VEGF) and suppression of thrombospondins. *Ras* signals may also influence the tumour microenvironment through induced expression of matrix metalloproteinases (MMPs) which degrade basement membrane and other components of the extracellular matrix[53].

As *Ras* regulates a multitude of downstream targets, some of which may contribute to tumour growth, Zhang, et al. suggested that dependent on whether the K-ras allele is wild-type or mutated, *Ras* can act as a proto-oncogene or a tumour suppressor gene[63]. It was shown that loss of one wild-type K-ras allele in mice predisposed them to chemically-induced lung tumours, displaying the importance of wild-type K-ras to prevent tumour initiation[63]. Furthermore, ectopic expression of wild-type K-ras *in vitro* was shown to inhibit colony formation and tumour development in cells with a mutation in the other K-ras allele[63]. Thus, oncogenic K-ras may be one of the key players in tumour initiation and progression, but wild-type K-ras may function in the reversal of such characteristics.

1.8 – Summary of Project

Since Oncostatin M has been shown to play a pro-tumorigenic role in various types of cancers, the main goal of this thesis was to determine the effects of Oncostatin M overexpression and mechanisms in the development of pulmonary tumours in mouse models. Previous experiments in the Richards' laboratory have indicated that OSM

induces inflammation (IL-6 and eosinophil accumulation) in non-tumour lung cells while supporting ectopic B16F10 and LLC cell tumour growth in mice. Confirmation and extension of these findings may have significant effect on the understanding of pulmonary tumour initiation and growth. It was hypothesized that Oncostatin M modulates the establishment and progression of pulmonary tumours in mice, such that elevation of cytokine level would increase tumour burden in an IL-6 and eosinophil-dependent fashion, and depletion or elevation of function decreases tumour burden.

To explore this hypothesis, two mouse models of lung cancer were employed: the B16 pulmonary melanoma metastases model (in wild type, IL-6 -/- and GATA-1 -/- mice) and the inducible oncogenic K-ras G12D mouse model. The B16F10 mouse model has been widely used to study a variety of pulmonary tumour burden stimulatory and inhibitory factors [64,65]. The established oncogenic K-ras G12D model was used to assess the effects of OSM signals on tumours initiated *in situ* in lungs (**Figure 1)**. This model has a point mutation in the K-ras gene, which is the mutation of glycine to aspartic acid in codon 12[53], as well as a Lox-Stop-Lox cassette inserted upstream of the mutated gene[66]. Pulmonary tumour growth was studied after ectopic delivery of B16F10 cells i.v (B16F10 mouse model) or after K-ras oncogene activation upon Cre expression in lungs of transgenic K-ras G12D mice. Using both models, the effects of OSM overexpression, as well as loss of function, on tumour burden were assessed. Additionally, potential mechanisms underlying the effects of OSM on tumour cell proliferation were examined using fibroblast-conditioned media and co-cultures of fibroblast and tumour cells.

Furthermore, co-cultures of tumour cells and macrophages conditioned *in vivo* were assessed to examine potential effects of lung macrophages on tumour cell proliferation.

CHAPTER 2: Materials and Methods

2.1 – Animals

K-ras G12D transgenic mice were purchased from The Jackson Laboratories (strain: B6.129S4-Kras$^{tm4Tyj/J}$), originally generated by Tyler Jacks[59]. These animals are heterozygous for the oncogenic K-ras G12D allele, consisting of a point transition mutation (G to A), resulting in a single amino acid substitution from glycine (G) to aspartic acid (D) at position 12. A lox-stop-lox cassette inserted upstream of the oncogenic K-ras allele prevents the expression of the mutant protein under normal conditions. However, Cre-mediated recombination deletes this transcriptional termination sequence, allowing expression of the oncogenic protein **(Figure 1).**

OSMRβ -/- mice were a generous gift from Minoru Tanaka and Atsushi Miyajima (University of Tokyo), and were subsequently bred in-house. These animals have a LacZ-neomycin phosphostransferase cassette inserted in the gene, resulting in disruption of OSMRβ transcription[67].

IL-6 -/- mice were purchased from The Jackson Laboratories as well, (strain: B6.129S2-Il6$^{tm1Kopf/J}$). These animals have a neomycin resistance cassette placed in the first coding exon of the IL-6 gene, resulting in the disruption of gene transcription and absence of IL-6 protein.

GATA-1 -/- mice were a gift from the Jordana laboratory at McMaster Immunology Research Center, previously purchased from The Jackson Laboratories (strain: C.129S1(B6)-Gata1$^{tm6Sho/J}$). In these animals, a targeting vector was used to replace the double GATA promoter site, upstream of the GATA-1 gene. Studies have

shown that this site is not required for GATA-1 expression by hematopoietic precursors, mast cells, and erythroid cells, but necessary for eosinophil development[68]**.**

Finally, C57Bl/6 mice were also purchased from Jackson Laboratories.

2.2 – Polymerase Chain Reaction (PCR) Protocol for IL-6, OSMR, and K-ras Genes

Genotyping parameters and primers for wild type and mutant IL-6 alleles were developed under the recommendations of Jackson Laboratory, as shown in **Figure 2**.

Wild type forward primer (σIMR0212): *5'* TTC CAT CCA GTT TTC TTG G *3'*

Wild type reverse primer (σIMR0213): *5'* TTC TCA TTT CCA CGA TTT CCC AG *3'*

Mutant reverse primer (oIMR0214): *5'* CCG GAG AAC CTG CGT GCA ATC C *3'*

PCR products were then run on a 1% agarose gel, as seen in **Figure 3:2a-b**.

Recommendations for the PCR protocol and primers that identify wild-type and mutant OSMRβ alleles were obtained from Tanaka *et al*[67], and shown in **Figure 2.**

Wild type forward primer: *5'* GTA ATC AGA CCA ATG GCT TTC TC *3'*

Wild type reverse primer: *5'* GAT CCA ACA GAG CAA TCA TGA AGC *3'*

Mutant reverse primer: *5'* GCA CAT CTG AAC TTC AGC *3'*

PCR products were then run on a 1% agarose gel (**Figure 3:3a-b**).

Transgenic K-ras G12D mice were genotyped using previously developed primers[69], and the presence of a 600 bp band indicated mutant K-ras allele (**Figure 3:1a)**. The use of these specific primers and the parameters of the PCR temperature and cycles were recommended and modified from the Jackson Laboratory.

To obtain the template for PCR, 1 mm tail ends were obtained from mice, and combined with 125 ul DirectPCR reagent (Viagen, CA USA) and 4.73 ul Proteinase K

(Viagen, CA USA) in eppendorf tubes (per tail snip). These tubes were heated at 55^{o}C overnight, then increased to 85^{o}C for 45 minutes to inactivate the Proteinase K. PCR was then performed according to manufacturer's guidelines using Platinum Taq (Life technologies, Burlington Ontario), where 1 ul of each primer and 1 ul of template were used to amplify the region identified by the forward and reverse primers (per reaction). Using the Mastercyler Gradient Thermocycler (Eppendorf, Mississauga Ontario) PCR was performed using the following parameters: initial denaturation at 94^{o}C for 3 mins (1 cycle) followed by 35 cycles of 94^{o}C for 30 seconds, 55^{o}C for 1 minute, and 72^{o}C for 1 minute, and final extension at 72^{o}C for 2 minutes. For PCR of K-ras alleles, the parameters were changed to 65^{o}C during extension, instead of 55^{o}C.

5 ul of Rapid-Load PCR Loading Dye (Origene, MD USA) was then added to the 25ul PCR product and 15 ul of this solution was loaded onto a 1% agarose gel. The agarose gel was prepared by combining 60 ml of 1x TBE with 0.6g agarose, heating it for 2 minutes, then adding 3 ul of RedSafe (Froggabio, ON CA). A 100 bp ladder (GeneRuler 100 bp Plus DNA-ladder, Fermentas, Burlington CA) was run alongside samples for 1.5 hours at 80V in 1x TBE (from 5x: 216g Tris, 110 g Boric acid, and 80 ml of 0.5M EDTA were added together in 4L of ddH_2O, and pH adjusted to 8.06 with addition of NaOH, to a final volume of 500 ml).

2.3 – Mouse Models of Lung Cancer

In the B16F10 pulmonary melanoma metastases model, ectopic delivery of B16F10 cells via tail vein injections was followed by endotracheal intubation of 50 ul of the desired adenovirus vector the next day. Animals were culled after 2 weeks, unless

otherwise specified, after which BAL fluid was collected, and the left lung was flash frozen in liquid nitrogen and stored at -80^{o}C, while the right lung was fixed in 10% formalin. After 48 hours, pictures were taken of the lungs, melanotic tumours were counted, and the lobes of the right lung were separated, placed in 70% ethanol, and processed for histology.

In the oncogenic K-ras mouse model, 50 ul of the indicated Ad vector was delivered by endotracheal intubation. CT scans were taken at indicated time points (weeks), in the McMaster Center Pre-clinical and Translational Imaging (MCPTI) facility. After 8-12 weeks, as indicated, animals were culled, after which BAL fluid was collected, the left lung was fixed in 10% formalin for 48 hours processed for histology, and the right lung was flash frozen in liquid nitrogen and stored at -80^{o}C.

2.4 - B16F10 Cell Injections

B16F10 cells obtained from the Bramson Laboratory (originally purchased from ATCC) were thawed and cultured until confluent (2 days) in DMEM supplemented with 10% heat-inactivated FBS, 1% penicillin-streptomycin, 1% L-glutamine, and 0.1% fungizone (Life Technologies, CA USA), at 37^{o}C in 5% CO_2. The cells were then split 1:4 and cultured for another 24 hours, after which the media was discarded and cells were washed with 5 ml of room temperature PBS. To lift cells off the plate, 1ml of 10% trypsin was applied and left for 5 minutes, after which the plate was knocked 4 times to dislodge the cells and 9ml of 10% FBS-DMEM was used to remove the cells off the surface of the flask. This 10 ml solution was added to a 50 ml falcon tube, and the plate was washed with another 5 ml of 10%FBS-DMEM and collected. These cells were then centrifuged at

1000 rpm for 5 minutes at 4^{o}C, after which the supernatant was discarded, cells were re-suspended in the residual volume by tapping the tube, and diluted in 50 ml of PBS. This process was repeated, and pelleted cells were re-suspended in 2 ml of 1x PBS and kept on ice. Cells were then counted and used to determine viability (only preparations with >90% viability was used). Cell suspensions were then diluted to achieve a 1x10^{5} cells per mouse (in 200 ul volume), which was intravenously injected into each mouse by Kyle Stephenson of the Lichty Laboratory.

2.5 – AdCre Precipitation

Adenovirus precipitation was performed using a previously established protocol[70]. Briefly, to prepare 1 ml of the virus diluent solution, 10 ul of 0.2 M L-glutamine was added to 100 ul of 10X Eagle's MEM (Sigma Aldrich, Oakville CA) and 890 ul sterile water. The appropriate amount of virus (indicated pfu) was diluted in this solution and 2ul of 2M $CaCl_2$ was added and mixed 20 minutes prior to the intubation at RT. This solution was used up to one hour after precipitation.

2.6– BALF Collection

Mice were anesthetized and then exsanguinated upon cutting the renal artery within the abdominal cavity. A polysterene tube was then used to canulate the trachea. After removal of the lungs from culled mice, 0.5 ml PBS was infused and retrieved (the conventional BAL), after which 3 more infusions of 0.5 ml PBS were retrieved (the exhaustive BAL). The conventional BAL was spun down at 13,000 rpm for 2 minutes at 4^{o}C, supernatants removed, and stored at -80^{o}C. The exhaustive BAL was also spun down at 13,000 rpm for 2 minutes at RT, after which cell pellets from both the conventional and

exhaustive BAL were combined and resuspended in 100 ul 1x PBS. These cells were then used to perform cell counts. A sample (100,000 cells) was spun onto slides using a cytocentrifuge and then stained using the Wright-Giemsa method (Thermo Fisher Scientific Inc.), for differential cell counting.

2.7 – Histological Processing and ImageJ Analysis

Depending on the model, either the left or right lung was used for histological processing. If the right lung was used, the lobes were separated and processed for histology. If the left lung was used, the lung was sectioned under the bronchial bifurcation and processed for histology. During histological processing, the cut edge was embedded in paraffin. 5 um sections were made 200 or 250 um apart (as indicated) and sections were placed on slides. These slides were than stained for H&E by MIRC Core Histology.

Using these slides and ImageJ software, the area of the tumour per section was measured. Photographs were taken using a Leica DMRA microscope and OpenLab Software (version 5.0.2) of the stained slides at 1.6x magnification. These images were then loaded on Image J software, where the freehand selection was used to select the tumour area. The values from each selection were then summed and the total value was divided by the number of sections of the lungs (8-12, varying on experiment and number of lobes sectioned).

2.8 – CT Scanning Analysis

CT scan images were analyzed using AMIRA software, purchased from Visage Imaging (San Diego, CA). Images were loaded onto the program using big endian and 512x512x512 dimensions. Using the Brush tool, the lung area within the rib cage was

first selected from the top of the lungs to the diaphragm and saved as the first "lung label". The heart and diaphragm were then removed from this first label, leaving only the lung area in the final lung label. To measure densities represented by Hounsfield Units (HU) within that label, a histogram was generated using the following properties: Range (-1025 to +275), Bin number (26). The histogram was saved as a .csv file, where the histogram.y values demonstrated the number of voxels (3D pixels) that are of a specific density. Using these values, the percentages of the lung label within specific ranges of Hounsfield Units were calculated and graphed using GraphPad Prism.

Colour overlays were generated using the lung label previously created. Using the terminology of the AMIRA software, three different new "materials" (colours) were added, and each "material" corresponded to a specific range of HUs: blue (-1000 to -200), yellow (-200 to 0), red (0 to +200). These materials were then applied to the original lung label, and will color each voxel with the corresponding density range. The dotted draw style (AMIRA terminology) was used in this thesis.

2.9 - Cell Culture

LLC cells were purchased from ATCC (Manassas, VA USA) and cultured at 37^{o}C (and 5% CO_2) in DMEM media supplemented with 10% heat-inactivated FBS, 1% penicillin-streptomycin, 1% L-glutamine, and 0.1% fungizone (Life Technologies, CA USA). These cells were cultured in T75 flasks, split 1:2 two days later, and plated at 1000 cells per well in 96-well tissue culture plates for experiments conducted the following day assessing proliferation.

B16F10 cells were cultured and prepared for proliferation assays in the same conditions as LLC cells, mentioned above.

LKR-13 cells were a gift from the Mossman Laboratory (originally obtained by Tyler Jacks, MIT), and cultured in the same conditions as mentioned above, except using RPMI media. These cells were split in 1:5 ratios and plated at 1000 cells per well for proliferation experiments the following day.

Mouse lung fibroblasts (MLFs) were obtained from explants of mouse whole lung tissue, using a protocol previously established in the laboratory[71]. These cells were cultured in the same conditions as mentioned above, except using MEM-F15 media. MLFs were cultured and passaged on tissue culture plates until adherent, and plated in densities specific to the experiment performed.

For *in vitro* proliferation studies, LLC and LKR-13 cells were plated at 1000 cells per well in 96-well tissue culture plates with corresponding media. After 24 hours, cells were treated in quadruplicate with either media, recombinant mIL-6, recombinant mOSM, recombinant human TGFβ, recombinant mTNFα, or recombinant mIL-18 (all from R&D) at concentrations 0.2, 2, or 20 ng/ml, and incubated at 37^{o}C and 5% CO_2 for 24 or 48 hours. After this time, cell proliferation was measured using the MTT assay and values were expressed as percent growth relative to tumour cells cultured with media alone.

2.10 –Conditioned Media Model

For conditioned media experiments, mouse lung fibroblasts were plated in 6-well Costar tissue culture plates and cultured until approximately 80% confluent. MLFs were

then treated with either media or 5ng/ml recombinant mOSM (R&D, MN USA), and left for 24 hours. During this time, FLuc-LLC and FLuc-B16F10 cells were plated at 1000 cells per well, and cultured for 24 hours, after which the media was discarded and conditioned media was applied (in quadruplicate). After the intended time passed, cell proliferation was measured using the luciferase assay.

2.11 - Co-culture Model

For co-culture experiments, mouse lung fibroblasts were plated in 96-well tissue culture plates until approximately 80% confluent. MLFs were then simultaneously treated with either media or 5ng/ml recombinant mOSM (R&D, MN USA), and co-cultured with FLucLLC or FLucB16F10 cells (1000 cells per well) in quadruplicate. After 24 or 48 hours, cell proliferation was measured using the luciferase assay.

2.12 - Reverse Transcription and Taqman

The RNA concentrations of samples obtained from a previous experiment (performed by D. Fritz) were quantified using the NanoVue Spectrophotometer (GE Healthcare, UK) and reverse transcribed to obtain cDNA using SuperScript II RT (Life Technologies, Burlington CA) using the manufacturer's instructions.

Samples were then examined for fibronectin and periostin mRNA levels by adding 20ul of a probe solution (containing 1.25 ul of the probe, 12.5 ul universal master mix, and 6.25 ul nuclease-free water) to 5ul of 2ng/ml cDNA in a MicroAmp Optical 96 well reaction plate. The plate was then sealed with parafilm, centrifuged, and mRNA levels were quantified using the 7900 HT Fast RealTime PCR System (Life

Technologies). The mRNA expression levels were calculated using the protocol outlined by Livak *et al* (2001)[72] and expressed relative to values of the 18S housekeeping gene.

2.13 - Primary Macrophage Culture

To obtain macrophage cultures, cells in the bronchoalveolar lavage (BAL) fluid were counted, and 20,000 cells per well (for macrophage and tumour cell co-cultures) or 25,000 cells per well (for arginase assays) were diluted in 10%FBS-DMEM, plated on 96 well plates, and incubated at 37^{o}C for 2 hours. After allowing cells to adhere, non-adherent cells were decanted and the wells were washed 3 times with 100 ul PBS to obtain the adherent population. Previous work in the Richards Laboratory has determined that the adherent population is largely composed of macrophages.

2.14 - Arginase Assay

The arginase assays were conducted on macrophages plated in 96-well tissue culture plates. Cells were washed with 100 ul PBS, and lysed with 25 ul of 0.1% Triton X-100 supplemented with a solution of protease inhibitors (for 1 ml of inhibitor solution: 5ul of 200 mM Na_3VO_4, 5ul of 1 mM PMSF, 1ul of 0.1 M DTT, and 30 ul aprotonin). The plate was then set on an orbital shaker for 15 minutes at room temperature. After cell lysis, 25 ul of 25 mM Tris-HCL was added, and 25 ul of each sample was then put into eppendorf tubes, where 2.5 ul of 10 mM $MnCl_2$ (dissolved in water) was added and samples were heated at 56^{o}C for 10 minutes. 25 ul of 0.5 M L-arginine (dissolved in water) was then added to each sample, and all samples were incubated at 37^{o}C for 30 minutes. During this time, the urea standard was prepared (7-point standard curve), using 0.12g urea and 100 ml H_2O to make 10mM urea. After this time, 200 ul of acid solution

(for 110 ml: 70 ml H_2O, 10 ml H_2SO_4, and 30 ml H_3PO_4) was added, followed by 10 ul of 9% α-ISPF (dissolved in 100% ethanol). Samples were then incubated at 95^oC for 30 minutes, and cooled, at which time the samples were transferred to a 96-well plate and absorption read at 550 nm using the ELx800 Absorbance Microplate Reader (BioTek, Vermont USA).

2.15 - MTT Assay

MTT (3-(4,5-dimethylthiazol-2-yl)-2,5-diphenyltetrazolium bromide) assays were conducted on cells plated in 96-well tissue culture plates. After 24 or 48 hours of cell proliferation (as indicated in the *Results* section), 20 ul of 5mg/ml MTT (Sigma-Aldrich, Oakville CA) was added to each well. The plate was then incubated at 37^oC for 4 hours in the dark. After this time, plates were spun down at 1000 rpm, the supernatant was removed, and 200 ul of DMSO was added to each well. After pipetting a few times to mix the solution, absorption was read at 550 nm using the ELx800 Absorbance Microplate Reader (BioTek, Vermont USA).

2.16 - Luciferase Assay

For an alternate method of calculating tumour cell proliferation, fluorescent LLC and B16F10 cells (a kind gift from Dr. Workenhe of the Mossman Lab), where retroviral transduction was used to integrate the reporter luciferase gene into the LLC1 and B16F10 cell DNA.

Cells were plated in 96-well tissue culture plates (1000 cells/well) and treated with the indicated conditions for 24 or 48 hours, after which 100 ul of 1x cell lysis buffer from the luciferase assay kit (Promega, WI USA) was added to each well and the plate was

incubated at room temperature for 15 minutes. After cell lysis, 50 ul of each sample lysate and 50 ul of luciferase substrate (from the kit) were added to a 96-well, white opaque OptiPlate (PerkinElmer, MA USA), and read using 5 second integration time on the Tropix TR717 Microplate Luminometer (Applied Biosystems, MA USA).

2.17 - ELISA

All ELISAs (mIL-6 and mOSM – purchased from R&D, Minneapolis, MN) were performed according to manufacturer's protocols and samples were measured at an optical density of 450 nm using the ELx800 Absorbance Microplate Reader (BioTek, Vermont USA). The limit of detection of the mIL-6 ELISA is 15.6 pg/ml, and the limit of the mOSM ELISA is 31.3 pg/ml.

2.18 - Statistical Analysis

All statistical analysis was performed using GraphPad Prism 5 Software (GraphPad Software Inc., San Diego USA). Student's t-test were used to determine statistical significant between 2 treatment groups, whereas one-way ANOVA was used when testing 3 or more treatment groups (unless otherwise specified). A p-value less than 0.05 was considered statistically significant.

Figure 1. Schematic Diagram of the Transgenic K-ras Mouse Model.

Transgenic K-ras mice have both a wild type K-ras and a silenced mutant K-ras allele. The mutant gene has a point mutation, resulting in an amino acid substitution from glycine to aspartic acid, and a Lox-Stop-Lox (LSL) cassette inserted upstream of the gene that blocks expression of mutant K-ras transcript. Upon administration of an adenovirus encoding Cre-recombinase, infected cells express Cre and a portion of the Lox-Stop-Lox site is excised that allows the oncogenic K-ras gene to be expressed.

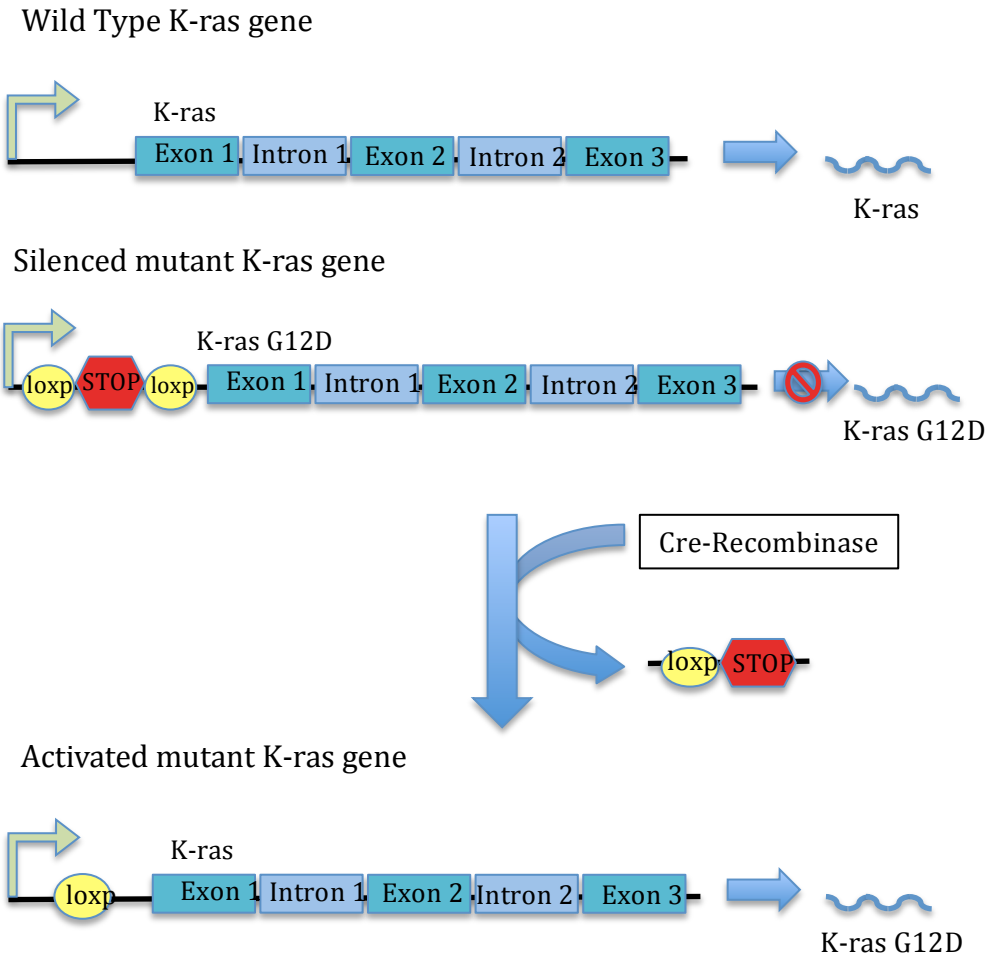
Wild Type K-ras gene
K-ras
Exon 1
Intron 1
Exon 2
Intron 2
Exon 3
K-ras
Silenced mutant K-ras gene
K-ras G12D
loxp
STOP
loxp
Exon 1
Intron 1
Exon 2
Intron 2
Exon 3
K-ras G12D
Cre-Recombinase
loxp
STOP
Activated mutant K-ras gene
K-ras
loxp
Exon 1
Intron 1
Exon 2
Intron 2
Exon 3
K-ras G12D

Figure 1.

Figure 2. Wild-type and Mutant IL-6 and OSMR DNA Sequences with Primer Binding Sites.

In the wild-type IL-6 DNA sequence (top), the 174 bp region spanning between the yellow arrow (primer oIMR0212) and the red arrow (primer oIMR0213) is the region present in all wild-type IL-6 alleles. Upon insertion of the neomycin-resistance cassette, as on the right, the mutant IL-6 alleles are identified via the 380 bp region spanning between the yellow arrow and grey arrow (primer oIMR0214). The OSMR knockout model is similar to the IL-6 knockout model, with the common forward and wild-type reverse primers recognizing the region spanning 364 bp (between the yellow and red sequences), while the common forward and mutant reverse primers recognize the region spanning 750 bp (between the yellow and grey sequences).


IL-6
CCAAGAACGATAGTCAATTCCAGAAACCGCTATGAAGTTCCTCTCTGCAAGTAAGTGAAGGCAGTTCCTTGCCCTCTGGCGG
AGCTATTGAGACTGTGAGAGAGGAGTGTGAGGCAGAGAGCCAGCATTGTGGGTTGGCCAGCAGCCATCAGCTAGCAGCAGGC
GCCCAACTGTGCTATCTGCTCACTTGCCGGTTTTCCCTTTTCTCCACGCAGGAGACTTCGATCCAGTTGCCTTCTTGGGACTGA
TGCTG *** NEOMYCIN CASSETTE ** GGATTGCAAGCAGGTTCTCCGG *** GTGACAACCACGGCCTTCCCTACTTCACAAGT
CCGGAGAGGAGACTTCACAGAGGATACCACTCCCAACAGACCTGTCTATACCACTTCACAAGTCGGAGGCTTAATTACACATGT
TCTCTGGGAAATCGTGGAAATGAGAAAAGAGGTGGGTAGGCTGTGAAACTGATGAAGACCCAGTGTGGGCGTCCATTCATTCT
CTTTGCTCTTGAATTAGAAATTCTCTGCTGGGATCTAGGGCCCTTAGGATTTGAAGCTAAAGGTCAGACTAGACTGTGTTC...
OSMR
CACTTCATGGGACAGGGAAATGTGCCTTCTTCCTCCAAAGACAGATGACAAGAGACACAGGTATGGGAGGAATAATGGAA
GACTTTCGTCCCACCTCTGACCACAGTTGCCCCCAAGAAGCATACCAGGAGTTAAAGCTATATAAAAGGCTCTTTCTTGTC
ATTTATCTTTTTCAGGTAATCAGACCAATGGCTTTCTCTGTGGTC *** LACZ-NEOMYCIN PHOSPHOTRANSFERASE
CASSETTE ** GCTGAAGTTCAGATGTGC *** CTTCATCCAGCCTTCCTCCTGGCAGTGCTGTCCCTGAGGGCATCCCGAAG
CGAAGGTGAGAGACAAGAACACGAGAAGGGAGCACGGAAAGGTGCTCCATCTGGTGCTTTGGAGAACGGTTAAGCAATTT
TCCTTCCTCAGAGCTGGTGATTAATTCACATGAGAGGTGGTAAATTTCTGGAAGCCACAATTGCCTCGGGCGTGTCCTCCC
TCAACTGATAGCACGTTTAGTAAGTCCACTCCTTAGCCCTGGCTGCCTGCTAGGTGCTCTGCTCATTGGTATGGTCGTGAG
CGGACCTGAGACTACAGACCTTCATGATTGCTCTGTTGGATCTACACCACTGCCAAGGTATTTCCTTCTGAACCTTGCTGC
GCAAGATGGAACAGCCCAGACTAGTTCTGGCTGCTGAGTTAGAACAAGTTCCAATGCCCCTTAGCCACACTTTGCTGAG...

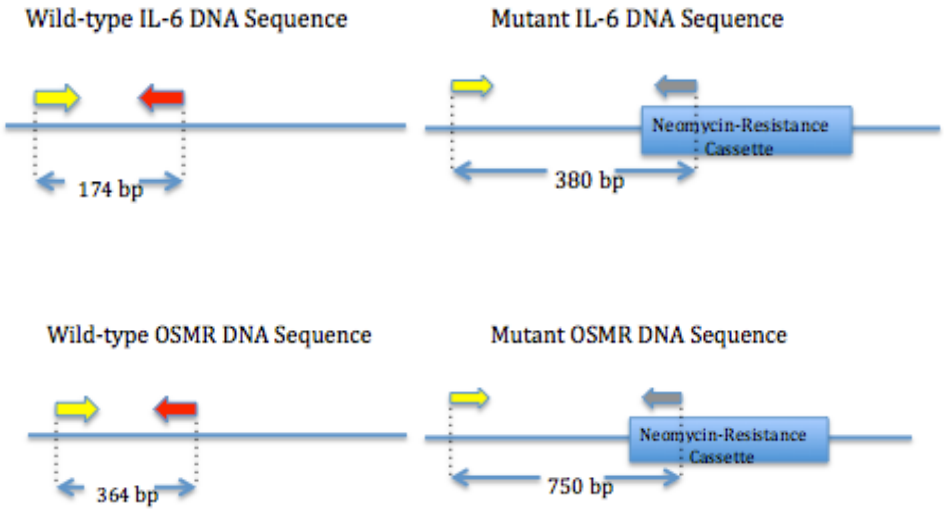
Wild-type IL-6 DNA Sequence
Mutant IL-6 DNA Sequence
174 bp
Neomycin-Resistance Cassette
380 bp
Wild-type OSMR DNA Sequence
Mutant OSMR DNA Sequence
364 bp
Neomycin-Resistance Cassette
750 bp

Figure 2.

Figure 3. Genotyping of IL-6 and OSMR by RT-PCR

(1a-e)DNA was extracted from a transgenic K-ras mouse via a 5 mm tail snip, and examined for (a) the mutant K-ras 600 bp band, (b) the wild-type IL-6 174 bp band, (c) the mutant IL-6 380 bp band, (d) the wild-type OSMR 364 bp band, and (e) the mutant OSMR 750 bp band, respectively.

(2a-b) DNA was extracted from an IL-6 heterozygous mouse via a 5 mm tail snip, and examined for (a) the wild-type IL-6 174 bp band, and (b) the mutant IL-6 380 bp band.

(3a-b) DNA was extracted from an OSMR heterozygous mouse and examined for (a) the wild-type OSMR 364 bp band, and (b) the mutant OSMR 750 bp band.

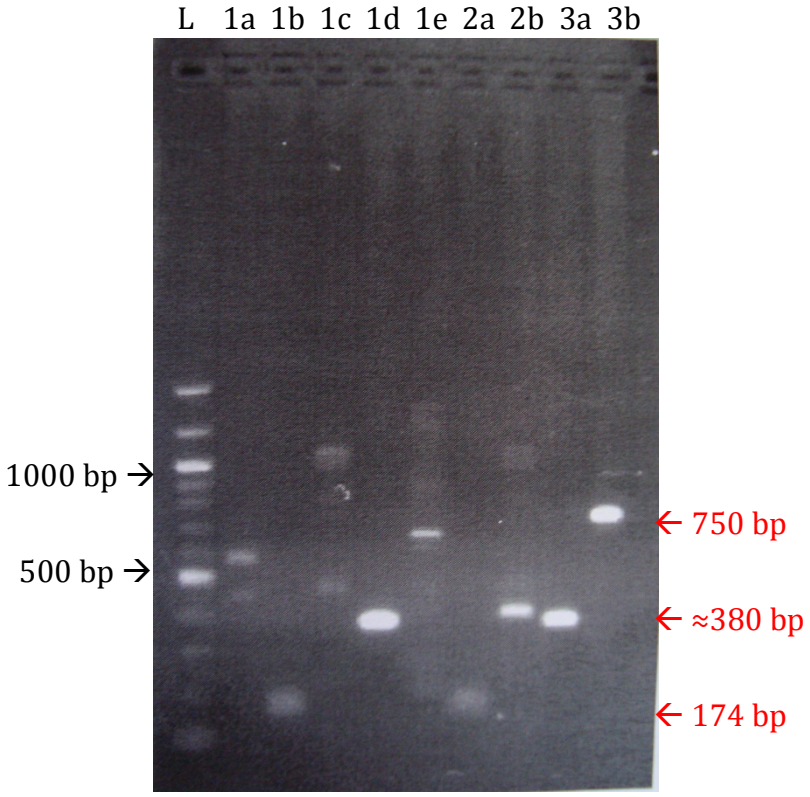

Figure 3.

CHAPTER 3: Effects of OSM overexpression in the B16F10 Mouse Model

In this chapter, the effects of overexpression of Oncostatin M or IL-6 on pulmonary tumour burden was examined using the B16F10 mouse melanoma model. To this extent, the tumour burden was examined by histopathology, calculation of tumour area and number, and BALF cell and cytokine constituents were measured. The role of IL-6 or eosinophils in OSM-induced tumour pathology was also examined using IL-6 -/- mice or GATA-1 -/- mice deficient in eosinophils.

3.1 - Pathology of OSM or IL-6 overexpression in the B16F10 mouse model

To examine the effects of OSM or IL-6 overexpression on tumour burden in the B16F10 melanoma model (described in *Materials and Methods*), 2 strains of mice, wild type and OSMRβ -/-, were intravenously injected with $1x10^5$ B16F10 cells per mouse, then intubated with an adenovirus vector on the following day. Wild type mice were endotracheally intubated with either $2x10^8$ pfu AdDel70 (n=5) as the control, $2x10^8$ pfu AdIL-6 (n=5), or $5x10^7$ pfu AdOSM (n=6). OSMRβ -/- mice were treated with $2x10^8$ pfu AdIL-6 (n=6). Two weeks after adenovirus administration, mice were culled, after which lungs were removed and BALF was collected for differential cell analysis and cytokine analysis by ELISA. The right lung was used to conduct tumour counts, then fixed and processed for histological sectioning and H&E staining, while the left lung was frozen for future DNA/RNA/protein extraction.

3.1.1 – Representative macroscopic and H&E-stained lung section images

Representative macroscopic pictures taken of the right lung are shown, which exhibited an increase in numbers of tumour nodules in lungs of wild type mice treated

with AdOSM compared to lungs of AdDel70 or AdIL-6 treatments, which ranged from few to none (**Figure 4A**). Lungs from OSMRβ -/- mice treated with AdIL-6 looked comparable to lungs from wild type mice treated with AdDel70. In subsequent experiments (data not shown here), lungs from wild type mice injected with B16F10 cells alone visually exhibited similar tumour nodule size and numbers as wild type mice injected with B16F10 cells and intubated with AdDel70. H&E stained sections of the lungs showed similar trends, demonstrating increased tumour burden in AdOSM-treated wild type mice, compared to all other treatments, while there was no visible difference among other treatments **(Figure 4B)**. Lung sections of AdDel70- or AdIL-6-treated wild type mice presented tumours characterized by diffuse hyperplastic regions located primarily on the outer surface of the lungs. This trend was also observed in lung sections from AdIL-6-treated OSMRβ -/- mice. In contrast, upon OSM overexpression in wild type mice, large and dense regions of tumour cell hyperplasia with disrupted alveolar structure and were found throughout the parenchyma and peribronchiolar space. These observations were consistent with previous studies examining the pathology following OSM overexpression in the B16F10 pulmonary metastases model[73].

3.1.2 – Analysis of tumour burden and number upon OSM or IL-6 overexpression

The H&E stained lung sections were used to generate quantitative data reflecting tumour area using Image J software, as described in the *Materials and Methods* section. This analysis confirmed trends observed macroscopically, as there was a statistically significant increase in tumour area per section upon OSM overexpression in wild type mice, increased approximately 10-fold compared to the AdDel70 control group **(Figure**

4C). There was no significant difference in tumour burden between wild type mice treated with AdDel70 or AdIL-6. In addition, OSMRβ -/- mice treated with AdIL-6 did not display changes in lung tumour burden, compared to AdDel70- or AdIL-6-treated wild type mice. Quantitative analysis of tumour burden was accompanied by tumour counts performed on the right lung, which revealed that upon OSM overexpression, there was a statistically significant increase in visible tumour nodules (2-fold) compared to the AdDel70 control group **(Figure 4D)**. The lungs of wild type mice treated with AdIL-6 also demonstrated a trend towards an increase in tumour nodule numbers compared to the control group. However, there were no statistically significant changes in tumour numbers between the AdDel70 control group and OSMRβ -/- mice treated with AdIL-6.

3.1.3 – Analysis of BALF constituents upon OSM or IL-6 overexpression

BAL fluid collected during the procedure was analyzed for IL-6 and OSM cytokine protein levels. Although average IL-6 protein levels in AdIL-6-treated wild type and OSMRβ knockout mice were elevated (approximately 1000 pg/ml and 300 pg/ml, respectively), compared to the AdDel70 control group (approximately 50 pg/ml), there were no statistically significant differences among all treatment groups **(Figure 5A)**. There were also consistently low OSM protein levels among all treatment groups, ranging from approximately 50-100 pg/ml **(Figure 5B)**. Significant differences were not expected, however, as cytokine analysis was conducted at day 14, likely missing higher peaks of cytokine levels as seen at earlier time points (day 2 and day 7) by previous observations in the laboratory.

BAL fluid was also assessed for cell numbers and differential cell analysis. Cell counts demonstrated a statistically significant increase in total BAL cells upon OSM overexpression in wild type mice, compared to the control group **(Figure 5C)**. In addition, total BAL cells counts from AdIL-6-treated OSMRβ -/- mice were significantly less compared to their wild type counterpart, though not statistically different from the AdDel70 control group. In differential cell analysis, there was a 20-fold, statistically significant increase in eosinophil recruitment due to OSM, but not IL-6, overexpression in wild type mice **(Figure 5D)**. Such eosinophil recruitment was also absent upon IL-6 overexpression in OSMRβ -/- mice. Finally, differential counts also demonstrated elevated lymphocyte recruitment among all treatment groups, compared to the AdDel70 control group.

3.2 – Pathology of OSM overexpression in wild type and IL-6 knockout mice using B16F10 mouse model

Previous studies have demonstrated that elevated OSM cytokine levels stimulates IL-6 production both *in vitro* and *in vivo*[35]. Thus, to assess whether IL-6 levels were required for the effects of OSM overexpression on tumour burden, a study was conducted using 2 strains of C57Bl/6 mice: wild type and IL-6 -/-. Each strain was intravenously injected with $1x10^5$ B16 cells, and endotracheally intubated with either $5x10^7$ pfu AdDel70 as the control (n=5 for wild type, n=3 for IL-6 -/-) or $5x10^7$ pfu AdOSM (n=3 for wild type, n=5 for IL-6 -/-) on the following day. Two weeks after adenovirus administration, mice were culled and lungs and BALF were analyzed as described above.

3.2.1 – Representative macroscopic and H&E-stained lung section images

Representative macroscopic pictures taken of the right lung suggest that the absence of IL-6 did not affect the increase in tumour nodule numbers upon OSM overexpression, as IL-6 -/- and wild type mice treated with AdOSM did not bear visual differences (**Figure 6A).** H&E stained sections of the lungs showed similar trends, as OSM overexpression in both wild type and IL-6 -/- mice resulted in increased tumour area, compared to their wild type counterparts **(Figure 6B)**. In accordance with the experiment described in *section 3.1*, OSM overexpression in wild type mice resulted in large and dense hyperplastic regions throughout the parenchyma, as well as near the outer surface of the lungs. Similar pathology was also observed upon OSM overexpression in IL-6 -/- mice. In comparison, AdDel70-treated wild type and IL-6 -/- mice presented with predominantly diffuse hyperplastic regions near the outer surface of the lungs, though they did have some smaller regions of dense tumour cell hyperplasia throughout the parenchyma.

3.2.2 – Analysis of tumour burden upon OSM overexpression in wild type and IL-6 -/- mice

The H&E stained lung sections were then used to generate quantitative data reflecting tumour area using Image J software, as described in the *Materials and Methods* section. This analysis confirmed trends observed previously, as there was a statistically significant increase in tumour area upon OSM overexpression in wild type mice, increasing tumour burden approximately 5-fold compared to the control group (**Figure 6C)**. Similarly, upon OSM overexpression in IL-6 -/- mice, there was a trend towards an

increase in tumour burden, resulting in a 3-fold increase in tumour area compared to AdDel70-treated IL-6 -/- mice. Importantly, there was no significant difference in tumour area per section measured upon OSM overexpression in either strain (approximately 2 mm^2 in both strains). Analysis of tumour counts performed on the right lung revealed that unlike experiment described in *section 3.1*, there were no statistically significant differences in tumour nodule number upon OSM overexpression in either wild type or IL-6 -/- mice, compared to AdDel70-treated wild type or IL-6 -/- mice, respectively **(Figure 6D)**.

3.2.3 – Analysis of BALF constituents upon OSM overexpression in wild type and IL-6 -/- mice

Although there was a statistically significant increase in IL-6 protein levels in BAL fluid upon OSM overexpression in wild type mice, compared to AdDel70 treatment, levels were relatively low in both treatment conditions, ranging from 10 to 50 pg/ml, and completely undetectable in IL-6 -/- mice, as expected **(Figure 7A)**. Similarly, OSM protein levels were generally low, ranging from 200-300 pg/ml, and not statistically significant among all treatment groups **(Figure 7B).**

Cell counts demonstrated no statistically significant differences in total BAL cell number among all treatment groups **(Figure 7C)**. Differential cell analysis demonstrated an increase in eosinophil numbers in BAL upon OSM overexpression in wild type mice, compared to undetectable levels in the BAL of AdDel70-treated wild type mice **(Figure 7D),** similar to the experiment described in *section 3.1*. There was significantly reduced eosinophil numbers upon OSM overexpression in IL-6 -/- mice compared to wild type

mice (reduced approximately 5-fold). Finally, low lymphocyte increases in BALF were consistent upon OSM overexpression compared to control in both wild type and IL-6 -/- mice.

3.3 – Eosinophil involvement in OSM-induced pathology in the B16F10 mouse model

Previous work in the Richards' laboratory has shown that OSM overexpression in lungs of C57Bl/6 mice induces a marked increase in eosinophil infiltration at 7 days, and this trend was also reported at day 14, as noted previously in *Section 3.1*. Therefore, to examine whether recruited eosinophils were involved in the effects on tumour pathology upon OSM overexpression in the B16F10 melanoma model, wild type C57Bl/6 and GATA-1 -/- mice (deficient in eosinophils) were intravenously injected with $1x10^5$ B16F10 cells each, then intubated with the Ad vector on the following day. Wild type mice were endotracheally intubated with either $2x10^8$ pfu AdDel70 as the control (n=5), or $5x10^7$ pfu AdOSM (n=6), while GATA-1 -/- mice received either $5x10^7$ pfu AdDel70 (n=4) or $5x10^7$ pfu AdOSM (n=4). 2 weeks after adenovirus administration, mice were culled, and the lungs and BALF were analyzed as described above. This experiment was completed in parallel with the experiment previously described in *Section 3.1*, thus the data for wild type mice treated with AdDel70 or AdOSM is the same and re-graphed here.

3.3.1 – Representative macroscopic and H&E-stained lung section images

As noted in *Section 3.1,* representative macroscopic pictures taken of the right lung reflected increased tumour number and size upon OSM overexpression, compared to AdDel70-treated wild type mice **(Figure 8A)**. Images of lungs from the GATA-1 -/- mice demonstrated that the absence of eosinophils did not appear to inhibit the tumour

development capacity in the B16F10 melanoma model, as AdDel70-treated GATA-1 -/- mice in fact exhibited more lung tumour nodules, compared to AdDel70-treated wild type mice. Representative images of the H&E stained sections of the lungs showed similar trends, as both GATA-1 -/- groups exhibited visibly more tumours than their control wild type counterparts (**Figure 8B)**. While the images of lung sections from wild type mice treated with AdDel70 showed diffuse hyperplastic regions near the outer surface of the lung, GATA-1 -/- mice treated with AdDel70 exhibited dense hyperplastic regions throughout the parenchyma, characteristic of B16F10 metastases observed upon OSM overexpression in wild type mice. In comparison, AdOSM-treated GATA-1 -/- mice exhibited larger dense hyperplastic regions, compared to the AdDel70-treated GATA-1 -/- mice.

3.3.2 – Analysis of tumour burden upon OSM overexpression in wild type and GATA-1 knockout mice

The H&E stained lung sections were then used to generate quantitative data using methods previously described. As previously noted in *Section 3.1*, there was a statistically significant increase in tumour area upon OSM overexpression in wild type mice **(Figure 8C).** There was also an increase in tumour burden upon OSM overexpression in GATA-1 -/- mice, increasing the tumour burden 3-fold compared to AdDel70-treated GATA-1 -/- mice. The increase in tumour burden in GATA-1 -/- mice was statistically significant via unpaired t-test, but not one-way ANOVA. When tested, there was no significant difference in tumour area per section of OSM-induced tumour burden in wild type or GATA-1 -/- mice. Tumour counts performed on the right lung revealed that AdDel70-

treated GATA-1 -/- mice showed an approximately 4-fold increase in lung tumour number, compared to the wild type counterpart, while AdOSM-treated GATA-1 -/- mice showed an approximately 2-fold increase in tumour number, compared to the wild type counterpart **(Figure 8D)**. Contrary to the trends observed with tumour area per section, however, there was no statistically significant difference in tumour counts between AdDel70- and AdOSM- treated GATA-1 -/- mice, where both groups showed high numbers of tumour nodules (80-100).

3.3.3 – Analysis of BALF constituents upon OSM overexpression in wild type and GATA-1 -/- mice

BAL fluid collected after culling animals was analyzed for IL-6 and OSM cytokine protein levels. There were consistently low levels of IL-6 protein among treatments in both strains, ranging from undetectable to 200 pg/ml **(Figure 9A)**. This trend was also observed when detecting OSM protein levels, with the exception of BAL samples from AdOSM-treated GATA-1 -/- mice **(Figure 9B)** which averaged 2000 pg/ml, a relatively high level in context of the two week time point.

As indicated earlier (*Section 3.1),* there was a statistically significant increase in total cell number in BALF upon OSM overexpression in wild type mice compared to the AdDel70 control group **(Figure 9C).** Despite similarity in measured tumour area, total BAL cell numbers were approximately 4.5-fold less upon OSM overexpression in GATA-1 -/- mice compared to wild type mice. There was a statistically significant increase in BAL lymphocyte cell numbers measured in AdOSM-treated wild type mice, but not in GATA-1 -/-mice **(Figure 9D).**

In addition, there was a trend towards a decrease in total cell and macrophage cell numbers in both GATA-1 -/- treatment groups, compared to wild type treatment groups**.** Finally, eosinophils were not detected in BAL samples from GATA-1 -/- mice, as expected due to the known phenotype of these animals.

3.4 – Effects of loss of function of OSMRβ in the B16F10 mouse model

Since accumulated results indicated that gain of OSM function increased tumour burden, the next experiments examined the effects of loss of function of OSMRβ in the B16F10 pulmonary melanoma metastases model. In this study, wild type and OSMRβ -/- mice were injected intravenously with either $1x10^5$ (n=5) or $5x10^4$ B16 cells (n=5). Three weeks after tumour cell injection, mice were culled. Lungs from these mice were not further analyzed. Lungs removed from mice treated with $5x10^4$ B16 cells were fixed and prepared for histology.

3.4.1 – Representative macroscopic and H&E-stained lung section images

Very high tumour numbers were observed macroscopically in mice that received $1x10^5$ B16 cells, and further analysis was not completed. However, representative macroscopic pictures taken of the right lung of wild type and OSMRβ -/- mice treated with $5x10^4$ B16 cells exhibited qualitatively similar tumour nodule numbers (**Figure 10A).** This trend suggests the lack of difference in tumour growth upon loss of function of OSMRβ. Representative images of the H&E stained sections of the lungs confirmed trends observed macroscopically, as both wild type and OSMRβ -/- mice exhibited large, dense tumours throughout the parenchyma of the lung **(Figure 10B).**

3.4.2 – Analysis of tumour burden upon loss of function of OSMRβ

Interestingly, tumour burden measured by tumour area per section in OSMRβ knockout mice was significantly greater (2-fold) than in wild type mice **(Figure 10C)**. Quantitative analysis of tumour counts on all lobes revealed that the lungs of OSMRβ knockout mice showed 2-fold greater number of tumours than lungs of wild type mice **(Figure 10D)**.

Figure 4. Analysis of lung tumour burden upon IL-6 overexpression in wild-type and OSMRβ -/- mice administered B16F10 melanoma cells.

Wild type and OSMRβ -/- mice were intravenously injected with $1x10^5$ B16F10 cells and the following day wild type mice were endotracheally intubated with either $2x10^8$ pfu AdDel70 (n=5), $5x10^7$ pfu AdOSM (n=6), or $2x10^8$ pfu AdIL-6 (n=5), while OSMRβ -/- mice were intubated with $2x10^8$ pfu AdIL-6 (n=6). After 2 weeks, the lungs of these animals were removed, BAL fluid was collected and the right lungs were analyzed for tumour numbers and area, as described in *Materials and Methods*. In (A) macroscopic pictures were taken of representative lungs. The lobes of the right lung were then separated and processed for H&E staining (B). Using the histological sections and Image J software, the tumour area per section for each mouse was calculated (C), and tumour counts were performed using only the right lung (D). Statistical significance is shown where *=$p<0.05$, **=$p<0.001$, and ***=$p<0.0001$.

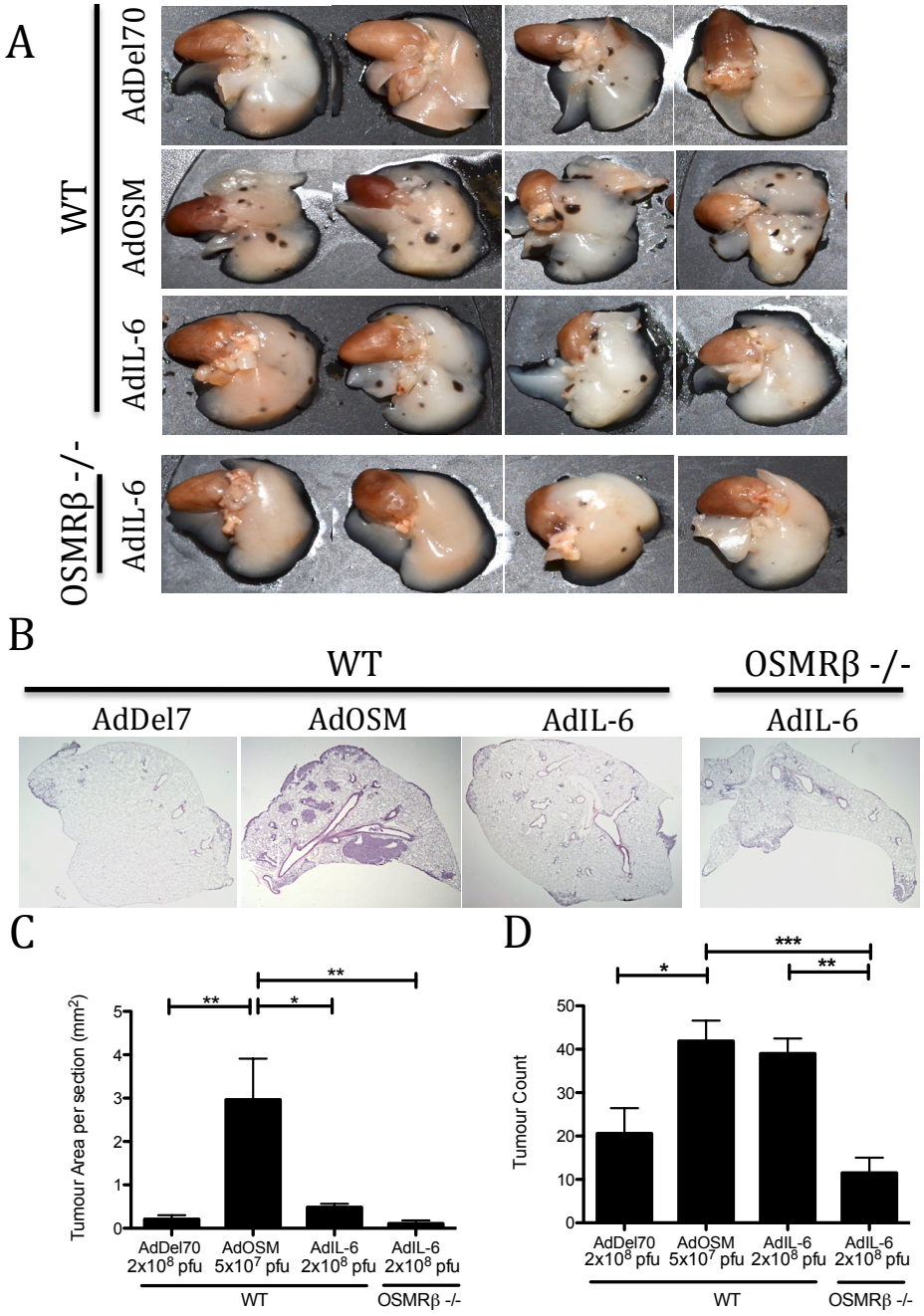
A
WT
OSMRβ -/-
AdDel70
AdOSM
AdIL-6
AdIL-6
B
WT
OSMRβ -/-
AdDel7
AdOSM
AdIL-6
AdIL-6
C
Tumour Area per section (mm²)
AdDel70 2x10⁸ pfu
AdOSM 5x10⁷ pfu
AdIL-6 2x10⁸ pfu
AdIL-6 2x10⁸ pfu
WT
OSMRβ -/-
D
Tumour Count
AdDel70 2x10⁸ pfu
AdOSM 5x10⁷ pfu
AdIL-6 2x10⁸ pfu
AdIL-6 2x10⁸ pfu
WT
OSMRβ -/-

Figure 4.

Figure 5. Analysis of alveolar lavage upon IL-6 overexpression in wild-type and OSMRβ -/- mice administered B16F10 melanoma cells.

In the same experiment described in *Figure 4*, IL-6 (A) and OSM (B) protein levels in the BALF were analyzed by ELISA, total cell counts were performed (C), and differential cell analysis of cytocentrifuged BAL fluid samples was conducted (D). Statistical significance is shown where ! = significance with unpaired t-test, or *=$p<0.05$, **=$p<0.001$, and ***=$p<0.0001$ using one-way ANOVA.

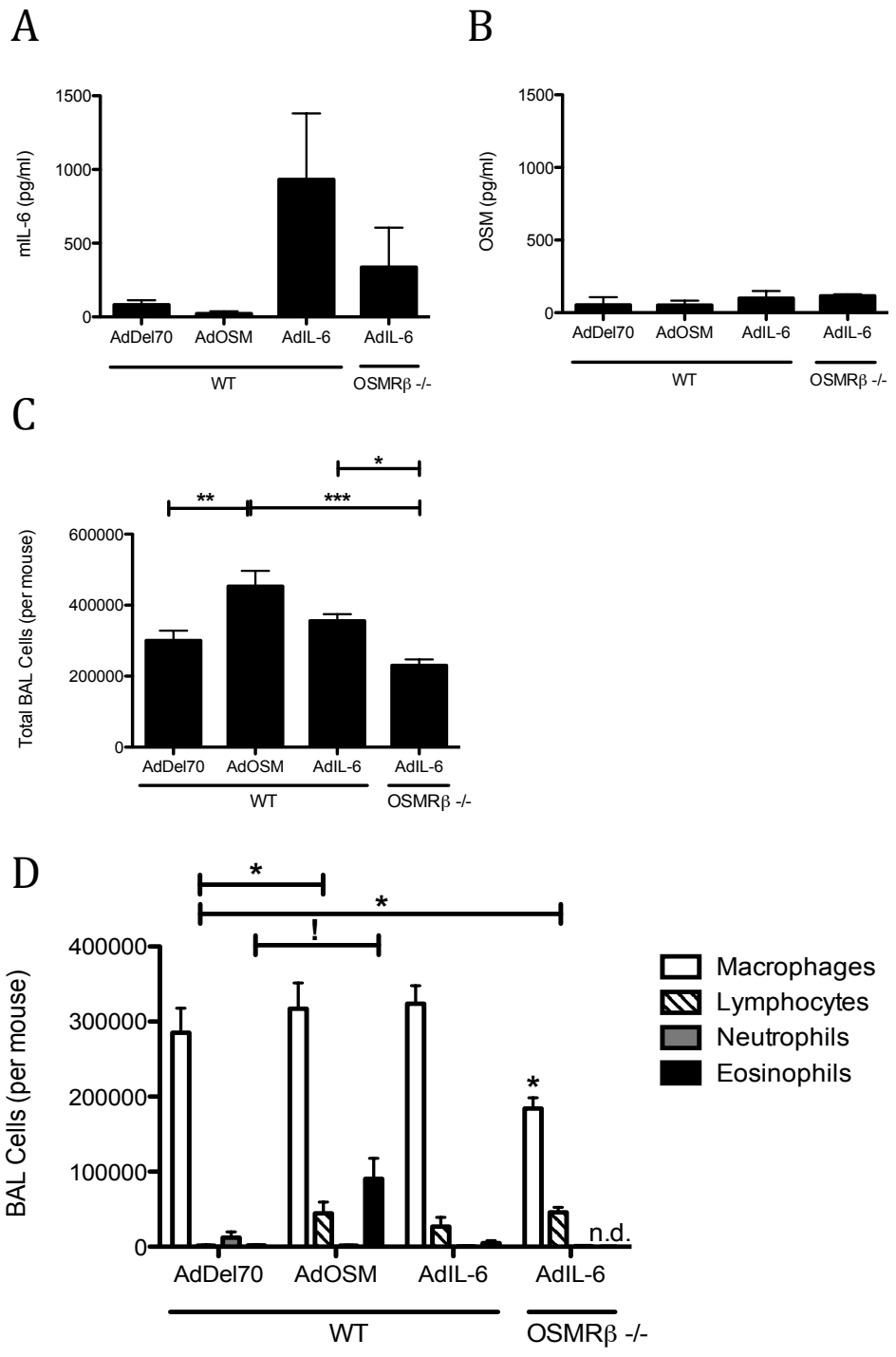
A
mIL-6 (pg/ml)
1500
1000
500
0
AdDel70
AdOSM
AdIL-6
AdIL-6
WT
OSMRβ -/-
B
OSM (pg/ml)
1500
1000
500
0
AdDel70
AdOSM
AdIL-6
AdIL-6
WT
OSMRβ -/-
C
*
**
***
Total BAL Cells (per mouse)
600000
400000
200000
0
AdDel70
AdOSM
AdIL-6
AdIL-6
WT
OSMRβ -/-
D
*
*
!
BAL Cells (per mouse)
400000
300000
200000
100000
0
*
n.d.
AdDel70
AdOSM
AdIL-6
AdIL-6
WT
OSMRβ -/-
Macrophages
Lymphocytes
Neutrophils
Eosinophils

Figure 5.

Figure 6. Analysis of lung tumour burden upon OSM overexpression in wild-type and IL-6 -/- mice administered B16F10 melanoma cells.

Wild type and IL-6 knockout mice were intravenously injected with $1x10^5$ B16F10 cells and endotracheally intubated the following day, with either $5x10^7$ pfu AdDel70 (n=5 for WT, n=3 for IL-6 KO) or $5x10^7$ pfu AdOSM (n=3 for WT, n=5 for IL-6 -/-). After 2 weeks, the lungs were removed, BAL fluid was collected, and the right lungs were analyzed for tumour numbers and area. In (A) macroscopic pictures were taken of representative lungs. The lobes of the right lung were then separated and processed for histological sectioning and H&E staining (B). Using the slides from histology and Image J software, the tumour area per section for each mouse was calculated (C), and tumour counts were performed using only the right lung (D). Statistical significance is shown where *=$p<0.05$ and **=$p<0.001$.

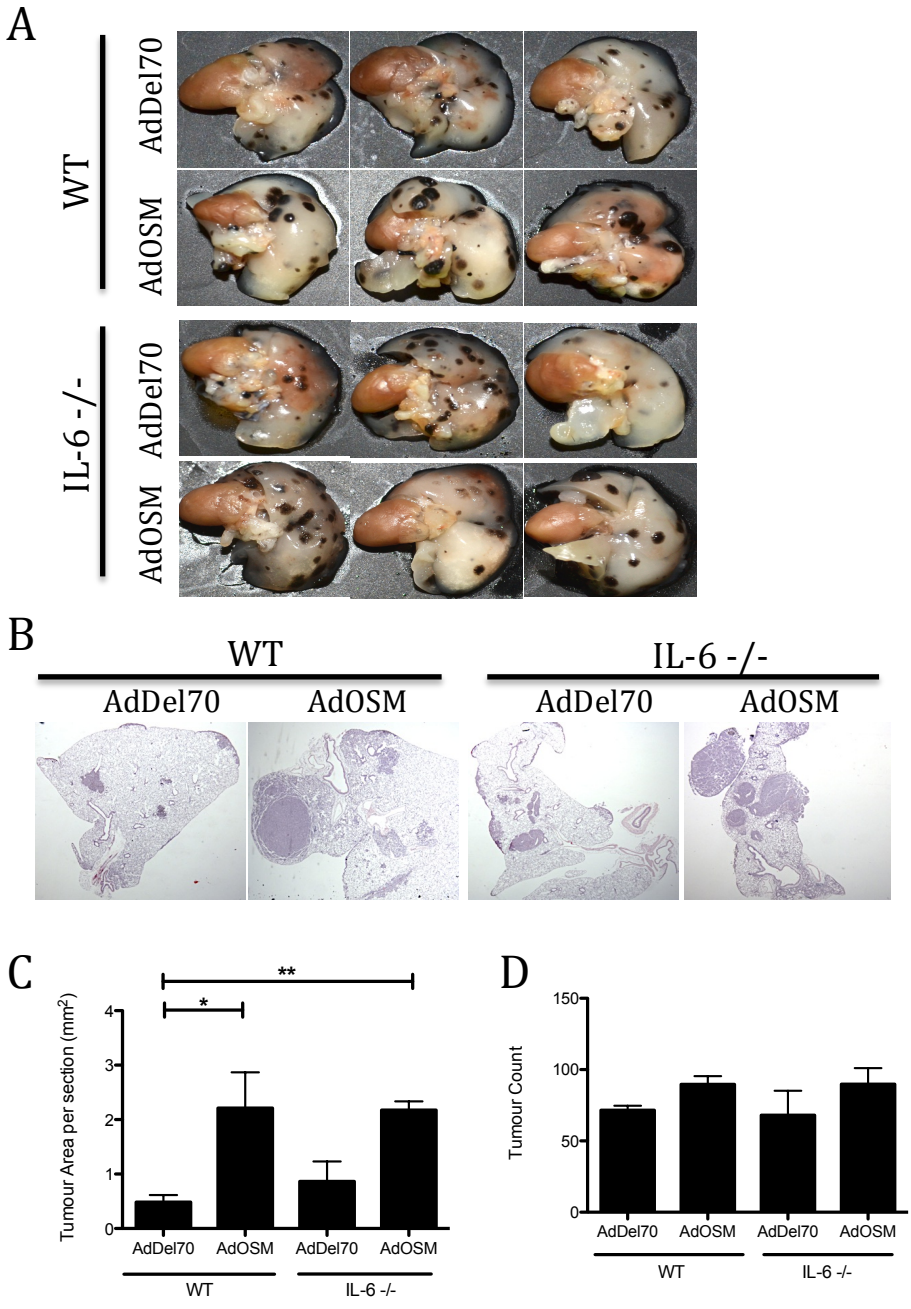
A
WT
AdDel70
AdOSM
IL-6 -/-
AdDel70
AdOSM
B
WT
IL-6 -/-
AdDel70
AdOSM
AdDel70
AdOSM
C
Tumour Area per section (mm²)
**
*
AdDel70
AdOSM
AdDel70
AdOSM
WT
IL-6 -/-
D
Tumour Count
AdDel70
AdOSM
AdDel70
AdOSM
WT
IL-6 -/-

Figure 6.

Figure 7. Analysis of alveolar lavage upon OSM overexpression in wild-type and IL-6 -/- mice administered B16F10 cells.

In the same experiment described in *Figure 6*, IL-6 (A) and OSM (B) protein levels in the BALF were analyzed by ELISA, total cell counts were performed (C), and differential cell analysis of cytocentrifuged BAL fluid samples was conducted (D). Statistical significance is shown where n.d. = not detectable,*=$p<0.05$, **=$p<0.001$, and ***=$p<0.0001$.

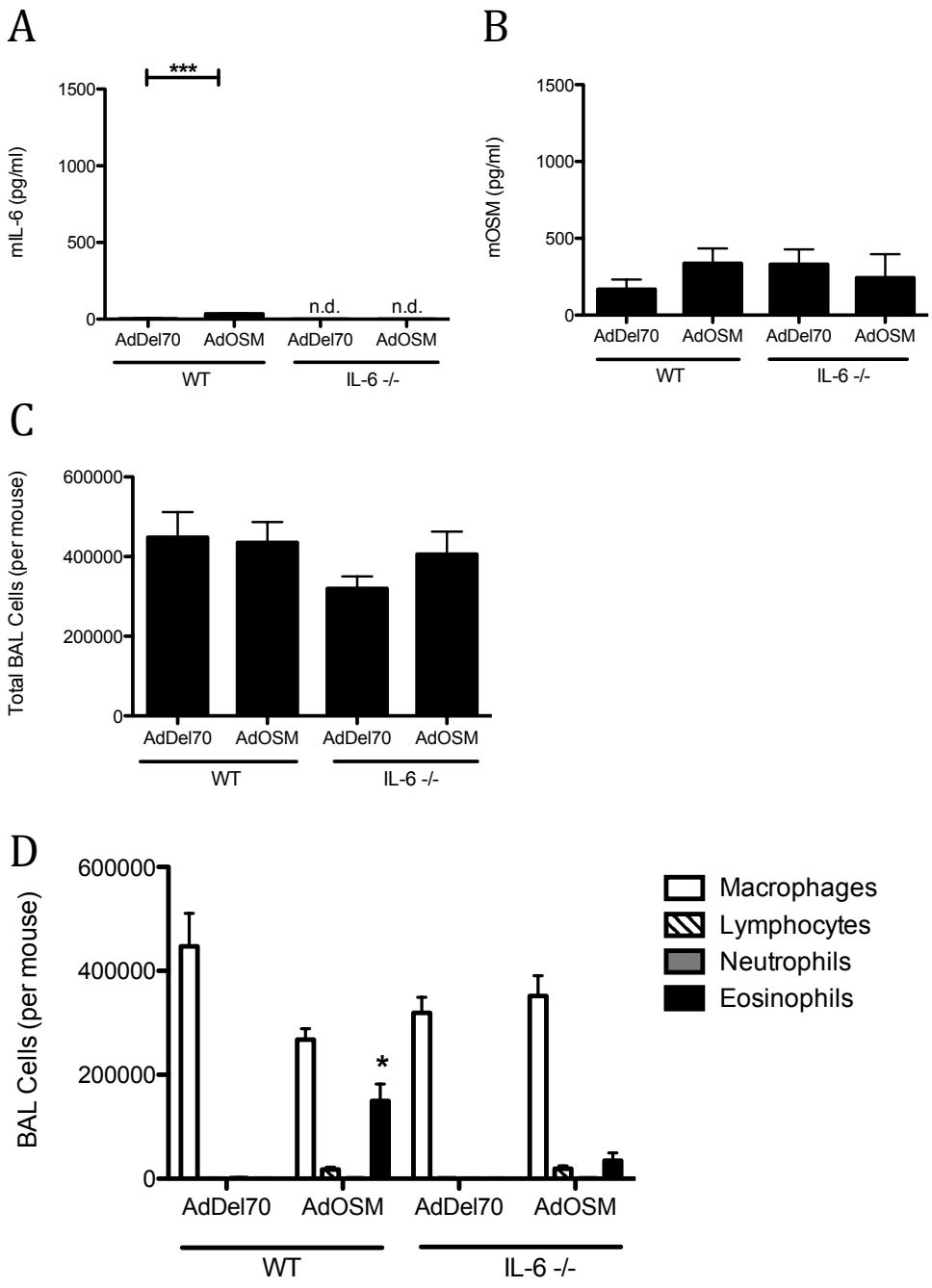
A
***
1500
1000
500
0
mIL-6 (pg/ml)
n.d.
n.d.
AdDel70
AdOSM
AdDel70
AdOSM
WT
IL-6 -/-
B
1500
1000
500
0
mOSM (pg/ml)
AdDel70
AdOSM
AdDel70
AdOSM
WT
IL-6 -/-
C
600000
400000
200000
0
Total BAL Cells (per mouse)
AdDel70
AdOSM
AdDel70
AdOSM
WT
IL-6 -/-
D
600000
400000
200000
0
BAL Cells (per mouse)
*
AdDel70
AdOSM
AdDel70
AdOSM
WT
IL-6 -/-
Macrophages
Lymphocytes
Neutrophils
Eosinophils

Figure 7.

Figure 8. Analysis of lung tumour burden upon OSM overexpression in wild-type and GATA-1 -/- mice administered B16F10 melanoma cells.

Wild type and GATA-1 -/- mice were intravenously injected with B16F10 cells and endotracheally intubated the following day with either AdDel70 (n=5 for WT, n=4 for GATA-1 -/-) or AdOSM (n=6 for WT, n=4 for GATA-1 -/-) at the doses indicated. After 2 weeks, the lungs of these animals were removed, BAL fluid was collected and lungs were analyzed for tumour numbers and area. In (A) macroscopic pictures were taken of the right lung. The lobes of the right lung were then separated and sent for histological sectioning and H&E staining (B). Using the slides from histology and Image J software, the tumour area per section for each mouse was calculated (C), and tumour counts were performed using only the right lung (D). Statistical significance is shown where ! = significance with unpaired t-test, *=$p<0.05$, **=$p<0.001$, and ***=$p<0.0001$.

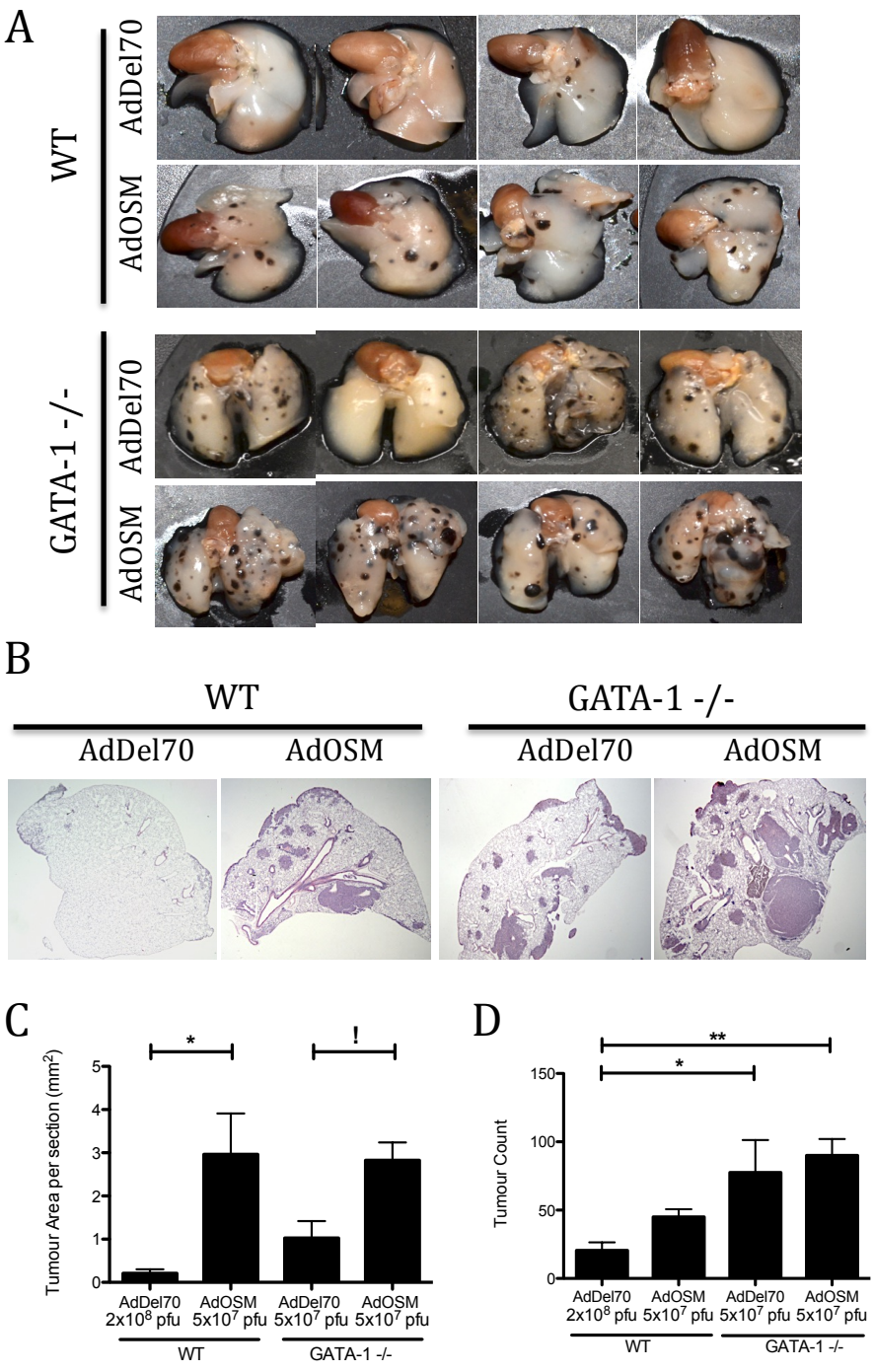
A
WT
AdDel70
AdOSM
GATA-1 -/-
AdDel70
AdOSM
B
WT
GATA-1 -/-
AdDel70
AdOSM
AdDel70
AdOSM
C
Tumour Area per section (mm2)
*
!
AdDel70 2x10^8 pfu
AdOSM 5x10^7 pfu
AdDel70 5x10^7 pfu
AdOSM 5x10^7 pfu
WT
GATA-1 -/-
D
Tumour Count
**
*
AdDel70 2x10^8 pfu
AdOSM 5x10^7 pfu
AdDel70 5x10^7 pfu
AdOSM 5x10^7 pfu
WT
GATA-1 -/-

Figure 8.

Figure 9. Analysis of alveolar lavage upon OSM overexpression in wild-type and GATA-1 knockout models.

In the same experiment described in *Figure 8*, IL-6 (A) and OSM (B) protein levels in the BALF were analyzed using ELISA kits, total cell counts were performed (C), and differential cell analysis of cytocentrifuged BAL fluid samples was conducted (D). Statistical significance is shown where n.d= not detectable, *=$p<0.05$, **=$p<0.001$, and ***=$p<0.0001$.

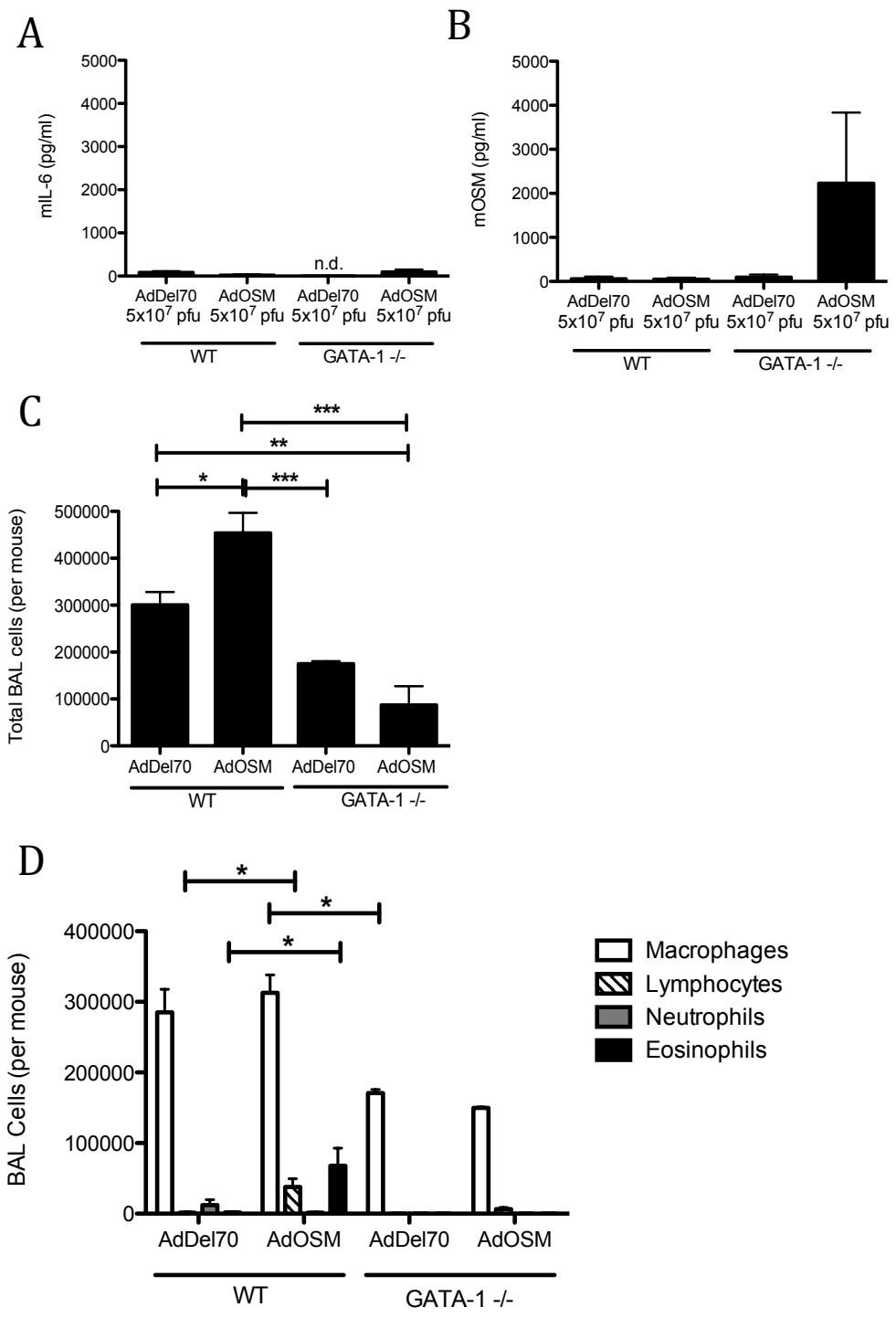
A
mIL-6 (pg/ml)
5000
4000
3000
2000
1000
0
n.d.
AdDel70 5x10^7 pfu
AdOSM 5x10^7 pfu
AdDel70 5x10^7 pfu
AdOSM 5x10^7 pfu
WT
GATA-1 -/-
B
mOSM (pg/ml)
5000
4000
3000
2000
1000
0
AdDel70 5x10^7 pfu
AdOSM 5x10^7 pfu
AdDel70 5x10^7 pfu
AdOSM 5x10^7 pfu
WT
GATA-1 -/-
C
***
**
*
***
Total BAL cells (per mouse)
500000
400000
300000
200000
100000
0
AdDel70
AdOSM
AdDel70
AdOSM
WT
GATA-1 -/-
D
*
*
*
BAL Cells (per mouse)
400000
300000
200000
100000
0
AdDel70
AdOSM
AdDel70
AdOSM
WT
GATA-1 -/-
Macrophages
Lymphocytes
Neutrophils
Eosinophils

Figure 9.

Figure 10. Analysis of lung tumour burden upon B16F10 cell injection in wild type and OSMRβ -/- mice.

Wild type and OSMRβ -/- mice were intravenously injected with $1x10^5$ B16 cells (n=5 for each) or $5x10^4$ B16 cells (n=5 for each) . After 3 weeks, the lungs of these animals were removed and lungs were analyzed for tumour numbers and area. In (A) macroscopic pictures were taken of the right lung. The lobes of the right lung were then separated and sent for histological sectioning and H&E staining (B). Using the slides from histology and Image J software, the tumour area per section for each mouse was averaged (C), and tumour counts were performed using only the right lung (D). Statistical significance is shown where *=$p<0.05$.

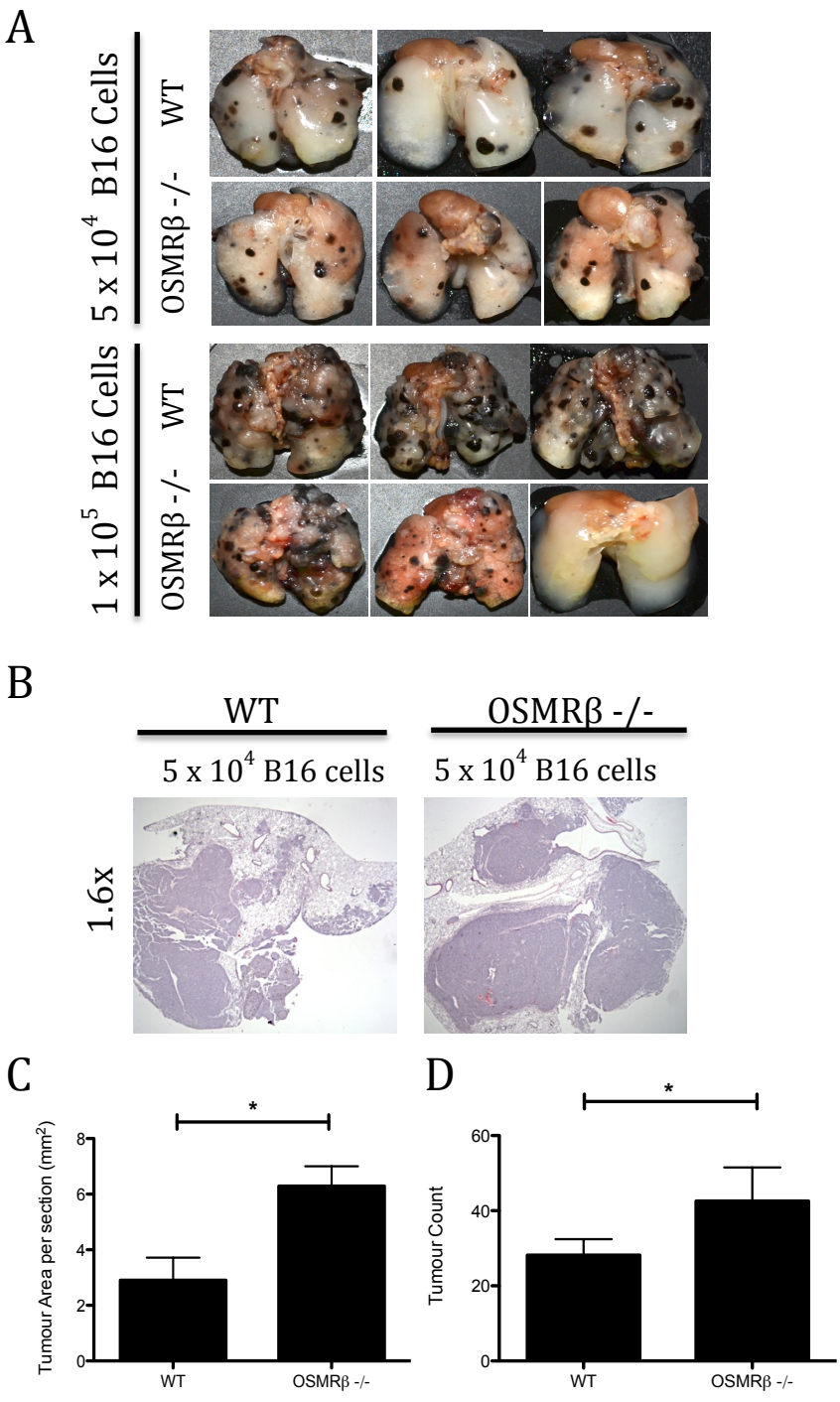
A
5 x 10^4 B16 Cells
WT
OSMRβ -/-
1 x 10^5 B16 Cells
WT
OSMRβ -/-
B
WT
OSMRβ -/-
5 x 10^4 B16 cells
5 x 10^4 B16 cells
1.6x
C
Tumour Area per section (mm^2)
0
2
4
6
8
*
WT
OSMRβ -/-
D
Tumour Count
0
20
40
60
*
WT
OSMRβ -/-

Figure 10.

CHAPTER 4: IL-6 and OSMR β Function in the Inducible K-ras Model

To assess potential roles of OSM and IL-6 in a different model of lung cancer, the conditional oncogenic K-ras mouse model, established by Tyler Jacks[59] and established previously in the Richards lab[69], was then used to examine the effects of diminished Oncostatin M or IL-6 on pulmonary tumour initiation and development. To this extent, the pathology of tumour burden upon AdCre administration in mutant K-ras +/- transgenic mice with deficiency in OSMRβ or IL-6 was examined by CT scan analysis, histopathology, calculation of tumour area and number, as well as BALF protein and cellular content. Additionally, the pathology of tumour burden upon overexpression of OSM in the mutant K-ras +/- transgenic mouse model was examined.

4.1 - Crosses

To obtain IL-6 deficient, mutant K-ras +/- transgenic mice, crosses between C57BL/6 IL-6 -/- mice (strain B6.129S6-*Il6*^{tm1Kopf}) and C57Bl/6 K-ras G12D transgenic mice (strain B65.129S4-Kras^{tm4Tyj}/J) were bred, as outlined in **Figure 11.** Offspring from the first pair of breeders were either IL-6$^{+/-}$ K-ras$^{+/+}$ or IL-6$^{+/-}$ mutant K-ras$^{+/-}$, as mice homozygous for the mutant K-ras alleles were embryonic lethal. Of this cross, heterozygotes for both the IL-6 gene and the K-ras mutation (IL-6$^{+/-}$ K-ras$^{+/-}$) were the targeted genotype. These offspring were then mated together, and of the second set of progeny, the mutant K-ras +/- transgenic, IL-6 -/- or IL-6 +/- mice were the focus of subsequent studies, identifiable using the established PCR protocol discussed in the *Materials and Methods* section. Unfortunately, mutant K-ras +/- transgenic IL-6 -/-mice were not generated, despite genotyping many offspring, and instead mutant K-ras +/- IL-

6+/- transgenic mice were used. As IL-6 -/- mice are healthy and viable, the lack of mutant K-ras +/- IL-6 -/- mouse generation may be due to inadequacy of decreased K-ras protein levels in implantation or embryonic development processes.

An identical approach was used to obtain mutant K-ras +/- transgenic OSMRβ -/- mice ($OSMR^{-/-}$ $K\text{-}ras^{+/-}$) as outlined in **Figure 12**. C57BL/6 OSMRβ -/- mice were obtained from Tanaka, M., et al[67] and have been established in-house since. Mutant K-ras +/-transgenic OSMRβ -/- mice and mutant K-ras +/- transgenic OSMRβ +/- mice were generated through these crosses and used for subsequent studies.

4.2 – AdCre-induced pathology in the oncogenic K-ras mouse model

To first confirm the functionality of the oncogenic K-ras mouse model, C57Bl/6 wild type (n=4) and mutant K-ras +/- transgenic mice (n=4) were endotracheally intubated with $5x10^8$ pfu AdCre. After intubation, CT scans were completed at weeks 0, 4, and 8, as described in *Materials and Methods*. Upon culling at week 10, the lungs were removed and BALF was collected for differential cell analysis. The left lung was fixed and prepared for histological sectioning and H&E staining, while the right lung was frozen for future DNA/RNA/protein extraction.

4.2.1 – Analysis of CT scans of K-ras transgenic mice upon AdCre administration

CT scans were analyzed using AMIRA software as outlined in the *Materials and Methods* section. This analysis demonstrated the development of areas of increased density in the left lung, characterized by increased yellow (-200 to 0 HU) and red (0 to +200 HU) labelled areas at week 8 compared to week 0 (representative CT scans shown in **Figure 13A).** The development of areas with increased density occurred between

weeks 4 and 8, as the CT scans of mutant K-ras +/- transgenic mice at week 4 appeared comparable to week 0.

4.2.2 – Analysis of H&E stained lung sections and tumour burden upon AdCre administration in K-ras transgenic mice

H&E stained sections of the lungs of AdCre-treated mutant K-ras +/- transgenic mice displayed both diffuse and dense hyperplastic regions throughout the parenchyma, characterized as grade 1 and grade 2 tumours, respectively, resulting in the disruption of alveolar wall morphology **(Figure 13B).** There was also noticeable cell infiltration, appearing as "pockets" of leukocytes surrounding the airways. In comparison, sections of the lungs of AdCre-treated K-ras wild type mice displayed regular alveolar structure lacking detectable leukocyte infiltration or hyperplasia. At a higher magnification (20x), the differences in alveolar morphology were more easily detected. Images of lungs from the K-ras wild type group showed normal alveolar structure and airways, whereas the mutant K-ras +/- transgenic group displayed an example of the multiple grade 2 tumours, accompanied by cellular infiltration near the airways and disrupted alveolar wall morphology **(Figure 13C)**.

The H&E stained lung sections were then used to generate quantitative data reflecting tumour area using Image J software, as described in the *Materials and Methods* section. In lung sections of mutant K-ras +/- transgenic mice, there was 0.14 mm^2 of grade 2 tumour area measured per section, compared to the complete absence of tumour area in K-ras wild type mice **(Figure 13D).** Additionally, tumour counts revealed that mutant K-ras +/- transgenic mice developed, approximately one grade 2 tumour per

histological section **(Figure 13E).** Consistent with the measured tumour area, there were no grade 2 tumours found in K-ras wild type mice.

4.2.3 - Analysis of BALF proteins and cell content upon AdCre administration in mutant K-ras +/- transgenic mice

Cells collected from BAL were used to determine cell counts and differential cell analysis. There was a significantly higher total cell number upon AdCre administration in mutant K-ras +/- transgenic mice (2-fold) compared to wild type mice **(Figure 13F).** Differential cell analysis demonstrated that there was a statistically significant increase in macrophage cell numbers, and a 4-fold higher level in lymphocyte cell numbers in BAL samples from mutant K-ras +/- transgenic mice compared to wild type mice.

4.3 – Pathology upon AdCre administration in the oncogenic K-ras mouse model

To confirm the effects of AdCre and to follow individual mice using CT, a study was conducted using mutant K-ras +/- transgenic mice endotracheally intubated with $5x10^8$ pfu AdCre (n=7), and CT scans were taken at weeks 0, 6, and 10. Upon culling at week 10, the lungs were removed and BALF was collected for differential cell analysis. The left and right lungs were analyzed as described above.

4.3.1 – Analysis of CT scans of K-ras transgenic mice upon AdCre intubation

CT scan analysis confirmed results observed in the previous experiment, as there was increased lung density throughout the lung area 10 weeks after AdCre intubation, depicted by the increase in yellow- (-200 to 0 HU) and red- (0 to 200 HU) labeled areas in the density overlays **(Figure 14A).** The representative CT scans in **Figure 14A** differ somewhat from those in the previous experiment **(Figure 13A)**, as the areas of increased

lung density was detected throughout the lung area, as opposed to restricted to one side of the lung.

The data generated by CT scan analysis were graphed and shown in **Figure 14B** for weeks 6 and 10. The histograms revealed that in comparison to week 0, where the majority of the lung label ranged from -450 to -200 HU, only approximately half of the lung label remained in the original density range at week 6, while the other half ranged from -200 to +200 HU, thereby demonstrating increased lung density overall. This increase was more pronounced at week 10, where the majority of the lung label was found in the -200 to +200 HU range. In **Figure 14C**, only the percentage of voxels between 0 to +200 HU were graphed, as they depicted areas of increased density that may be indicative of solid tissue (tumour development) as 0 HU is the density of water, and >250 HU is the density of cortical bones[74]. This graph exhibited statistical significance between the percent of voxels within the 0 to +200 HU range at week 0 and week 10 post-AdCre intubation.

4.3.2 – Analysis of tumour burden upon OSM overexpression in the oncogenic K-ras mouse model

In addition to the 7 mutant K-ras +/- transgenic mice intubated with AdCre, K-ras +/- transgenic mice of a preliminary study were intubated with both $5x10^8$ pfu AdCre and $5x10^7$ pfu AdOSM (n=2). All post-culling procedures were conducted similarly, except these mice were sacrificed at week 8, instead of week 10, as they reached endpoint guidelines sooner than mutant K-ras +/- transgenic mice treated with AdCre alone. H&E stained sections of the lungs of mutant K-ras +/- transgenic mice intubated with AdCre

alone displayed increased dense hyperplastic regions throughout the parenchyma, characterized as grade 2 tumours in **Figure 15A**, compared to mutant K-ras +/- transgenic mice in the study presented in *Section 4.2*. Due to these grade 2 tumours, there was considerable disruption of alveolar wall morphology, as well as thickening of alveolar septae. In comparison, mutant K-ras +/- transgenic mice treated with both AdCre and AdOSM demonstrated large areas of diffuse hyperplasia, as well as smaller and denser hyperplastic regions throughout the parenchyma. Lung sections of these mice also exhibited thickening of alveolar septa due to cell hyperplasia. In **Figure 15B**, images of the lung sections at a higher magnification (20x) illustrated the differences in pathology of tumour burden, as mutant K-ras +/- transgenic mice intubated with AdCre alone had more patchy areas of dense hyperplasia, while these areas were larger in mice intubated with both AdCre and AdOSM.

In lung sections from both treatment groups, there was approximately 1 mm^2 total tumour area measured per section using Image J software, completed as per *Materials and Methods* section **(Figure 15C)**. Thus, mutant K-ras +/- transgenic mice treated with both AdCre and AdOSM exhibited similar total tumour area per section at week 8 as mutant K-ras +/- transgenic mice treated with AdCre alone at week 10, possibly indicating accelerated tumour development. In **Figure 15D**, grade 1 tumour area measurements demonstrated a trend towards an increase in mutant K-ras +/- transgenic treated with both treatments compared to AdCre treatment alone, whereas the opposite trend was observed with grade 2 tumour area measurements **(Figure 15E)**, however the lack of sufficient sample size in the AdOSM/AdCre group precluded statistical analysis.

4.3.3 – Analysis of BALF constituents upon OSM overexpression in the oncogenic K-ras mouse model

BAL fluid was analyzed for IL-6 and OSM cytokine protein levels, and showed consistently low levels of IL-6 protein in both treatment groups, ranging from undetectable to 50 pg/ml **(Figure 16A)**. This trend was also observed when measuring OSM protein levels, shown in **Figure 16B**, where protein levels did not exceed 200 pg/ml. These low levels may not reflect levels earlier in this model, as cytokine analysis was conducted only at day 70.

Cells collected during broncho-alveolar lavage were then used to complete cell counts and differential cell analysis. Cell counts demonstrated that there was a 2-fold decrease in total cell number upon AdCre and AdOSM intubation in mutant K-ras +/- transgenic mice compared to AdCre intubation alone **(Figure 16C).** Upon differential cell analysis, BAL samples mice intubated with AdCre and AdOSM also exhibited 2-fold less macrophage cell numbers, while lymphocyte cell numbers remained similar. As these results were unexpected, the data was then analyzed as percentage of immune cells in the BAL, in contrast to number of immune cells **(Figure 16D).** This graph revealed that, in both treatment groups, macrophages accounted for approximately 98% of BAL cells, and thus there was no decrease in macrophage proportion, rather total cell numbers. This may be due to technical issues where obtaining samples of alveolar spaces could be affected by the alterations in lung pathology.

4.4 – Pathology of tumour burden upon loss of function of OSMRβ or IL-6 in the oncogenic K-ras mouse model

As overexpression of OSM in this model appeared to lead to accelerated tumour development, the subsequent step was to examine whether loss of function of OSMRβ or IL-6 would affect tumour initiation and growth. To do so, mice obtained from the crosses described in *Section 4.1* were used. There were four strains of mice used in total: mutant K-ras +/- transgenic, mutant K-ras +/- transgenic OSMRβ +/-, mutant K-ras +/- transgenic OSMRβ -/-, and mutant K-ras +/- transgenic IL-6 +/-. All groups were endotracheally intubated with precipitated Ad-Cre, and mice were CT scanned at weeks 0, 6, and 10. Upon culling at week 10, the lungs were removed, BALF samples taken, left lung processed in histology, and right lung frozen for future use. This experiment was completed in parallel with the experiment previously described in *Section 4.3*, and thus the results discussed for mutant K-ras +/- transgenic mice intubated with AdCre are identical.

4.4.1 – Analysis of CT scans of K-ras transgenic mice upon loss of function of OSMRβ or IL-6

CT scans were analyzed using AMIRA software as outlined in the *Materials and Methods* section. This analysis demonstrated that upon AdCre intubation, there were similar increases in lung density throughout the whole lung area in mutant K-ras +/- transgenic and mutant K-ras +/- transgenic IL-6 +/- mice, as assessed visually by the similar levels of yellow and red-labeled areas **(Figure 17)**. CT scans of mutant K-ras +/- transgenic OSMRβ +/- or mutant K-ras +/- transgenic OSMRβ -/- mice revealed increases

in lung density as well. The mutant K-ras +/- transgenic OSMRβ +/- and mutant K-ras +/- transgenic OSMRβ -/- mice consistently demonstrated less areas of increased density, in comparison to mutant K-ras +/- transgenic or mutant K-ras +/- transgenic IL-6 +/- mice, depicted qualitatively by more blue- (-1000 to 0) labeled areas visible.

The histograms generated by CT scan analysis were graphed for each strain and shown in **Figure 18A** at weeks 6 and 10. These data revealed that in comparison to week 0, where the majority of the lung label ranged from -450 to -200 HU across all strains, approximately 80% of the lung label was found in the -200 to +200 HU range at week 6 (across all strains). At week 10, approximately 95% of the lung label of mutant K-ras +/- transgenic and mutant K-ras +/- transgenic IL-6 +/- mice ranged from -200 to +200 HU, whereas 85% of the lung label of mutant K-ras +/- transgenic OSMRβ +/- and mutant K-ras +/- transgenic OSMRβ -/- mice was found in this density range (calculations not shown here). In **Figure 18B**, only the percentage of voxels between 0 to +200 HU were graphed, as they estimated areas of increased density that may be indicative of solid tissue (tumour development). This graph exhibited statistical significant differences between the percent of voxels within the 0 to +200 HU range at week 0 and week 10 post-AdCre intubation only in mutant K-ras +/- transgenic and mutant K-ras +/- transgenic IL-6 +/- mice, which correlated with the trends observed visually.

4.4.2 – Analysis of tumour burden upon loss of function of OSMRβ or IL-6 in the oncogenic K-ras mouse model

Serial H&E stained sections of the lungs confirmed grade 1 and grade 2 tumour development in all strains, while revealing variability in frequency of diffuse and dense hyperplastic regions throughout the parenchyma within each strain used **(Figure 19A).** Quantitative analysis of grade 1 and 2 tumour area exhibited different trends than those suggested from CT scan analysis. In contrast to the CT scan data that exhibited increased lung density in mutant K-ras +/- transgenic and mutant K-ras +/- transgenic IL-6 +/- compared to the other two strains, there were no statistically significant differences in grade 1 **(Figure 19B)** or grade 2 **(Figure 19C)** tumour area per section among all mutant K-ras transgenic strains. Upon calculation of total tumour area per section, approximately 1-1.5 mm^2 tumour area was measured for mutant K-ras +/- transgenic, mutant K-ras +/- transgenic OSMR+/-, and mutant K-ras +/- transgenic OSMR -/-, whereas less (0.3 mm^2 tumour area per section) was measured for mutant K-ras +/- transgenic IL-6 +/- mice, although this was not statistically significant. Thus, in contrast to CT data, there were no detectable statistically significant differences in tumour area among all mutant K-ras transgenic strains used. Difference in trends may be due to the lack of sensitivity in CT scans, compared to histological analyses.

4.4.3 – Analysis of BALF constituents upon loss of function of OSMRβ or IL-6 in the oncogenic K-ras mouse model

BAL fluid collected at the termination of the experiment showed low levels of IL-6 protein measured among all strains, ranging from approximately 0 to 50 pg/ml **(Figure 20A)**. OSM protein levels, shown in **Figure 20B**, were also consistently low, as measurements did not exceed 200 pg/ml.

There were no detectable differences in cell number in BAL among the mutant K-ras transgenic strains, as shown in **Figure 20C**. Differential cell analysis of the BALF demonstrated similar trends, as there were no detected differences in measured numbers of macrophages and lymphocytes among the mutant K-ras transgenic strains, while neutrophils and eosinophils were not detected. Thus, loss of function of OSMRβ or IL-6 in the oncogenic K-ras mouse model did not appear to influence detectable differences in tumour development or inflammatory cell recruitment at the time point examined.

Figure 11. Schematic of Cross-breeding to Obtain IL-6 -/- K-ras Transgenic Mice. IL-6 -/-, K-ras wild-type mice were crossed with IL-6 wild-type, transgenic K-ras mice and the F1 generation had mice with the IL-6 heterozygote, wild-type K-ras genotype, as well as the IL-6 heterozygote, transgenic K-ras mice. The mice with the latter genotype were selected using previously mentioned PCR protocols, and mated. Of the F2 generation, mice homozygous for the mutant K-ras alleles will be embryonic lethal. The targeted genotype from the crosses was the IL-6 -/-, K-ras transgenic mice, as indicated by the oval.

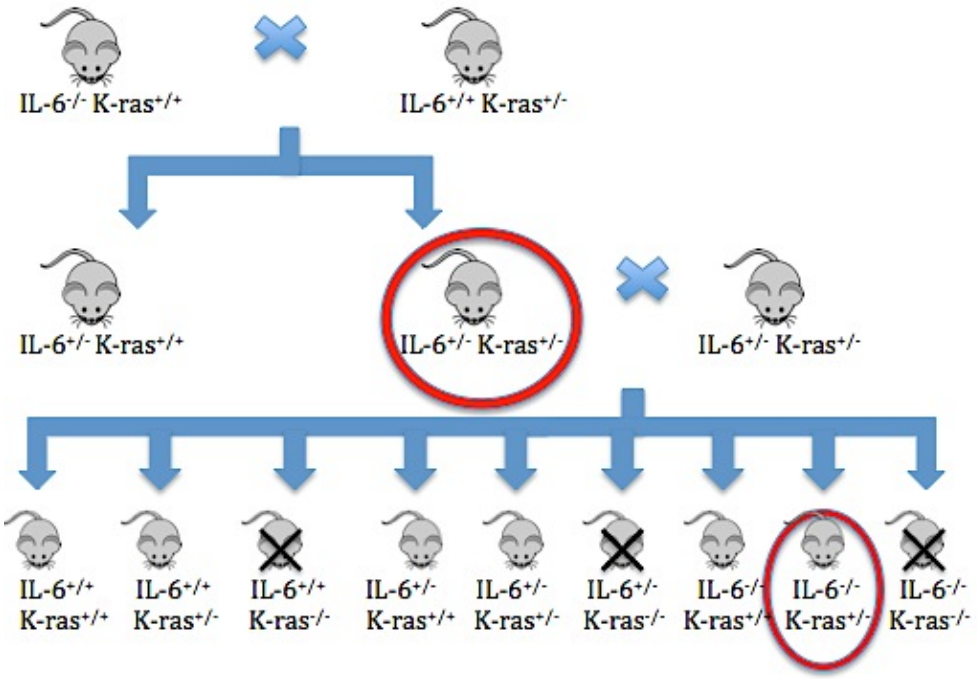
IL-6-/- K-ras+/+
IL-6+/+ K-ras+/-
IL-6+/- K-ras+/+
IL-6+/- K-ras+/-
IL-6+/- K-ras+/-
IL-6+/+ K-ras+/+
IL-6+/+ K-ras+/-
IL-6+/+ K-ras-/-
IL-6+/- K-ras+/+
IL-6+/- K-ras+/-
IL-6+/- K-ras-/-
IL-6-/- K-ras+/-
IL-6-/- K-ras+/-
IL-6-/- K-ras-/-

Figure 11.

Figure 12. Schematic of Cross-breeding to Obtain OSMRβ -/- K-ras Transgenic Mice.

OSMRβ -/-, K-ras wild-type mice were crossed with OSMRβ wild-type, transgenic K-ras mice and the F1 generation had mice with the OSMRβ heterozygote, wild-type K-ras genotype, as well as the OSMRβ heterozygote, transgenic K-ras mice. The mice with the latter genotype were selected using previously mentioned PCR protocols, and mated. Of the F2 generation, mice homozygous for the mutant K-ras alleles will be embryonic lethal. The targeted genotype from the crosses was the OSMRβ -/-, K-ras transgenic mice, as indicated by the oval.

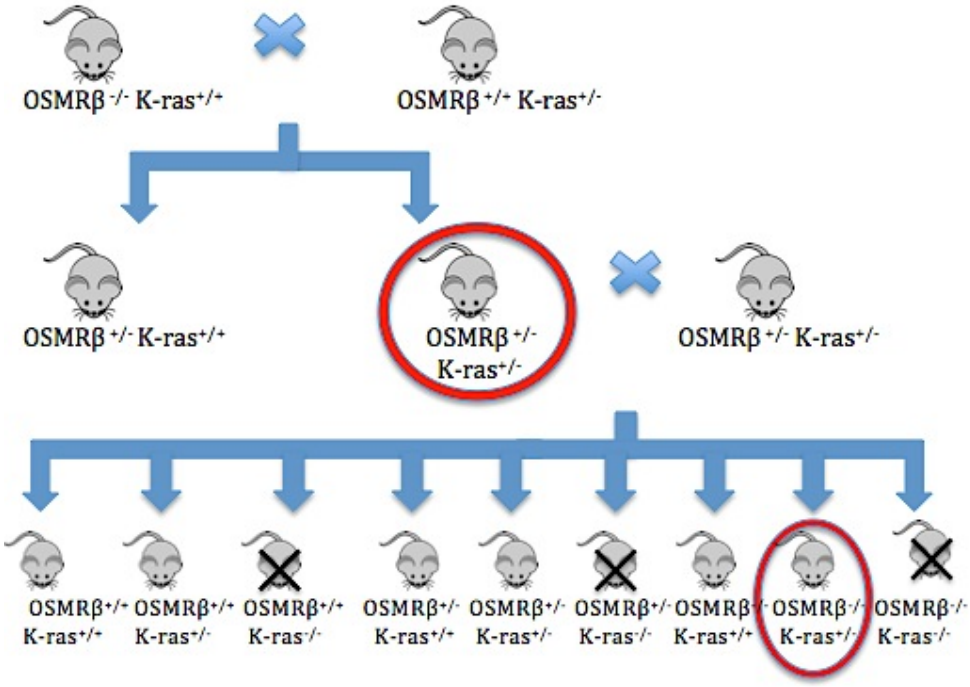
OSMRβ -/- K-ras+/+
OSMRβ +/+ K-ras+/-
OSMRβ +/- K-ras+/+
OSMRβ +/- K-ras+/-
OSMRβ +/- K-ras+/-
OSMRβ+/- K-ras+/+
OSMRβ+/+ K-ras+/-
OSMRβ+/+ K-ras-/-
OSMRβ+/- K-ras+/+
OSMRβ+/- K-ras+/-
OSMRβ+/- K-ras-/-
OSMRβ-/- K-ras+/+
OSMRβ-/- K-ras+/-
OSMRβ-/- K-ras-/-

Figure 12.

Figure 13. Representative CT scans and analysis of tumour burden upon Cre Recombinase treatment in the K-ras G12D mouse model. K-ras wild type (n=5) and transgenic mice (n=5) were endotracheally intubated with $5x10^8$ pfu Ad-Cre Recombinase. CT scans of K-ras transgenic mice were taken at weeks 0, 4, and 8, as indicated, and analyzed using AMIRA software to generate density overlays. These overlays represent varying density ranges using 3 colours: blue (-1000 → -200 HU), yellow (-200 → 0 HU), red (0 → +200 HU). In (A) representative CT scan images with density overlays of K-ras transgenic mice are shown at each indicated week and are taken at 6 sections ranging from the first rib to the diaphragm. Lungs were removed at week 10, the left lung was cut at the major bifurcation and sent for sectioning and H&E staining (B) and (C). Using the slides from histology and Image J software, the grade 2 tumour area per section for each mouse was calculated (D), and tumour counts were performed (E). Differential cell analysis of cytocentrifuged BAL fluid samples was also conducted (F). Statistical significance is shown where *=$p<0.05$ and **=$p<0.001$.

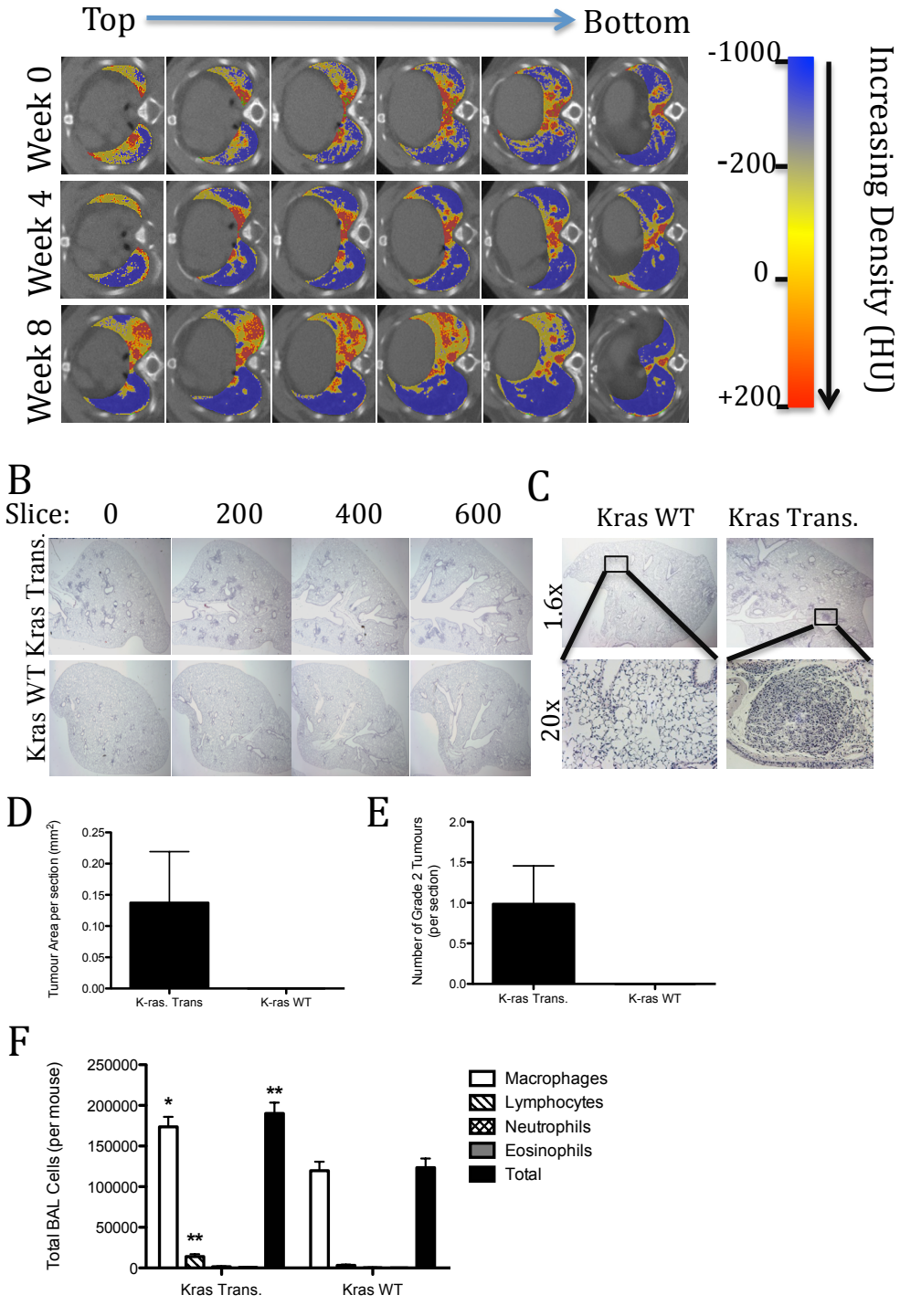
Top
Bottom
Week 0
Week 4
Week 8
-1000
-200
0
+200
Increasing Density (HU)
B
Slice: 0 200 400 600
Kras Trans.
Kras WT
C
Kras WT
Kras Trans.
1.6x
20x
D
Tumour Area per section (mm²)
0.25
0.20
0.15
0.10
0.05
0.00
K-ras. Trans
K-ras WT
E
Number of Grade 2 Tumours (per section)
2.0
1.5
1.0
0.5
0.0
K-ras Trans.
K-ras WT
F
Total BAL Cells (per mouse)
250000
200000
150000
100000
50000
0
*
**
**
Kras Trans.
Kras WT
Macrophages
Lymphocytes
Neutrophils
Eosinophils
Total

Figure 13.

Figure 14. Quantitative analysis of CT scans upon Cre Recombinase treatment in the K-ras G12D mouse model. K-ras transgenic mice were endotracheally intubated with $5x10^8$ pfu Ad-Cre Recombinase (n=7). CT scans were taken at weeks 0, 6, and 10 and analyzed using AMIRA software to generate density overlays. These overlays represent varying density ranges using 3 colours: blue (-1000 → -200 HU), yellow (-200 → 0 HU), red (0 → +200 HU). In (A) representative CT scan images with density overlays are shown at each weeks 0, 6, and 10, and are taken at 6 sections ranging from the first rib to the diaphragm. The density overlays generated from the CT scans were used to produce histograms over the range of -1000 HU to +250 HU with 26 bins. The values in each histogram were summed, and each value was then expressed as a percent of the total lung label. In (B), the average of these percentages are shown at weeks 0 (in black) 6 and 10 and in (C) only the percentage of the lung label between 0 to 200 HU at each time point are shown. Statistical significance is shown where *=$p<0.05$.

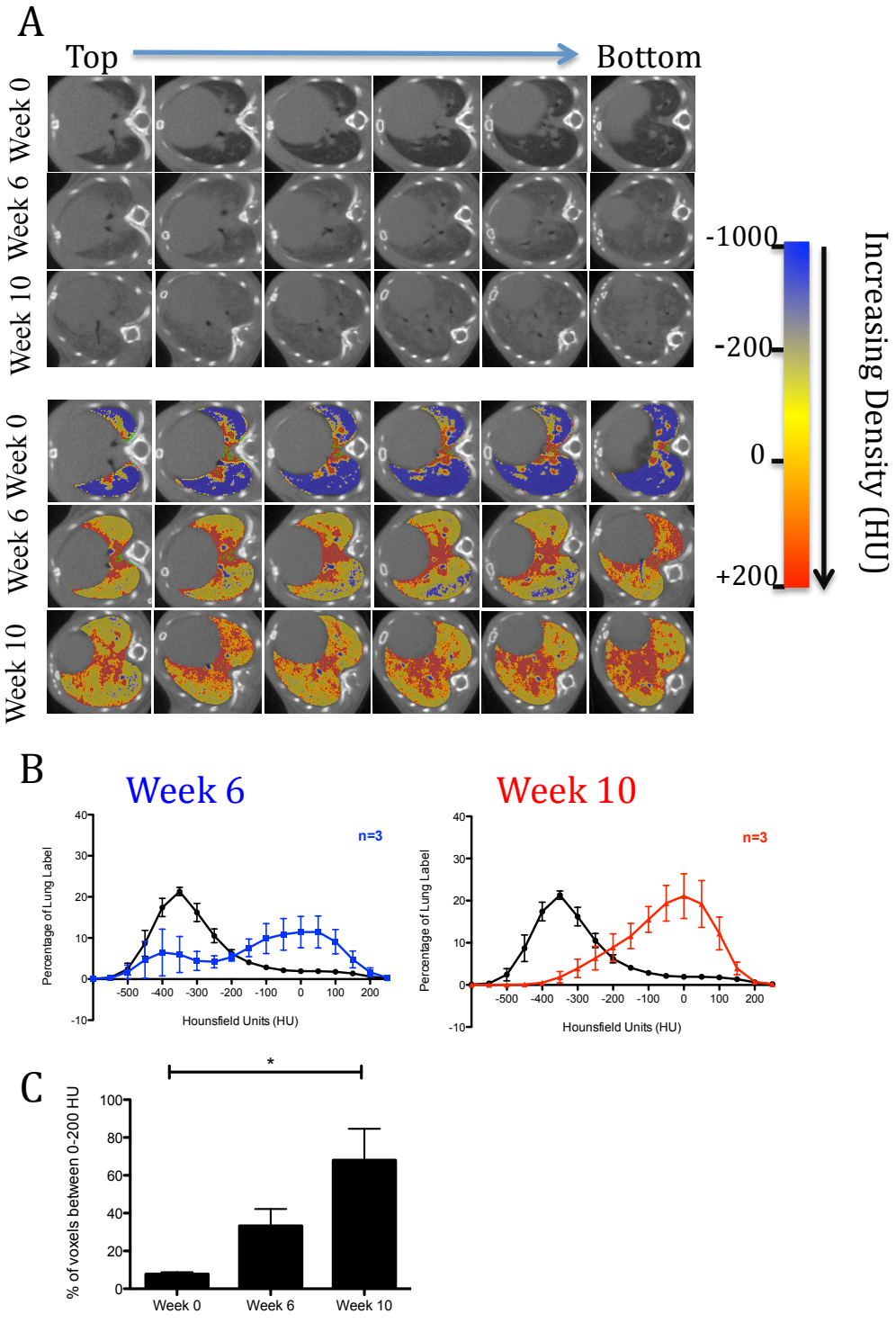
A
Top
Bottom
Week 0
Week 6
Week 10
-1000
-200
0
+200
Increasing Density (HU)
B
Week 6
Week 10
n=3
n=3
Percentage of Lung Label
Hounsfield Units (HU)
C
*
% of voxels between 0-200 HU
Week 0
Week 6
Week 10

Figure 14.

Figure 15. Analysis of tumour burden upon OSM overexpression in the K-ras G12D mouse model. In the same experiment described in *Figure 14,* an additional group of K-ras transgenic mice were treated with both $5x10^7$ pfu AdCre and $5x10^7$ pfu AdOSM (n=2) and sacrificed after 8 weeks due to reaching endpoint conditions. Upon sacrifice, the left lungs were cut at the major bifurcation, sectioned, and sent for H&E staining. In (A) representative histology images are shown of the two treatment groups, cut in 250 micron intervals with a close up (B) of the resulting cell hyperplasia and tumour growth. Using the slides from histology and Image J software, the tumour area per section for each mouse was calculated as total tumour area per section (C), total grade 1 tumour area per section (D), and total grade 2 tumour area per section (E). Statistical significance is shown where *=$p<0.05$, **=$p<0.001$, and ***=$p<0.0001$.

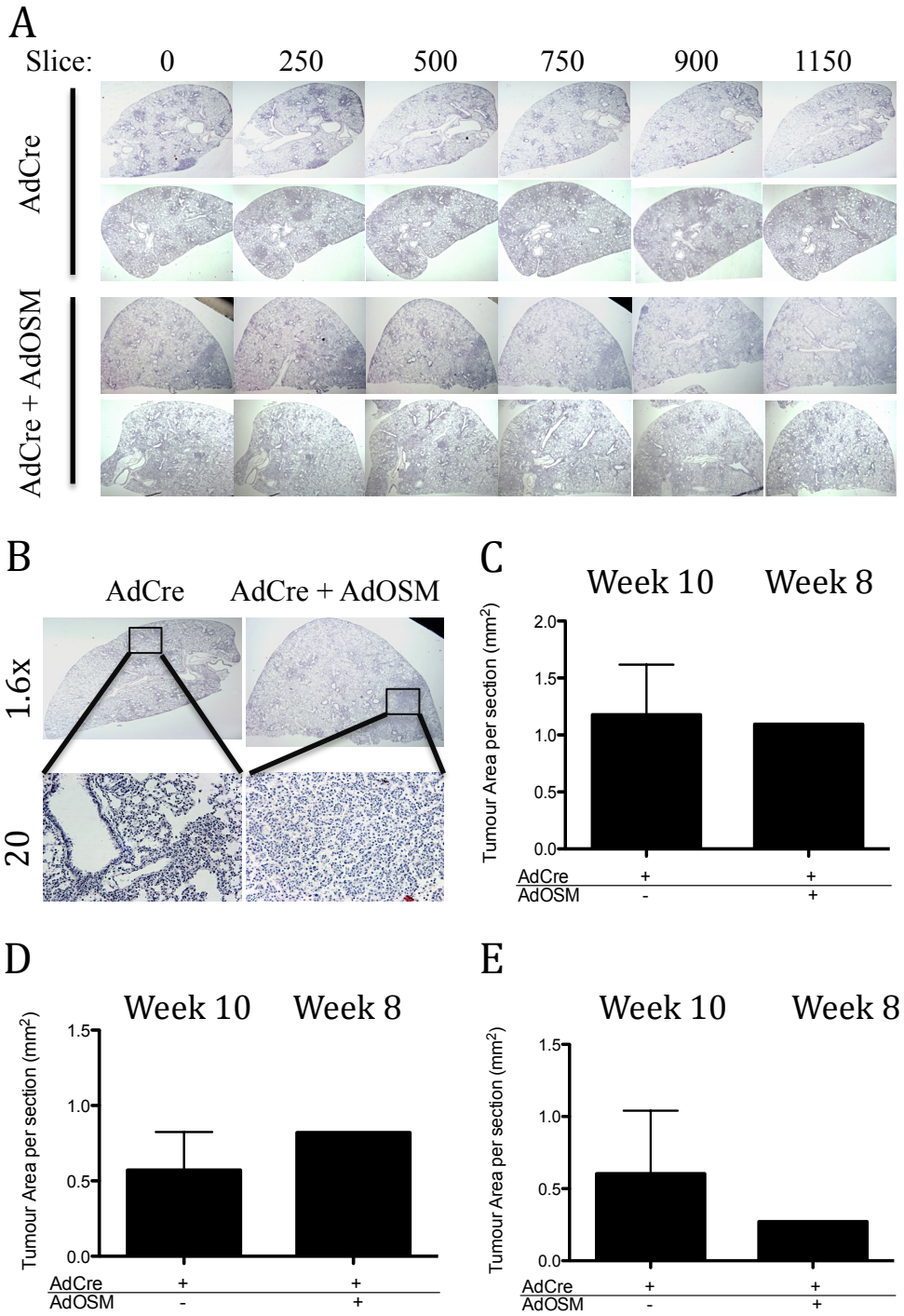
A
Slice: 0 250 500 750 900 1150
AdCre
AdCre + AdOSM
B
AdCre
AdCre + AdOSM
1.6x
20
C
Week 10
Week 8
Tumour Area per section (mm2)
2.0
1.5
1.0
0.5
0.0
AdCre + +
AdOSM - +
D
Week 10
Week 8
Tumour Area per section (mm2)
1.5
1.0
0.5
0.0
AdCre + +
AdOSM - +
E
Week 10
Week 8
Tumour Area per section (mm2)
1.5
1.0
0.5
0.0
AdCre + +
AdOSM - +

Figure 15.

Figure 16. Analysis of alveolar lavage upon OSM overexpression in the K-ras G12D mouse model.

In the same experiment described in *Figure 15*, IL-6 (A) and OSM (B) protein levels in the BALF were analyzed using ELISA kits, and differential cell analysis of cytocentrifuged BAL fluid samples was conducted (C). Immune cell populations are also shown as a percentage of total cells (D). There was no statistical significance using the one-way ANOVA test between the two groups.

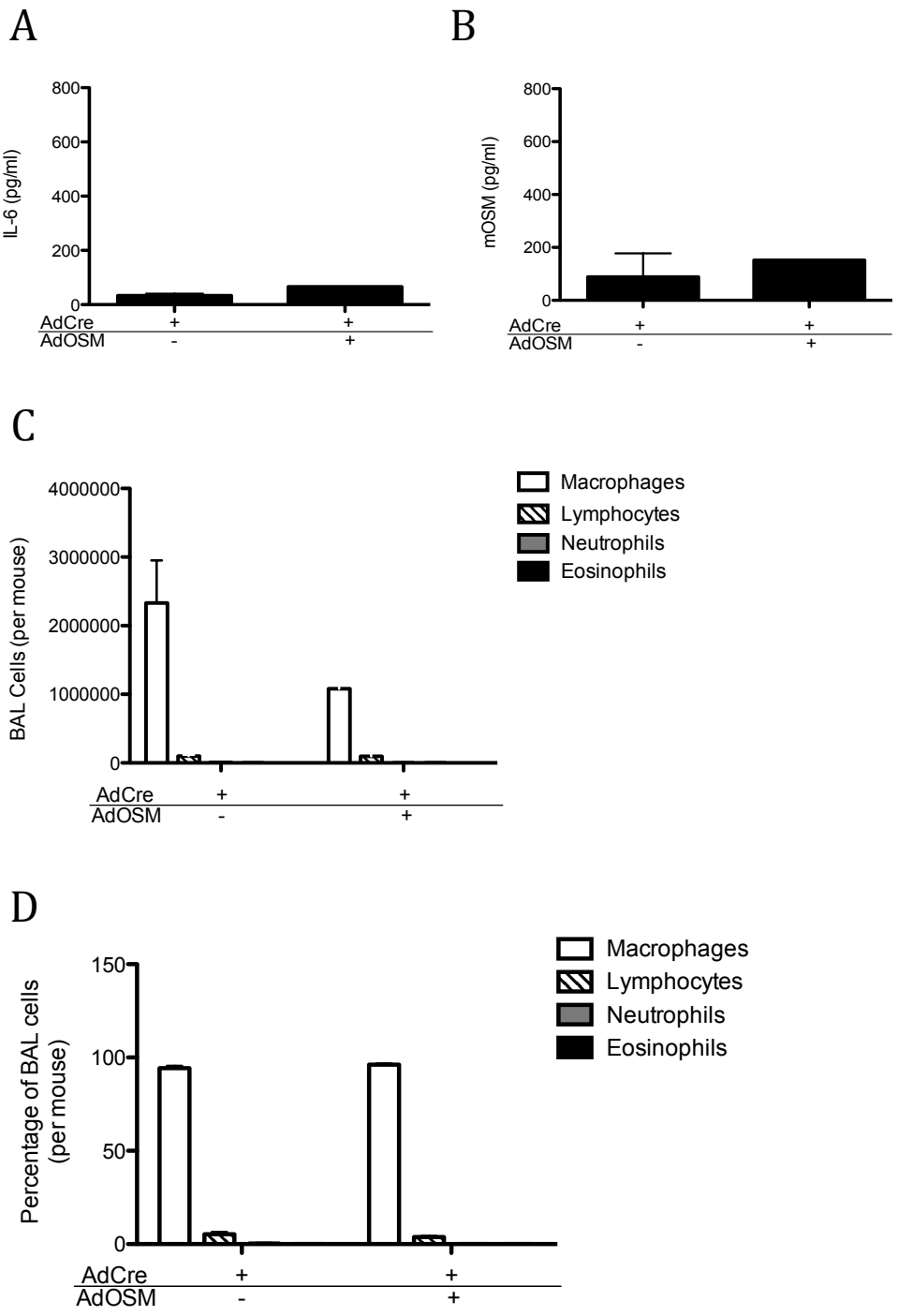
A
IL-6 (pg/ml)
800
600
400
200
0
AdCre + +
AdOSM - +
B
mOSM (pg/ml)
800
600
400
200
0
AdCre + +
AdOSM - +
C
BAL Cells (per mouse)
4000000
3000000
2000000
1000000
0
AdCre + +
AdOSM - +
Macrophages
Lymphocytes
Neutrophils
Eosinophils
D
Percentage of BAL cells (per mouse)
150
100
50
0
AdCre + +
AdOSM - +
Macrophages
Lymphocytes
Neutrophils
Eosinophils

Figure 16.

Figure 17. Representative CT scans upon loss of function of OSMRβ or IL-6 in the K-ras G12D mouse model.

K-ras transgenic (n=7), K-ras transgenic, OSMRβ +/- (n=4), K-ras transgenic, OSMRβ -/- (n=7), and K-ras transgenic, IL-6 +/- (n=6) mice were endotracheally intubated with $5x10^8$ pfu Ad-Cre Recombinase. CT scans were taken at weeks 0, 6, and 10, and analyzed using AMIRA software to generate density overlays. These overlays represent varying density ranges using 3 colours: blue (-1000 → -200 HU), yellow (-200 → 0 HU), red (0 → +200 HU). In (A) representative CT scan images with density overlays are shown at week 10, and are taken at 6 sections ranging from the first rib to the diaphragm.

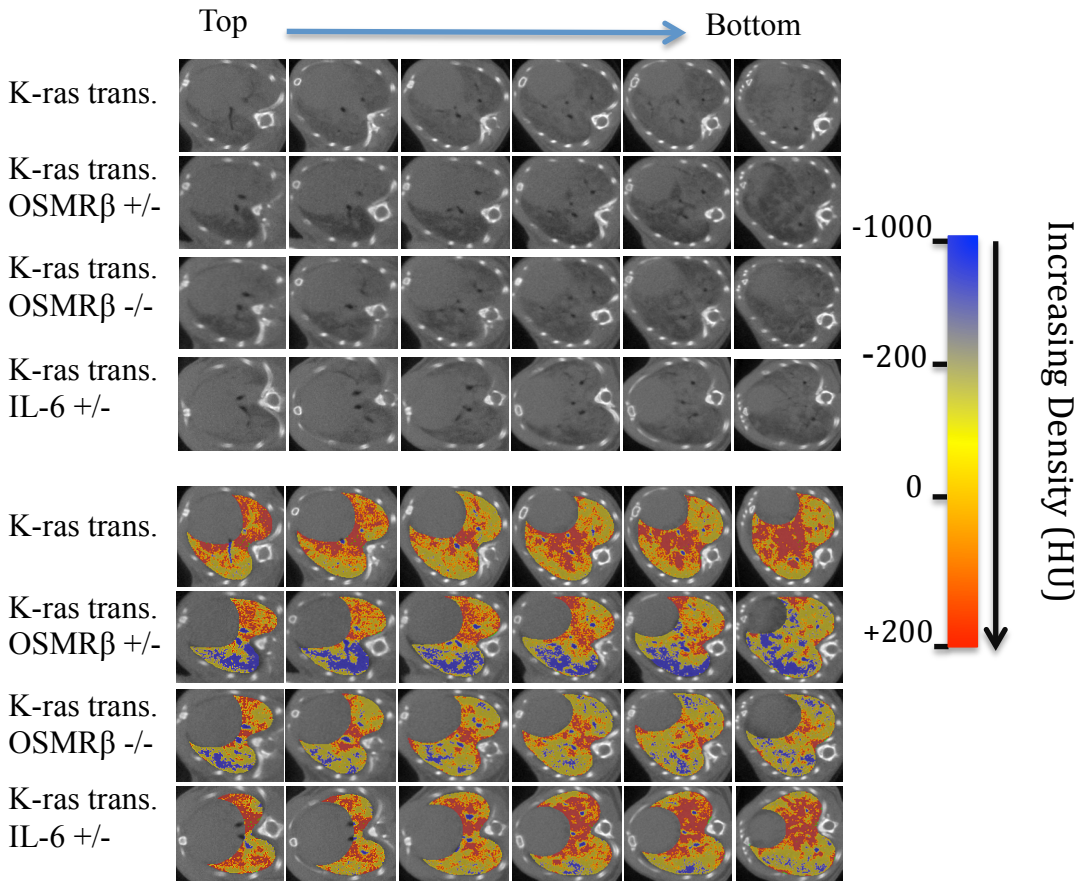
Top
Bottom
K-ras trans.
K-ras trans. OSMRβ +/-
K-ras trans. OSMRβ -/-
K-ras trans. IL-6 +/-
K-ras trans.
K-ras trans. OSMRβ +/-
K-ras trans. OSMRβ -/-
K-ras trans. IL-6 +/-
-1000
-200
0
+200
Increasing Density (HU)

Figure 17.

Figure 18. CT scan analysis upon loss of function of OSMRβ or IL-6 in the K-ras G12D mouse model.

In the same experiment described in *Figure 17*, the density overlays generated from the CT scans were used to produce histograms over the range of -1000 HU to +250 HU with 26 bins. The values in each histogram were summed, and each value was then expressed as a percent of the total lung label. In (A), the averages of these percentages are shown at weeks 0 (black), 6 (blue), and 10 (red). In (B) only the percentage of the lung label between 0 to 200 HU at each time point were graphed. Statistical significance is shown where *=$p<0.05$, **=$p<0.001$, and ***=$p<0.0001$.

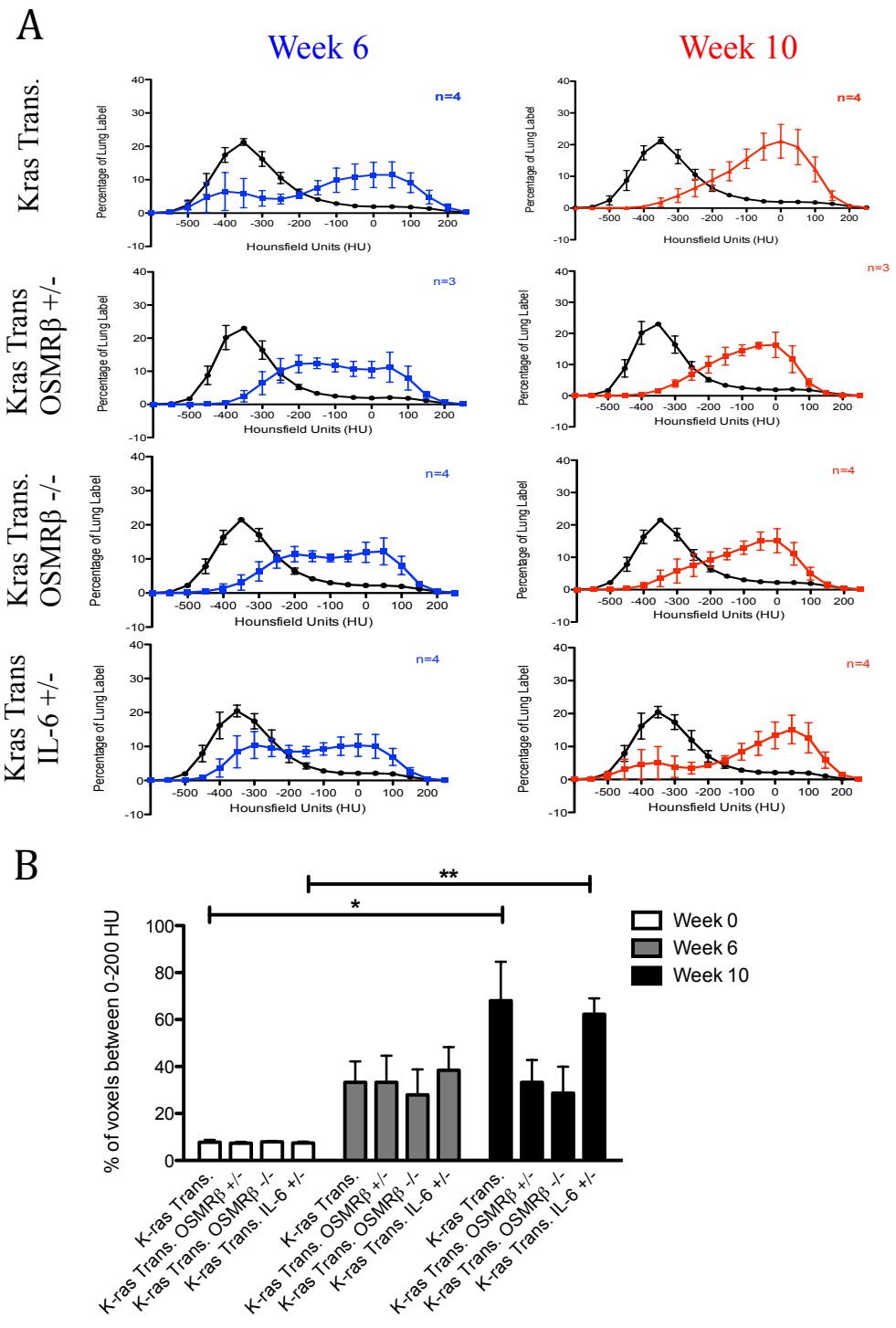
A
Week 6
Week 10
Kras Trans.
Kras Trans OSMRβ +/-
Kras Trans. OSMRβ -/-
Kras Trans IL-6 +/-
Percentage of Lung Label
Hounsfield Units (HU)
n=4
n=3
B
% of voxels between 0-200 HU
Week 0
Week 6
Week 10
*
**
K-ras Trans.
K-ras Trans. OSMRβ +/-
K-ras Trans. OSMRβ -/-
K-ras Trans. IL-6 +/-

Figure 18.

Figure 19. Analysis of tumour burden upon loss of function of OSMRβ or IL-6 in the K-ras G12D mouse model.

In the same experiment described in *Figure 17,* lungs were cut at the major bifurcation, sectioned, and H&E stained. In (A) representative histology images are shown, cut in 250 micron intervals. Using the slides from histology and Image J software, the tumour area per section for each mouse was calculated as total grade 1 tumour area per section (B), total grade 2 tumour area per section (C), and total tumour area per section (D).

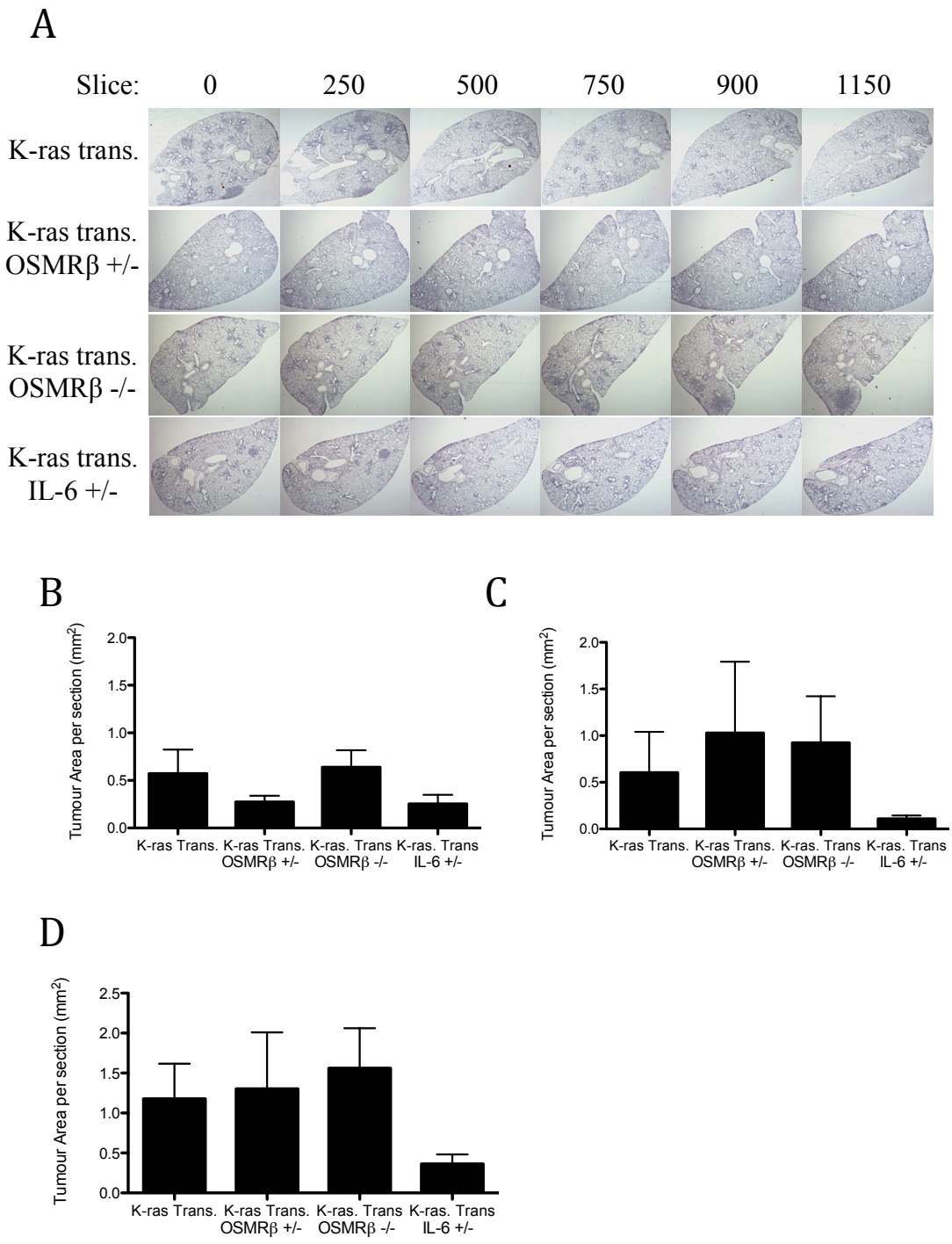
A
Slice: 0 250 500 750 900 1150
K-ras trans.
K-ras trans. OSMRβ +/-
K-ras trans. OSMRβ -/-
K-ras trans. IL-6 +/-
B
Tumour Area per section (mm²)
2.0
1.5
1.0
0.5
0.0
K-ras Trans.
K-ras Trans. OSMRβ +/-
K-ras. Trans OSMRβ -/-
K-ras. Trans IL-6 +/-
C
Tumour Area per section (mm²)
2.0
1.5
1.0
0.5
0.0
K-ras Trans.
K-ras Trans. OSMRβ +/-
K-ras. Trans OSMRβ -/-
K-ras. Trans IL-6 +/-
D
Tumour Area per section (mm²)
2.5
2.0
1.5
1.0
0.5
0.0
K-ras Trans.
K-ras Trans. OSMRβ +/-
K-ras. Trans OSMRβ -/-
K-ras. Trans IL-6 +/-

Figure 19.

Figure 20. Analysis of alveolar lavage upon loss of function of OSMRβ or IL-6 in the K-ras G12D mouse model.

In the same experiment described in *Figure 17*, IL-6 (A) and OSM (B) protein levels in the BALF were analyzed using ELISA kits, and differential cell analysis of cytocentrifuged BAL fluid samples was conducted (C). Statistical significance is shown where *=$p<0.05$, **=$p<0.001$, and ***=$p<0.0001$.

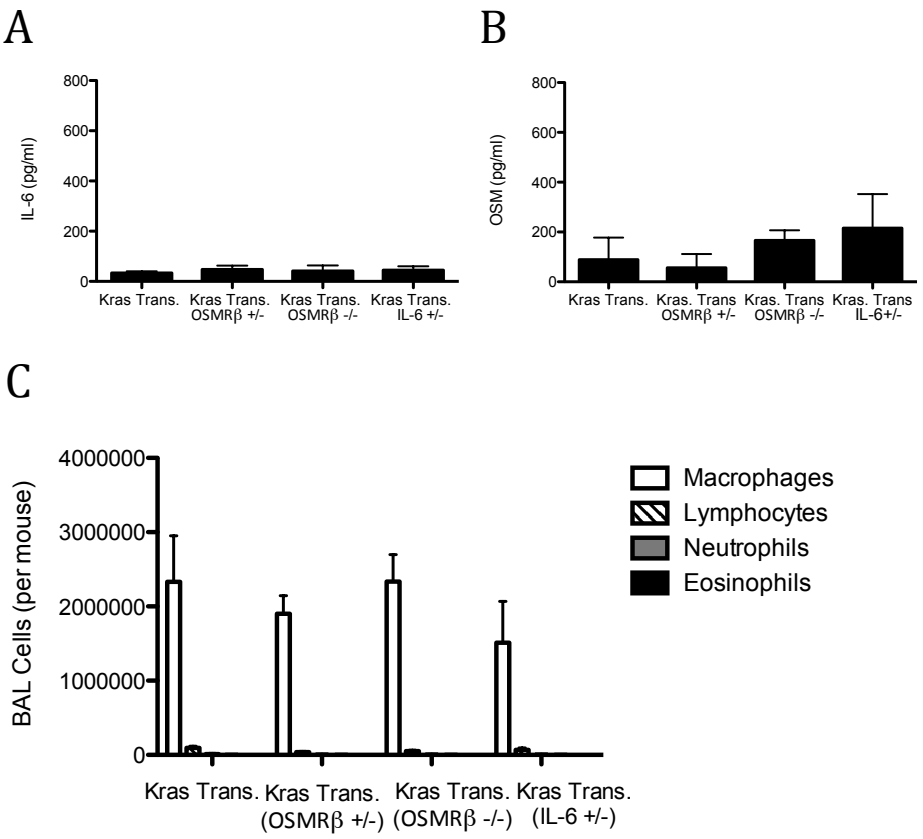
A
IL-6 (pg/ml)
800
600
400
200
0
Kras Trans.
Kras Trans. OSMRβ +/-
Kras Trans. OSMRβ -/-
Kras Trans. IL-6 +/-
B
OSM (pg/ml)
800
600
400
200
0
Kras Trans.
Kras. Trans OSMRβ +/-
Kras. Trans OSMRβ -/-
Kras. Trans IL-6+/-
C
BAL Cells (per mouse)
4000000
3000000
2000000
1000000
0
Kras Trans.
Kras Trans. (OSMRβ +/-)
Kras Trans. (OSMRβ -/-)
Kras Trans. (IL-6 +/-)
Macrophages
Lymphocytes
Neutrophils
Eosinophils

Figure 20.

CHAPTER 5: Mechanisms of OSM-mediated Effects on Tumour Burden

In this chapter, potential mechanisms underlying the effects of OSM overexpression on tumour growth were examined *in vitro* using mutant K-ras cell lines LKR-13 and Lewis Lung Carcinoma (LLC) cells, as well as B16F10 melanoma cells. Through direct and indirect methods of stimulation, effects of rOSM on tumour cell proliferation was assessed in this collection of work. Indirect methods of stimulation utilized conditioned media and co-culture models of tumour cell lines with lung cells such as mouse lung fibroblasts and macrophages.

5.1 – Direct stimulation of mutant K-ras cell lines with recombinant OSM, IL-6, TGFβ, TNFα, or IL-18 cytokines

As the overexpression of Oncostatin M enhanced tumour burden in the work presented in earlier chapters, the effects of direct cytokine stimulation on LLC, FLUC-LLC, and LKR-13 cell proliferation was examined to determine if Oncostatin M influenced tumour growth by acting directly on tumour cells. Thus, tumour cell lines were treated with inflammatory mediators rOSM, IL-6, TGFβ, TNFα, or IL-18 at varying doses of 0.2, 2, and 20 ng/ml, or media as a control. Cells were treated in quadruplicate for 24 or 48 hours, after which an MTT assay was conducted to measure mitochondrial activity as an indicator of cell numbers.

The MTT assays in **Figure 21** demonstrated that LLC, FLuc-LLC, and LKR-13 cells were unresponsive to direct stimulation with rOSM, IL-6, TNFα, or IL-18 at both 24 hour and 48 hour time points, regardless of dose. There was a trend towards a decrease in cell activity of LKR-13 and LLC cells upon TGFβ stimulation at both 2ng/ml and 20

ng/ml after 48 hours, however this was not statistically significant. Thus, OSM presence *in vitro* did not directly alter K-ras mutant tumour cell proliferation in these conditions as assessed by the MTT assay.

5.2 –Relative luciferase activity and FLuc-LLC and FLuc-B16 cell proliferation

As an alternative to utilizing MTT assays to indicate cell proliferation, relative luciferase activity of FLuc-LLC and FLuc-B16 cells was measured to also assess cell proliferation. To ensure relative luciferase activity was proportional to cell numbers, FLuc-LLC and FLuc-B16 cells were plated at 500, 1000, 1500, or 2000 cells per well and 24 hours later, relative luciferase activity was measured. For both FLuc-LLC **(Figure 22A)** and FLuc-B16 cells **(Figure 22B)**, increase in cell numbers was roughly linearly proportional to luciferase activity measured. Thus, FLuc-LLC and FLuc-B16 cells were used for subsequent tumour cell proliferation studies.

5.3 – Indirect stimulation of tumour cells with rOSM using mouse lung fibroblasts

As direct stimulation of LKR-13 and LLC tumour cells with recombinant OSM did not yield changes in cell proliferation, subsequent experiments examined potential indirect mechanisms of tumour cell regulation. Recently, the tumour stroma has been identified as a key player in the promotion of tumour growth, and fibroblasts have been found to be a common cell type in the tumour stroma[75]. Thus, to examine whether fibroblasts, upon stimulation with OSM, release soluble factors that influence tumour cell proliferation, mouse lung fibroblasts cell lines obtained from normal mouse lungs were treated with either media or 25 ng/ml rOSM. After 24 hours, the conditioned media was removed and added to either FLuc-LLC or FLuc-B16 cells and relative luciferase activity

was measured after 24 and 48 hours. To also examine whether cell-to-cell contact was necessary for potential fibroblast-mediated tumour cell proliferation upon rOSM stimulation, mouse lung fibroblasts and FLuc-LLC or FLuc-B16 cells were co-cultured and treated with either media as a control, 5 ng/ml rOSM, or 5 ng/ml TGFβ. A luciferase assay was completed after 24 and 48 hours.

5.3.1 – FLuc-LLC and FLuc-B16 proliferation upon OSM stimulation in MLF-conditioned media model

Although conditioned media from fibroblasts did not influence FLuc-LLC cell luciferase activity after 24 hours, there was a small but statistically significant increase in LLC cell proliferation after 48 hours upon application of either untreated- or rOSM-treated MLF-conditioned media, increasing 1.5-fold in comparison to tumour cells stimulated with rOSM-treated media alone (**Figure 22C**). Unlike the trends measured in FLuc-LLC cells, MLF-conditioned media did not alter FLuc-B16 cell luciferase activity at either time point **(Figure 22D)**.

5.3.2 – FLuc-LLC and FLuc-B16 proliferation upon co-culture with MLFs

To examine whether cell-to-cell contact may be necessary between stromal cells and tumour cells for influence on tumour cell proliferation, cultures with OSM and TGFβ alone, or co-cultures with MLFs (unstimulated or stimulated with OSM or TGFβ) were completed. To also determine if the tissue culture substrate had influence on MLF activity, conditions of culture were assessed on standard plastic-ware compared to plastic-ware pretreated with collagen. Although tumour cell luciferase activity was not altered after 24 hours of FLuc-LLC and MLF co-culture on plastic **(Figure 23A)**, TGFβ

treatment inhibited tumour cell proliferation after 48 hours upon either direct application to tumour cells, or in MLF-LLC co-culture **(Figure 23B).** Similar trends were observed in FLuc-LLC culture on collagen, as TGFβ treatment inhibited cell proliferation slightly at 24 hours **(Figure 23C)** and 1.5-fold at 48 hours **(Figure 23D)** only upon direct application to tumour cells. In FLuc-B16 and MLF co-culture studies on plastic, TGFβ stimulation inhibited tumour cell proliferation (approximately 1.5-fold), only upon stimulation under co-culture conditions at 48 hours **(Figure 23F)**, but not 24 hours **(Figure 23E).**

5.4 – Steady-state fibronectin and periostin mRNA levels in whole lung tissue upon OSM overexpression *in vivo*

Fibronectin and periostin, proteins of the extracellular matrix that are elevated in NSCLCs[76, 77], are primarily produced by fibroblasts, and have been implicated in the support of tumour growth and metastasis[78–81]. Thus, measuring trends in expression levels upon OSM stimulation *in vivo* were of interest. mRNA expression levels of periostin and fibronectin were assayed in whole lung tissue obtained from wild type mice endotracheally intubated with either $5x10^7$ pfu AdDel70 or $5x10^7$ pfu AdOSM (3 experiments, previously completed in the laboratory) and culled after day 5 (Expt 1) or day 7 (Expt 2 and 3). These samples have previously been shown to display AdOSM-induced increase in several genes, as published by Fritz *et al* (2011) and Botelho *et al* (2013). Upon extraction of RNA from whole lung tissue, mRNA levels of fibronectin and periostin were analyzed using qRT-PCR. In all three experiments, there was an increase in fibronectin mRNA expression **(Figure 24A)** and expression was found to be

statistically significant in samples at day 7 time point, increasing 7- and 15-fold, whereas no changes in periostin mRNA levels were detected **(Figure 24B)**.

5.5 – Steady state fibronectin and periostin mRNA levels in mouse lung fibroblasts treated with OSM *in vitro*

To examine whether the trends seen in *Section 5.4* were also observed upon *in vitro* rOSM stimulation of fibroblasts, MLFs were treated with 25 ng/ml rOSM for 24 hours. After 24 hours, RNA was extracted, and probed for fibronectin or periostin.In contrast to the results demonstrated *in vivo*, *in vitro* rOSM stimulation of MLFs did not alter fibronectin **(Figure 24C)** mRNA levels. Regulation of periostin mRNA was not altered and consistent with results *in vivo* **(Figure 24D)**.

5.6 – Arginase activity regulation in alveolar and peritoneal macrophages upon stimulation *in vitro*

Previous experiments in the laboratory have demonstrated that AdOSM induces an increase in the number of macrophages in lungs that display an M2 phenotype, as assessed by Arg1 expression[73]. Whether this results from direct regulation of the M2 phenotype is not known, thus the potential ability of OSM to directly influence M2 phenotype differentiation was assessed. Using a model developed in a collaborator's laboratory (A. Askhar) using peritoneal macrophages, C57Bl/6 mice were culled and peritoneal and alveolar macrophages were obtained by lavage (see *Materials and Methods*). The cells from both collections were stimulated with either M1 stimuli (IFNγ, LPS), M2 stimuli (IL-4, IL-13), or rOSM (25 ng/ml or 5 ng/ml) for 24 hours. After 24

hours, an arginase assay of lysates was conducted using the urea produced as an indicator of arginase 1 activity.

Regardless of the stimulus used, alveolar macrophages remained unresponsive, determined by unchanged urea levels that remained at approximately 1.5 mM (**Figure 25A)**. In contrast, stimulation of peritoneal macrophages with M2 ligands resulted in a statistically significant elevation of arginase activity, increasing urea levels 2-fold compared to the urea levels of control or M1-stimulated macrophages (**Figure 25B)**. Thus, resident alveolar macrophages responded differently to IL-4/IL-13 stimulation than peritoneal macrophages.

5.7 – Co-cultures of FLuc-LLC cells with BAL cells from AdDel70 or AdOSM-treated mice

As resident alveolar macrophages were non-responsive to stimulation *in vitro*, the subsequent study used macrophages obtained from animals treated with either AdDel70 or AdOSM, to assess whether populations conditioned by inflammation *in vivo* could influence tumour cells *in vitro* upon co-culture. Mice were endotracheally intubated with either $5x10^7$ pfu AdDel70 or AdOSM. Seven days after intubation, they were culled, BALF was collected, and cells were cultured. After 2 hours of adherence, designated wells were washed to assess the adherent population (termed adherent pop.), and others were left unwashed to assess the total BAL cell population (termed total BALF). FLUC-LLC cells were then co-cultured with these cells, and cell proliferation was determined using the luciferase assay.

After 24 hours of co-culture, no significant difference was measured between unstimulated FLUC-LLC cells, and FLUC-LLC cells in co-culture with the pooled adherent or total population from AdDel70 and AdOSM-treated mice **(Figures 26B)**. The trends of FLuc-LLC cell luciferase activity in co-culture conditions with the pooled adherent population were similar to those in **Figure 26D**, where the adherent population from each mouse was plated in quadruplicate to assess variability within treatment groups. After 48 hours, however, co-culture conditions with the pooled total cell population from AdDel70 or AdOSM treatments increased FLUC-LLC luciferase activity 2-3 fold (**Figures 26C).** In both **Figure 26C and D**, the co-cultures of pooled or separate adherent cell populations, respectively, did not influence FLuc-LLC luciferase activity. IL-6 and OSM ELISAs were completed to confirm that the intubation was successful. As predicted, there was an increase in IL-6 protein levels **(Figure 26F)** and OSM protein levels in the BAL from AdOSM-treated mice **(Figure 26G)**, indicating that the AdOSM treatment functioned similarly to that established previously[82,83].

Figure 21. Direct stimulation of LLC, Fluc-LLC, and LKR-13 tumour cells.

Tumour cells were plated at 1000 cells/well in 96 well plates and treated in quadruplicate with the indicated concentration of cytokines (at the bottom of the figure). After 24 (left) and 48 hours (right), an MTT assay was performed to measure cell proliferation. The OD values obtained were then expressed as a percentage relative to unstimulated cells to illustrate percentage of growth increase. No statistical significance was detected using the one-way ANOVA test.

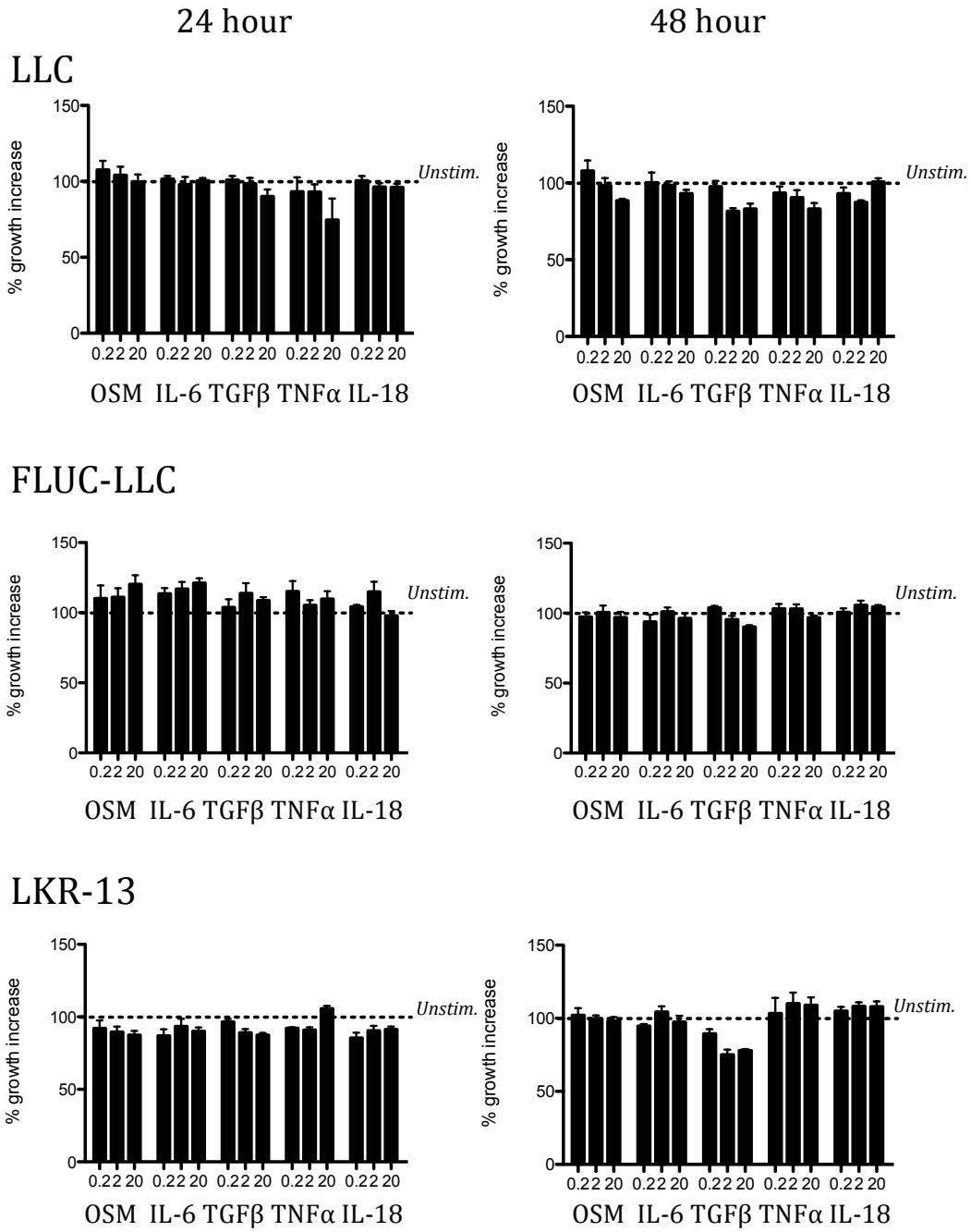
24 hour
48 hour
LLC
FLUC-LLC
LKR-13
% growth increase
150
100
50
0
Unstim.
0.2 2 20 0.2 2 20 0.2 2 20 0.2 2 20 0.2 2 20
OSM IL-6 TGFβ TNFα IL-18

Figure 21.

Figure 22. Effects of fibroblast-conditioned media and OSM overexpression on FLuc-LLC or FLuc-B16 cell proliferation.

Mouse lung fibroblasts, plated at 2000 cells per well were treated, upon reaching 90% confluency, with either media or 5ng/ml rOSM for 24 hours. FLuc-LLC and FLuc-B16 cells, plated at 1000 cells per well, were then treated with either of 4 conditions: media, 5ng/ml rOSM, conditioned media, or conditioned media with 5ng/ml rOSM. Luciferase assays were conducted 24 hours (left) and 48 hours (right) post-treatment to measure tumour cell proliferation. Statistical significance is shown where *=$p<0.05$, **=$p<0.001$, and ***=$p<0.0001$.

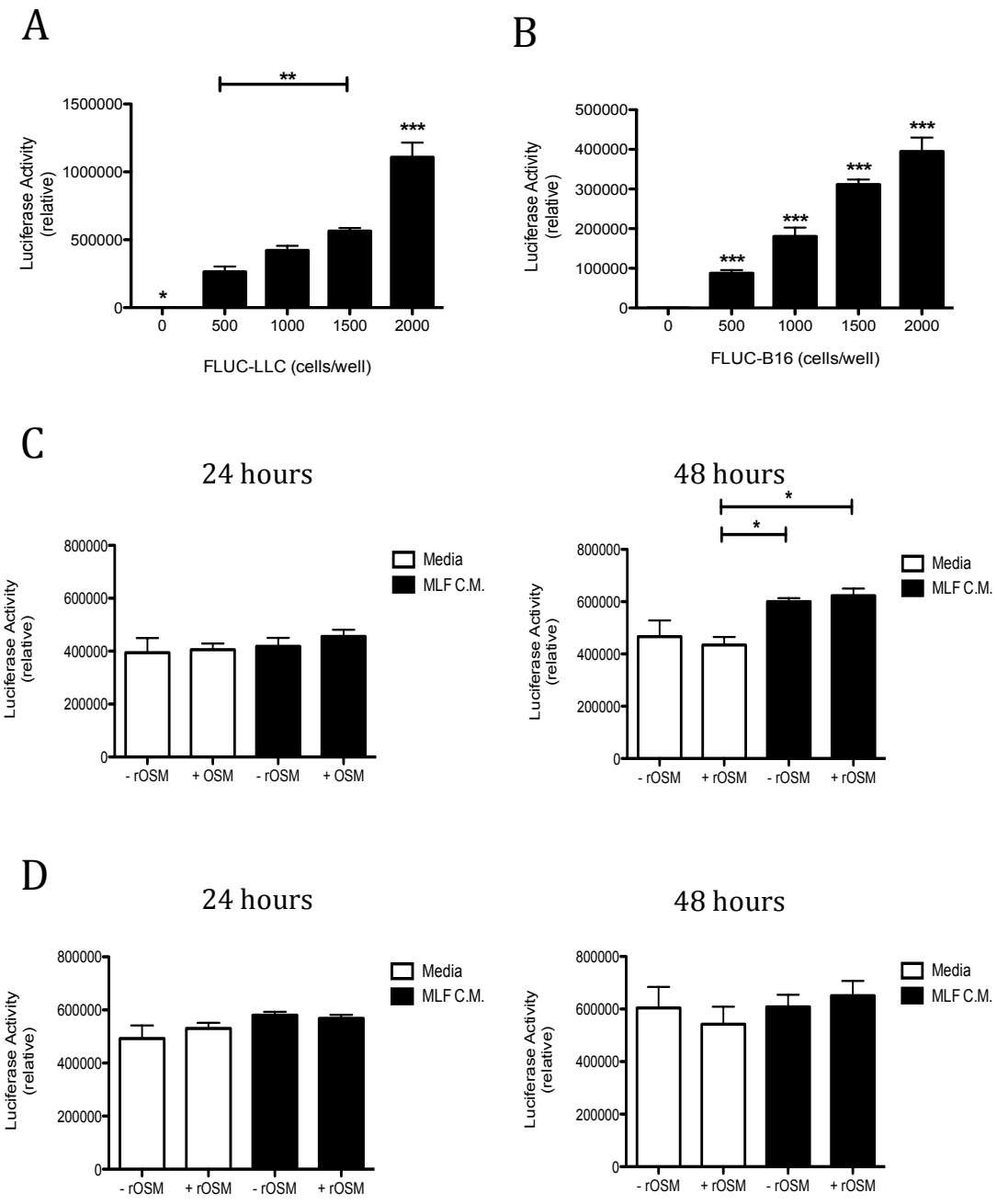
A
B
C
D
Luciferase Activity (relative)
FLUC-LLC (cells/well)
FLUC-B16 (cells/well)
24 hours
48 hours
Media
MLF C.M.
- rOSM
+ OSM
+ rOSM

Figure 22.

Figure 23. Co-culture of MLF and Fluc-LLC or FLuc-B16 cells.

(A-B) MLFs, FLUC-LLC cells, or co-cultures of MLF and FLUC-LLC cells were plated on either plastic (A) or collagen-coated (B) wells, and treated with either media, 5ng/ml rOSM, or 5ng/ml hTGFβ. After 24 (left) or 48 (right) hours, a luciferase assay was conducted to measure the relative luciferase activity as an indication of LLC cell proliferation. Statistical significance is shown where *=$p<0.05$, **=$p<0.001$, and ***=$p<0.0001$.

(C) MLFs, FLuc-B16 cells, or co-cultures of MLF and FLuc-B16 cells were plated on plastic and treated with either media, 5 ng/ml rOSM, or 5 ng/ml hTGFβ. After 24 (left) or 48 (right) hours, a luciferase assay was conducted to measure the relative luciferase activity as an indication of B16 cell proliferation. Statistical significance is shown where *=$p<0.05$ and**=$p<0.001$.

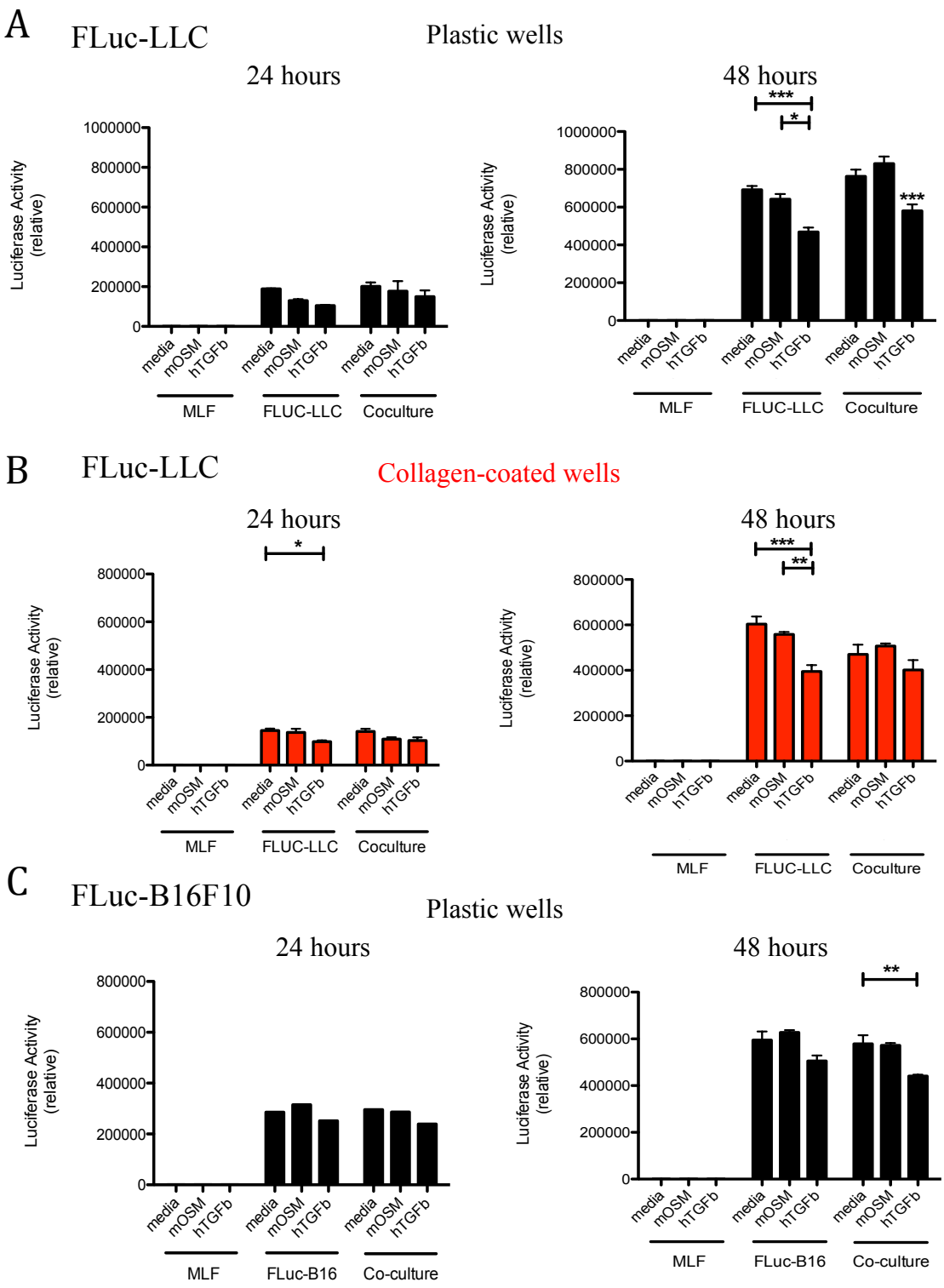
A
FLuc-LLC
Plastic wells
24 hours
48 hours
Luciferase Activity (relative)
1000000
800000
600000
400000
200000
0
media
mOSM
hTGFb
MLF
FLUC-LLC
Coculture
***
*
B
FLuc-LLC
Collagen-coated wells
**
C
FLuc-B16F10
Plastic wells
FLuc-B16
Co-culture

Figure 23.

Figure 24. Analysis of fibronectin and periostin mRNA levels with *in vivo* or *in vitro* OSM stimulation.

For *in vivo* experiments, mice were treated with either $5x10^7$ pfu AdDel70 or $5x10^7$ pfu AdOSM and sacrificed one week later. RNA was extracted from whole lung tissue and probed, using real-time quantiative PCR, for fibronectin (mFn-1) and periostin (mPstn) mRNA levels (A) and (C), respectively. For the *in vitro* experiment, mouse lung fibroblasts isolated from wild type C57bl/6 mice were stimulated with either media or 25 ng/ml rOSM for 24 hours. RNA was then extracted from the cells and probed for fibronectin and periostin mRNA levels (B) and (D), respectively. Statistical significance is shown where *=$p<0.05$, **=$p<0.001$, and ***=$p<0.0001$.

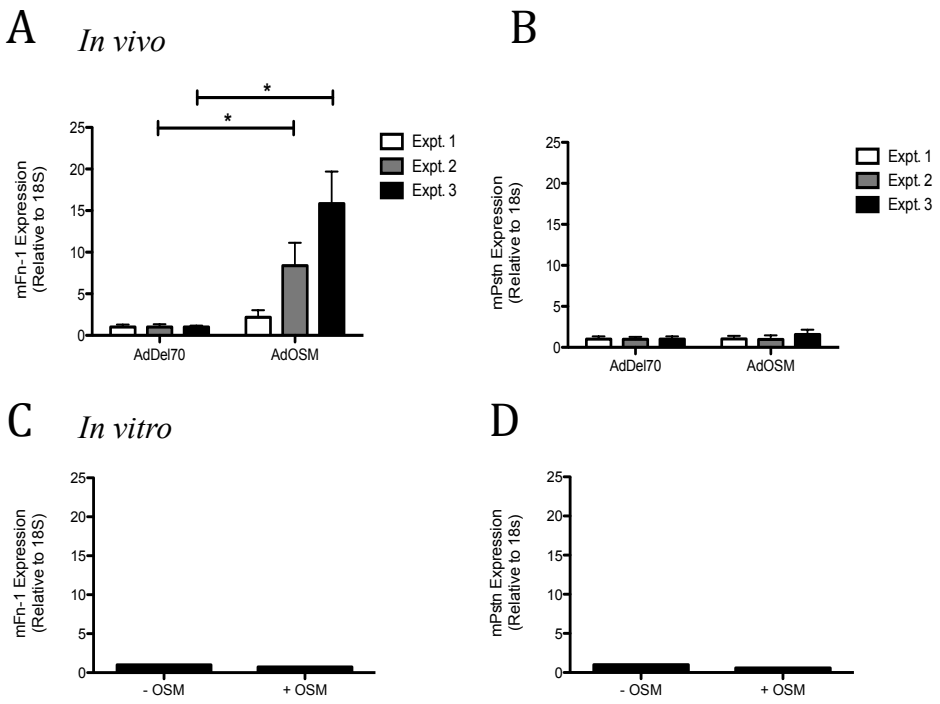
A
In vivo
B
C
In vitro
D
mFn-1 Expression (Relative to 18S)
mPstn Expression (Relative to 18s)
Expt. 1
Expt. 2
Expt. 3
AdDel70
AdOSM
- OSM
+ OSM
*
*
0
5
10
15
20
25

Figure 24.

Figure 25. Alveolar and peritoneal macrophage stimulation.

Using wild type naïve mice, cells were collected from the peritoneal cavity using 10 mmol EDTA solution, and BAL was collected from the lungs using 1x PBS. These cells were then plated and left to adhere for 2 hours. The wells were then washed, and the adherent population was treated with either media, M1 ligands (2 ng/ml LPS and 5 ng/ml IFNγ), M2 ligands (10 ng/ml IL-4 and 25 ng/ml IL-13), or rOSM at the indicated doses. An arginase assay was conducted after 24 hours. This data is representative of 2 experiments. Statistical significance is shown where *=$p<0.05$ and **=$p<0.001$.

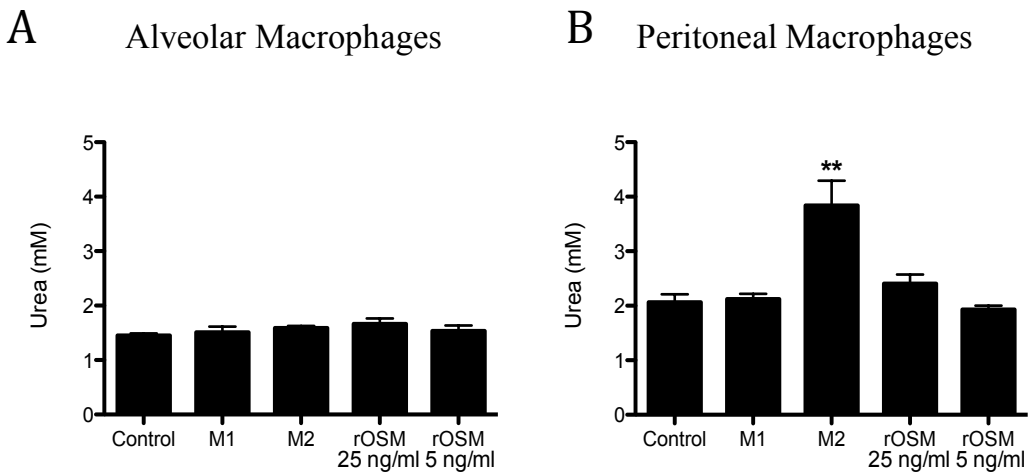
A
Alveolar Macrophages
B
Peritoneal Macrophages
Urea (mM)
0
1
2
3
4
5
**
Control
M1
M2
rOSM 25 ng/ml
rOSM 5 ng/ml

Figure 25.

Figure 26. Co-culture of FLUC-LLC cells and total BAL cells.

In (A) FLUC-LLC were plated at the indicated densities, and a luciferase assay was conducted after 24 hours to assess cell proliferation.

In (B)-(G), wild type mice were intubated with either $5x10^7$ AdDel70 or AdOSM, and culled 1 week later. BALF was collected and cells from each mouse were plated in quadruplicates (D) and (E), or pooled together based on treatment (AdDel70 or AdOSM), and plated (B) and (C). Cells were left to adhere for 2 hours, after which they were either washed (termed the adherent population) or left unwashed (termed the total BALF) and co-cultured with FLUC-LLC cells. After 24 hours or 48 hours, a luciferase assay was conducted on these various co-cultures. IL-6 and OSM protein levels were assessed in the BALF by ELISA (F) and (G) respectively. Statistical significance is shown where *=$p<0.05$, **=$p<0.001$, and ***=$p<0.0001$.

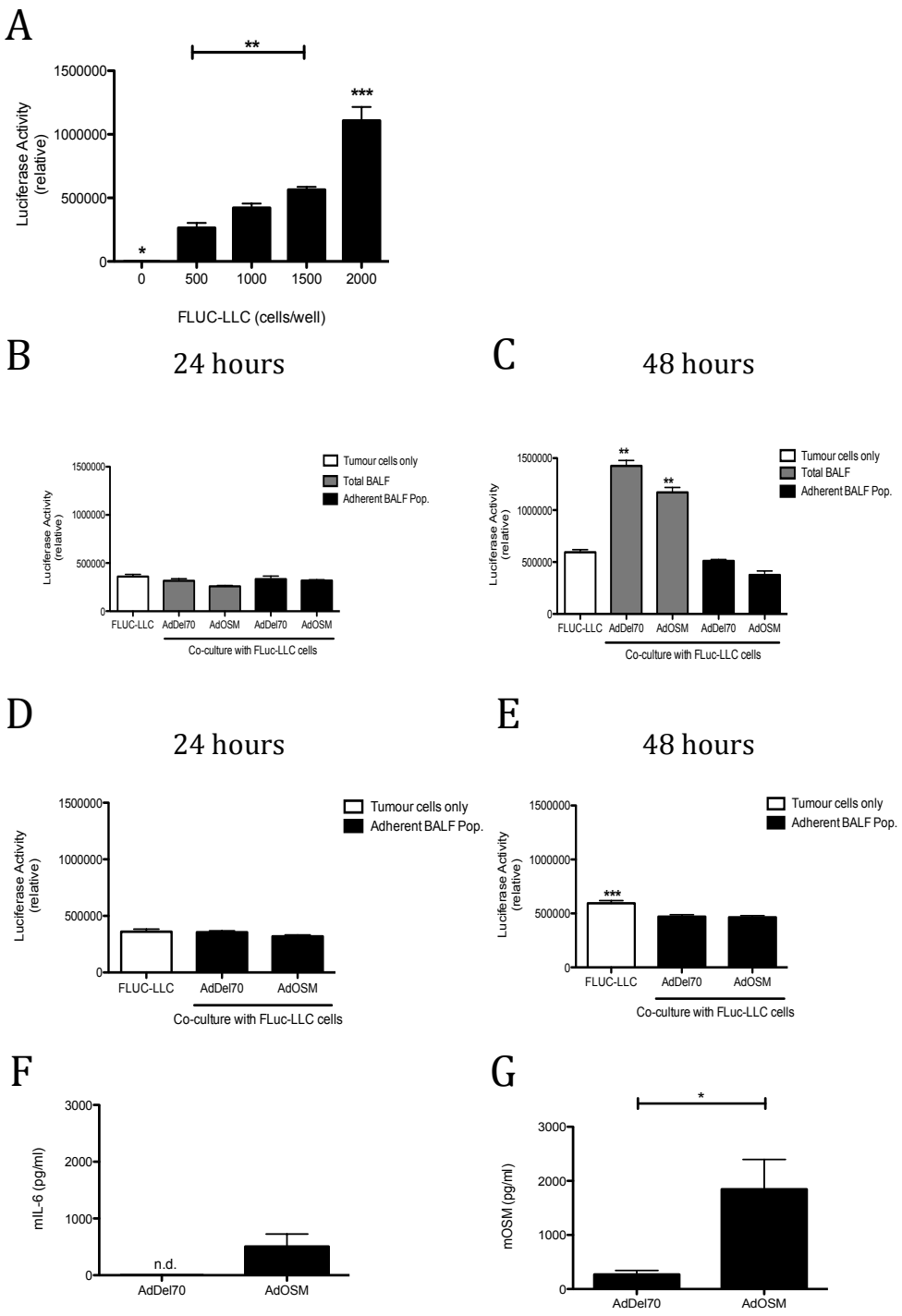
A
Luciferase Activity (relative)
1500000
1000000
500000
0
**
***
*
0
500
1000
1500
2000
FLUC-LLC (cells/well)
B
24 hours
Tumour cells only
Total BALF
Adherent BALF Pop.
FLUC-LLC
AdDel70
AdOSM
AdDel70
AdOSM
Co-culture with FLuc-LLC cells
C
48 hours
D
24 hours
E
48 hours
F
mIL-6 (pg/ml)
3000
2000
1000
0
n.d.
AdDel70
AdOSM
G
mOSM (pg/ml)
*

Figure 26.

CHAPTER 6: Discussion

6.1 – Summary of Findings

Results gathered from *in vivo* studies using the B16F10 pulmonary melanoma metastases model demonstrated that pulmonary overexpression of Oncostatin M resulted in increased tumour nodule numbers, as well as tumour area per section, illustrated by the large and dense hyperplastic regions throughout the parenchyma **(Figures 4B-D)**. In contrast, overexpression of IL-6 in wild type mice did not result in changes in tumour burden as assessed by histology, although tumour nodule numbers were comparable to those induced upon OSM overexpression. Moreover, experiments using IL-6 -/- mice demonstrated that IL-6 was not required for OSM-induced tumour pathology, as both the tumour area per section measured and tumour nodule number counted upon OSM overexpression in wild type and IL-6 -/- mice were very similar **(Figures 6C and D)**. In addition to increased tumour size, overexpression of OSM caused lymphocyte and eosinophil recruitment to the lungs, suggesting these cells may play a role in Oncostatin M-mediated effects on tumour development **(Figure 5D).** However, subsequent experiments using eosinophil-deficient GATA-1 -/- mice revealed that eosinophils were not required for OSM-induced tumour growth, as tumour areas per section calculated in wild type and GATA-1 -/- mice were very similar **(Figure 8C)**. Finally, though unexpected, tumour burden and tumour nodule number assessed in OSMRβ -/- mice upon ectopic delivery of B16F10 cells alone were significantly increased after 3 weeks, compared to wild type mice, suggesting that OSMRβ -/- mice were more susceptible to tumour development **(Figures 10C and D)** upon ectopic delivery of B16 melanoma cells.

To compare such activity of OSM in a model where tumours are derived within lung tissue, the induced oncogenic K-ras mouse model system of lung cancer was used to examine the effects of OSM overexpression, as well as loss of function of OSMRβ or IL-6, on pulmonary tumour development. Results confirmed previous characterization of the model[59], with a gradual development of grade 1 and 2 tumours over a span of 10 weeks upon endotracheal intubation of an adenovirus encoding Cre recombinase, as demonstrated with histological analyses **(Figure 13)**. Subsequent experiments also demonstrated the use of CT scanning technology as a reasonable method of monitoring tumour development in mice. Over the span of 10 weeks, data from CT scans exhibited a gradual increase in percentage of voxels between 0-200 HU, indicative of increased lung density that was associated with tumour development **(Figures 14, 17, and 18).** Upon OSM overexpression in K-ras +/- transgenic mice, similar tumour area per section was measured 8 weeks after intubation as that in K-ras +/- transgenic mice after 10 weeks of AdCre intubation alone, suggesting that elevated Oncostatin M expression accelerated tumour development **(Figure 15C)**. However, loss of function of OSMRβ did not affect tumour development at the time point examined in this model, suggesting that OSMRβ was not necessary for oncogenic K-ras-driven lung adenocarcinoma in mice **(Figure 19D)**.

In vitro experiments designed to test possible mechanisms by which Oncostatin M induced increased tumour cell proliferation were completed. Data demonstrated that OSM did not directly act on mutant K-ras cell lines LLC and LKR-13, as changes in tumour cell proliferation were not detected by MTT assay **(Figure 21)**. In testing whether OSM

could stimulate fibroblasts to indirectly regulate tumour cells, mouse lung fibroblast-conditioned media, untreated or treated with rOSM, was applied to FLuc-LLC cells and FLuc-B16 cells. While both conditions increased FLuc-LLC cell proliferation approximately 1.5-fold after 48 hours, FLuc-B16 cell growth was not affected **(Figures 22C and D)**. This increase in LLC cell proliferation suggests that MLFs release soluble factors that can mediate cell proliferation. However, this increase in proliferation was small and not modulated by OSM, thus results did not support this mechanism of OSM-induced tumour growth in vivo. In co-culture models of MLFs and tumour cells, rOSM did not stimulate changes in FLuc-LLC **(Figures 23A and B)** or FLuc-B16 cell proliferation **(Figure 23C)**. In comparison, TGFβ1 treatment significantly inhibited both FLuc-LLC and FLuc-B16 cell proliferation in co-culture with MLFs after 48 hours when plated on plastic **(Figures 23A and C)**. Effects of OSM overexpression on mouse lung fibroblast secretion of ECM proteins were also assessed both *in vivo* and *in vitro.* Upon OSM overexpression in C57Bl/6 mice, there was significant increase in steady-state fibronectin, but not periostin, mRNA levels in whole lung tissue **(Figures 24A and B)**. These results were not obtained upon rOSM stimulation of MLFs *in vitro*, as very low mRNA levels were detected of both fibronectin and periostin **(Figures 24C and D)**.

In experimentation with cell culture systems with macrophages, alveolar macrophages were shown to be unresponsive to M1 and M2 ligand stimulation *in vitro*, while peritoneal macrophages assumed an M2-like phenotype upon IL-4 and IL-13 stimulation, as assessed by the increased arginase activity **(Figures 25A and B)**. Using the adherent population in BAL fluid collected from AdOSM-treated mice, co-culture

systems with FLuc-LLC cells did not demonstrate modulation of LLC cell proliferation after either 24 and 48 hours **(Figures 26D and E)**. Interestingly, co-cultures of tumour cells with the total BALF population from either AdDel70- or AdOSM-treated mice increased FLuc-LLC cell proliferation 3-fold **(Figures 26B and C)**.

6.2 – OSM- and IL-6-induced tumour pathology in the B16 pulmonary melanoma metastases model

The B16F10 pulmonary melanoma metastases model is widely used to study the function of genes in tumour development and metastasis[84,85], as well as test therapeutic drugs and vaccines[86,87]. Overexpression of Oncostatin M in this model significantly increased tumour burden and tumour nodule numbers, demonstrated by histological analyses **(Figure 4B)**, measurements of tumour area **(Figure 4C)** and calculation of tumour nodule numbers using the right lung **(Figure 4D)**. This is consistent with previous results reported by Lauber *et al,* 2014 who showed that OSM overexpression in this model resulted in a statistically significant increase in tumour burden, increasing tumour area per section approximately 9-fold, compared to the AdDel70 control group[73]. There are a few caveats with the use of this model as a reflection of human lung cancer, namely the method of tumour cell delivery, the dosage of Oncostatin M used, and the duration chosen for assessment of tumour development. Though tail vein injections of B16F10 cells ensure delivery of tumour cells to the lungs, this type of tumour initiation and growth is more relevant to studies of tumour metastases to the lung, as it uses ectopic delivery of melanoma cells. In addition, the levels of OSM present in this model may not necessarily reflect the quantity of OSM protein present in the human pulmonary tumour

microenvironment. Another aspect of interest is the duration of tumour development used in this model. The effects of OSM on tumour burden has been demonstrated after 2 weeks, however, effects are unknown at different time points in that whether OSM accelerates tumour progression at early or later (or both) stages of tumour growth is not clear.

Although Oncostatin M was initially identified as an inhibitor of tumour cell proliferation in A375 melanoma cells[88,36], as well as lung A549 cells, 95-D carcinoma cells, HTB10 neuroblastoma cells and a variety of breast cancer cell lines *in vitro*[88–90], recent studies demonstrate stimulatory effects in a variety of cancers, including prostate, breast, and cervical cancers[91,92,93], as well as the use of OSM protein levels as a negative prognostic indicator[47,94,95]. These studies suggest that in contrast to the effects of direct tumour cell regulation *in vitro,* OSM may promote tumour progression by enhancing angiogenesis, epithelial-mesenchymal transition, and/or the metastatic/invasiveness capacity of tumour cells. As the effects of Oncostatin M on pulmonary tumour development were established *in vivo* in the thesis work, the potential mechanisms by which Oncostatin M acted to increase B16F10 tumour burden were explored. Experiments were designed to examine potential indirect methods of OSM-regulated tumour cell proliferation through fibroblasts, which are a prominent cellular component of the stroma. OSM has been reported to play a role in fibroblast phenotype modulation, increasing alpha smooth muscle actin expression and fibroblast chemotaxis upon stimulation[96], as well as other gp130 cytokines[97]. However, upon application of MLF-conditioned media, either untreated or treated with rOSM, there were no observed

changes in B16 tumour cell proliferation after 24 or 48 hours **(Figure 22D and 22E).** There was also no effect observed on tumour cell proliferation under co-culture conditions with mouse lung fibroblasts and rOSM treatment after 24 or 48 hours **(Figure 23C)**. These results suggest that stimulation of fibroblasts may not contribute to mechanisms by which OSM stimulates increased B16 tumour cell proliferation in vivo. Previous studies have shown that fibroblasts assume a myofibroblast phenotype when cultured on stiff substrates such as plastic, compared to soft substrates such as silicone[98,99,100]. Thus, a possible limitation of the interpretation is that it may be that fibroblasts used in the study have already assumed an altered phenotype due to continuous passage on plastic, and can not be regulated further toward a myofibroblast or CAF phenotype by OSM. Another possible explanation is that effects of OSM on fibroblasts *in vivo* are not recaptured *in vitro,* indicating the insufficiency of the conditioned media and co-culture systems as designed in this study in modeling the actual tumour microenvironment. As noted in *Section 1.2,* the tumour microenvironment is composed of a variety of stromal and immune cell types and further experiments could be designed with different co-culture systems, where stromal cells, immune cells, and tumour cells are incorporated *in vitro*. In a system used by Fu *et al* (2013), conditioned media was collected from co-cultures of CAFs and epithelial ovarian carcinoma cells, and then applied again to epithelial ovarian carcinoma cells, where it was found to stimulate tumour cell proliferation, invasion, and migration[101]. This system highlights the importance of stromal and epithelial cell cross-talk in the production of soluble factors that are able to stimulate proliferation and survival of tumour cells.

Another potential mechanism underlying Oncostatin M's effects on tumour burden *in vivo* could be modulation of tumour angiogenesis. Indeed OSM has shown angiogenic properties[102,103], including upregulation of vascular endothelial growth factor (VEGF) significantly in both prostate[50] and cervical squamous carcinoma cells[104], inducing a pro-angiogenic phenotype. Reports have also shown that OSM stimulation upregulated angiopoietin 2 levels in human endothelial cells[105]. Under normal conditions, angiopoietin 2 disrupts blood vessel formation and promotes cell death[106]. However, in conjunction with VEGF, angiopoietin 2 has been reported to promote neo-vascularization[106]. Angiopoietin 2 has also been identified to promote the growth of ovarian cancer in mouse models[107], and specifically in lung cancer, serum levels of angiopoietin 2 were higher in cancer patients and demonstrated a positive correlation with tumour stage[108]. In the system examined in this thesis, it is known that AdOSM induces VEGF[109], whereas it is not known whether angiopoietins or other factors involved in angiogenesis are regulated. Despite this, there is a growing body of evidence that Oncostatin M stimulates a pro-angiogenic phenotype in tumours, possibly through induction of VEGF and angiopoietin 2 or other angiogenic factor expression[110].

In contrast to rOSM, hTGF-β1 treatment inhibited B16 cell proliferation upon direct stimulation, as well as in co-culture conditions with MLFs **(Figure 23C)**. TGFβ has been previously reported to act as a tumour suppressor in normal and early carcinoma cells by inhibition of cell proliferation and cell immortalization[111,112]. It plays a dual role, however, as it also acts as a tumour promoter in later stages of cancer progression by EMT induction, and increases tumour migration and invasion[111]. Though it is not clear

whether TGFβ is involved in the OSM-induced effects in the present model in vivo, Wong et al (2014) have shown that despite the induced upregulation of a number of genes by AdOSM, TGFβ mRNA levels were not altered[109].

Overexpression of IL-6 in wild type mice did not increase tumour burden, as demonstrated by histological analyses **(Figure 4B)** and measurements of tumour area **(Figure 4C)**, where the tumour area calculated was comparable to that of AdDel70-treated wild type mice. In contrast, tumour nodule numbers were similar to numbers in AdOSM-treated wild type mice, though differences were observed regarding characterizations of the tumours resulting from each treatment. Histological sections revealed that tumours in AdIL-6 treated mice were more restricted to the surface of the lungs and those in the parenchyma were characterized as relatively smaller, diffuse hyperplastic regions, whereas tumours observed in AdOSM-treated mice were large and dense hyperplastic regions found throughout the parenchyma. These differences in tumour pathology suggest that overexpression of OSM engages mechanisms to increase tumour burden but IL-6 did not. In a slightly different model published by De Galdeano *et al* (1998), B16F10 cells themselves were treated *in vitro* with IL-6 prior to ectopic delivery via tail vein injection and exhibited increased metastatic foci, as well as percentage area covered by metastatic foci in lungs compared to the control[113]. This study suggests that trends observed upon direct stimulation of tumour cells, is not necessarily a reflection of the effects *in vivo*, as cytokines may play a different role upon overexpression by the tumour microenvironment.

6.3 – Role of IL-6 in OSM-induced tumour pathology in the B16 pulmonary melanoma metastases model

Increased Oncostatin M expression has been shown to induce the upregulation of a variety of cytokines, one of which is the pro-inflammatory molecule IL-6[114]. Thus, the potential role of IL-6 in OSM-induced tumour pathology was tested using IL-6 -/- mice, which demonstrated that the effects of OSM overexpression on tumour burden in wild type and IL-6 -/- mice were similar **(Figures 6B and 6C)**. These results suggest that in the B16F10 melanoma metastases model, IL-6 is not required for OSM-induced tumour expansion. These are novel findings regarding the effects of IL-6 in tumour development, as previously published literature has identified IL-6 as a promoter in a variety of cancers[115,116]. However, the results in this thesis accentuate differences in action of OSM from IL-6 in modulation of lung cancer models.

Upon overexpression of OSM in wild type mice, increased lymphocyte and eosinophil recruitment was evident **(Figure 5D and 7D).** However, there was a significant decrease in eosinophil recruitment upon OSM overexpression in IL-6 -/- mice. These trends are consistent with findings reported by Botelho, *et al* (2013) who showed that 7 days after AdOSM administration, there was an increase in BAL macrophage, lymphocyte, neutrophil and eosinophil numbers in wild type mice, compared to the AdDel70 control group, but a significant decrease of those cells in IL-6 -/- mice[83]. Additionally, the same study demonstrated a significant decrease in MCP-1, KC, and eotaxin-2 protein levels in the BALF[83]. Since tumour burden upon OSM overexpression in IL-6 -/- mice was very similar to that in wild type mice, despite the decreased

eosinophil recruitment and chemokine presence, the results suggest that IL-6-mediated inflammation mechanisms were not necessary for tumour development in this model of lung cancer.

Upon OSM overexpression, IL-6 ELISA protein levels at day 14 exhibited a significant increase in one experiment **(Figure 7A)** compared to the AdDel70 control group, whereas there was a trend towards a decrease in a separate experiment **(Figure 5A)**. Though different trends are reported, the IL-6 protein levels were near the limit of detection and thus it is probable that the differences were of low biological significance.

6.4 – Role of eosinophils in OSM-induced tumour pathology in the B16 pulmonary melanoma metastases model

Overexpression of Oncostatin M in wild type mice resulted in significant eosinophil recruitment to mouse lungs. Thus, the role of eosinophils in OSM-induced tumour pathology in the B16 mouse model was examined using GATA-1 -/- mice. GATA-1 is a transcription factor required for proper erythroid and megakaryocyte maturation, mast cell differentiation, and eosinophil development[68,117,118]. In GATA-1 -/- mice, the deletion of the double GATA site in the GATA-1 promoter results in selective loss of eosinophil development, while erythroid, megakaryocyte and mast cell lineages are left unaffected[68]. Using the B16F10 model, OSM overexpression yielded similar tumour burden in both wild type and GATA-1 -/- mice **(Figure 8C),** suggesting that eosinophils were not required in OSM-induced tumour pathology. These findings are novel, as GATA-1 -/- mice have yet to be extensively studied. One of the assumptions of the methodological approach used is that the trends observed with the averaged tumour

area per section accurately estimates differences in tumour burden in the whole lung of each mouse (histological assessments used 8 sections of the lungs). However, since samples were taken at the same anatomical location and then multiple sections were examined, this is a reasonable approach in context of the literature.

Interestingly, GATA-1 -/- mice treated with AdDel70 exhibited a trend towards an increase in tumour area per section (3-fold) compared to AdDel70 treatment in wild type mice **(Figure 8C)**. Although this increase was not statistically significant, further study may indicate that it is plausible that GATA-1 -/- mice show increased tumour susceptibility due to eosinophil deficiency compared to wild type mice. In a number of different types of cancer, eosinophils have been identified as players in the anti-tumour response[119–121]. High levels of eosinophilic infiltration were found in tumour tissues taken from NSCLC patients[122], and in a case report of a patient with NSCLC and serum eosinophilia, removal of the tumour normalized eosinophil counts[121]. Thus, the absence of eosinophils in GATA-1 -/- mice may lead to increased tumour susceptibility.

In contrast to the consistently low levels of IL-6, high OSM protein levels (approx. 2ng/ml) were detected in BAL samples of GATA-1 -/- mice treated with AdOSM **(Figure 9B)** at day 14. These results were unexpected, as the peak of cytokine production is typically 2-7 days in the Ad vector system used here. It is possible that high endogenous OSM protein production was maintained. A potential explanation is that GATA-1 is involved in the regulation of OSM expression. Alternatively GATA-1 mice may have altered immune responses to Ad vectors allowing longer expression of virus-encoded cytokine.

6.5 – Effects of loss of function of OSMRβ on tumour pathology in the B16 pulmonary melanoma metastases model

In the B16F10 mouse model, there was a significant increase in tumour area per section, as well as nodule numbers, in OSMRβ -/- mice after 3 weeks, compared to the wild type group **(Figure 10C and 10D).** This result was unexpected, as the loss of function of OSMRβ was predicted to result in decreased tumour burden, based on previous results demonstrating increased tumour burden upon OSM overexpression after 2 weeks. One possible explanation for these results is that basal OSM signalling levels actually inhibit tumour growth, while overexpression of OSM stimulates tumour growth. Another possible explanation is that the lack of IL-31 signaling upon loss of function of OSMRβ results in increased tumour susceptibility. IL-31 is another member of the gp130 cytokine family, which binds to IL-31RA and OSMRβ to activate a variety of pathways, including JAK/STAT, MAPK, and PI3K/AKT pathways[123]. Importantly, loss of function of OSMRβ would abolish IL-31 signaling as well as OSM signaling. Recently, IL-31 has been identified to negatively regulate type 2 inflammation in the intestines as well as the lung following infection[124,125]. This may result in increased Th2 responses in knockout animals which would conceivably facilitate down-regulation of anti-tumour immunity by release of type 2 cytokines including IL-10 and inhibition of Type 1 inflammation[126]. To examine this possibility, future experiments could incorporate IL-31 -/- mice to study the role of IL-31 in the B16F10 mouse model independently of OSM.

6.6 – Role of OSM in the oncogenic K-ras mouse model

The role of OSM was also studied in the oncogenic K-ras model of lung cancer. In this model, intubation of K-ras G12D transgenic mice with an adenovirus encoding Cre-Recombinase activates the oncogenic K-ras gene, and induces the development of lung adenocarcinoma. There are a number of advantages and limitations of this model. The main benefit of the model is its ability to recapitulate the sporadic growth of tumour cells due to one of the most common genetic mutations in lung cancer - K-ras, supporting relevancy to the human disease. This model also allows researchers to monitor tumour development over a longer period of time, as tumours develop over a span of several weeks, in contrast to the rapid development in the B16F10 melanoma model. Limitations of the model, however, include the presence of the oncogenic K-ras mutations in all cells of the target tissue. In the human disease, sporadic tumours generally arise from a few malignant cells in an environment largely composed of normal cells[127]. In this model, however, delivery of AdCre activates the expression of oncogenic K-ras presumably in all cells of the lungs that become infected. Another limitation includes the lack of uniformity of adenoviral delivery to the lungs. As observed in **Figure 13A**, adenoviral intubation did not always affect the entire lung evenly, as determined by the increase in density on only one side of the lung. Furthermore, the system does not reflect the process of K-ras mutation in cancer development.

The oncogenic K-ras model demonstrated gradual grade 1 and 2 tumour development over a span of 10 weeks after AdCre intubation, as demonstrated with histological analyses **(Figure 14)**. CT scanning technology, used to monitor increasing

lung density, proved to be a reliable method of monitoring lung pathology as well as endpoint succession of mice, using percentage of voxels between 0-200 HU, and comparison between weeks 0 and 10 **(Figure 14C).** Although preliminary data suggested that AdOSM accelerated tumour development **(Figure 15C),** further studies are required to interpret the effects of OSM overexpression in this model. Interestingly, in a study by Lauber, *et al* (2014), a model similar to the B16F10 model was used with ectopic delivery of LLC cells that have a K-ras G12C mutation[73]. In this study, there was a 10-fold increase in tumour burden upon OSM overexpression, compared to the AdDel70 group, demonstrating the effects of overexpression of Oncostatin M on the growth of mutant K-ras tumour cells *in vivo*[73].

Possible mechanisms underlying the effects of OSM on mutant K-ras tumour cells were examined, first using direct methods of stimulation. Upon stimulation with a variety of cytokines including rOSM, there were no changes in LLC, LKR-13, or FLuc-LLC cell proliferation detected with an MTT assay **(Figure 21)**. These results are similar to those demonstrated by Lauber *et al* (2014)[73], and suggest that OSM does not act directly on mutant K-ras cells. Thus, subsequent experiments examined possible indirect mechanism of OSM-mediated tumour cell proliferation using conditioned media and co-culture systems with mouse lung fibroblasts. However, there was no effect on tumour cell proliferation upon application of MLF-conditioned media either untreated or treated with rOSM, as well as under co-culture conditions with mouse lung fibroblasts, plated on either plastic or collagen, and rOSM treatment after 24 or 48 hours **(Figures 22B-C, 23A-B)**. Similar to that noted previously with B16F10 cells, these results suggest that OSM

may not regulate tumour cell proliferation through effects on fibroblasts. Alternatively, as mentioned in *Section 6.2*, the lack of change in tumour cell proliferation exhibited in conditioned media and co-culture systems may be due to the insufficiency of these systems to mimic the tumour microenvironment, such as the potential role of OSM in neovascularization. Also as noted previously, the phenotype of the MLFs used in this study mauy not accurately reflect lung fibroblast phenotype *in vivo.* Thus, fibroblasts used in future co-culture studies could be passaged on collagen upon explant from whole lung tissue, to minimize phenotypic changes. In contrast to rOSM, hTGF-β1 treatment of LLC tumour cells inhibited LLC cell proliferation approximately 1.5-fold after 48 hours upon direct stimulation as well as co-culture conditions on plastic with MLFs **(Figure 23A)**. Although this trend was not present upon co-culture on collagen, hTGF-β1 directly inhibited LLC cell proliferation approximately 1.5 fold at both 24 and 48 hours **(Figure 23B)**. Direct hTGF-β1 inhibition of LLC cell proliferation was not consistent with results using the MTT assay. One possible explanation for this inconsistency is that the MTT assay used to detect changes in cell proliferation assesses metabolically active mitochondria, and may result in overestimation of viable cells[128]. Luciferase activity of the FLuc-LLC or FLUc-B16F10 cells may be a more accurate measurement of cell proliferation than the MTT assay.

As results from the co-culture systems of fibroblasts and tumour cells suggested that direct stimulation of fibroblasts may contribute to the mechanisms by which OSM regulates tumour cell proliferation, co-culture systems involving macrophages were also examined. Many studies have focused on the role of TAMs in tumour development, and

recently Tripathi, et al. (2014) reported that conditioned media collected from hypoxic MDA-MB-231 and MCF-7 breast cancer cells and applied to macrophages resulted in increased M2 marker expression (CD206) measured via flowcytometric analysis[110]. Upon further studies, not only were Oncostatin M and Eotaxin cytokines found to be newly synthesized and released by the hypoxic cancer cells, compared to levels in conditioned media from normoxic cancer cells, but blockade of the two cytokines using neutralizing antibodies decreased recruitment and skewing of macrophages into the M2 phenotype[110]. Thus, macrophages may play a role in the oncogenic K-ras or the B16 and LLC ectopic models examined in this thesis. The responsiveness of alveolar macrophages *in vitro* to stimulatory ligands was measured. In this model, developed by the Ashkhar laboratory, macrophages were polarized *ex vivo* into either the M1 phenotype, using IFNγ and LPS, or the M2 phenotype, using IL-4 and IL-13 as stimuli. In contrast to the 2-fold increase in arginase activity upon stimulation with M2 ligands in peritoneal macrophages, there were consistently low levels of arginase activity amongst all treatments **(Figure 25A and 25B)** of the alveolar macrophage populations. These results suggest that resident alveolar macrophages are not as responsive as resident macrophages from other locations, such as the peritoneum, to these exogenous stimuli. These findings are novel, and are in accordance with other data that suggests alveolar macrophages are less responsive to other stimuli such as LPS[129,130]. Resident alveolar macrophages are located in a unique environment, generally found near the lung epithelium and exposed to exogenous antigens and stimuli every day[130]. Interestingly, rOSM stimulation of peritoneal macrophages did not yield increased arginase activity and future iNOS assays would help

to determine whether rOSM stimulation of peritoneal macrophages instead stimulates an M1 phenotype. As alveolar macrophages were not responsive to polarization *ex vivo, in vivo*-conditioned alveolar cells were tested by removal of BAL cells from mice intubated 7 days earlier with AdDel70 or AdOSM and used for co-culture experiments. Though co-culture of adherent macrophages from either AdDel70- or AdOSM-treated mice did not alter FLuc-LLC cell proliferation, co-culture of the total BALF population from either AdDel70- or AdOSM-treated mice increased FLuc-LLC cell proliferation 3-fold **(Figure 26B and 26C)**. These results were unexpected, as cells removed from AdDel70-treated mice exhibited stimulatory properties towards tumour cells. These results pose numerous suggestions. Firstly, it suggests that either macrophages are not the cell type that modify tumour growth, or that macrophages require the presence of other cell types to promote tumour cell proliferation. More interestingly, these results suggest that adenoviral treatment alone may stimulate cells found in the bronchoalveolar lavage into a phenotype that facilitates tumour cell proliferation. One alternate cell type involved may be the neutrophil. Recent work conducted with human breast cancer cells demonstrated that co-cultures of tumour cells and neutrophils stimulate OSM production by neutrophils, which in turn is involved the upregulation of a variety of pro-angiogenic factors[93].

6.7 – Effects of loss of function of IL-6 or OSMRβ in the oncogenic K-ras mouse model

As the results obtained upon OSM overexpression in the oncogenic K-ras model suggested accelerated tumour development, the effects of loss of function of IL-6 or OSMRβ on tumour development in the model were examined using the crosses generated in-house **(Figures 11 and 12)**. However, the attempted cross of K-ras and IL-6 -/- mice

did not yield transgenic, homozygous IL-6 -/-, and the heterozygous IL-6+/- mice were used as a comparator. It is not known if these mice showed a loss of IL-6 expression or IL-6 protein in comparison to the wild type, and future analysis would be required in order to assess this. Histological analyses and calculation of tumour area exhibited no significant differences in grade 1 or grade 2 tumour burden after 10 weeks, upon loss of function of OSMRβ or the IL-6-/+ genotype **(Figure 19B-D).** These results did not support the hypothesis as the loss of function of OSMRβ was postulated to decrease tumour burden. Instead, these results suggest that OSMRβ was not necessary for tumour development or growth in the K-ras transgenic mouse model. One caveat with this experiment, however, is that there was high variability in tumour area calculated within treatment groups, and it is possible that increasing the sample size per group may yield different results. It may also be interesting to extend the time point past 10 weeks to observe longer-term effects of loss of OSM signaling on tumour burden in this model.

Interestingly, there was a trend towards a decrease in tumour area per section measured in IL-6 +/-, K-ras transgenic mice. Though publications regarding the role of OSM in mutant K-ras models are scarce, in a recent study using tumorigenic human kidney cells, Ancrile, *et al* (2007) showed that oncogenic Ras (G12V) induced high levels of IL-6 secretion, and upon IL-6 shRNA treatment, there was a significant decrease in tumour size, and delay in tumour development[131].

CHAPTER 7: Conclusions

The focus of interest of this thesis was the role of Oncostatin M in pulmonary tumour development. Although Oncostatin M was originally identified as an inhibitor of human melanoma tumour cell proliferation, recent studies have demonstrated pro-tumorigenic functions for OSM in a variety of cancer models, as well as in the B16F10 pulmonary melanoma metastases model. The original hypothesis regarding the role of Oncostatin M in tumour development was that elevation of Oncostatin M would increase tumour burden in an IL-6 and eosinophil dependent fashion, and that depletion of function would decrease tumour burden. In accordance with the hypothesis, OSM overexpression was shown to increase pulmonary tumour burden by at least 15-fold, compared to the control group in the B16F10 mouse model. However, increased tumour development due to OSM overexpression did not require IL-6 levels or eosinophil recruitment, suggesting the involvement of other cells in the tumour microenvironment. In contrast to the original hypothesis, OSMRβ -/- mice exhibited increased tumour burden upon B16 cell administration alone, compared to the wild type control after 3 weeks, suggesting that the loss of OSM and/or IL-31 signaling may increase susceptibility to pulmonary tumour development in this model. Thus, OSM functions upon overexpression appear different than those at basal levels. Alternatively, future experiments may show that IL-31 has protective functions against melanoma tumour growth.

The role of Oncostatin M was also studied in the inducible oncogenic K-ras G12D mouse model. In accordance with the hypothesis, preliminary results suggested that OSM overexpression using AdOSM induced accelerated tumour development, although further experimentation would be needed to confirm this trend. To examine the function of IL-6 and OSMRβ in the development of tumours, mutant K-ras +/- transgenic mice were crossed with either IL-6 -/- or OSMRβ -/- mice to obtain mutant K-ras +/- IL-6 +/-, mutant K-ras +/- OSMRβ +/-, and mutant K-ras +/- OSMRβ -/- mice. In subsequent experiments with AdCre administration, loss of function of OSMRβ resulted in significant decreases in density of lungs as assessed by CT scan technology, but did not significantly alter tumour burden at the time point examined (10 weeks) as assessed histologically, suggesting that OSMRβ was not required for tumour development in this model.

Potential mechanisms underlying Oncostatin M's effects *in vivo* were also examined *in vitro*. OSM did not stimulate B16F10, LLC, or LKR-13 tumour cell proliferation directly or indirectly through fibroblast conditioned media and co-culture experiments. Finally, results from co-cultures of BAL macrophages with K-ras tumour cells suggested that adherent macrophage populations (from either AdOSM or control vector-treated mice) were not sufficient to alter tumour cell proliferation. Collectively, the findings presented in this thesis suggest that OSM overexpression has pro-tumorigenic functions in mouse models of pulmonary tumours. Although these appear independent of IL-6 presence or eosinophil accumulation in lungs, further investigation is necessary to identify mechanisms of

OSM action in these models. Such work may lead to new approaches in the treatment of cancer growth in lungs.

CHAPTER 8: References

1. Lung Cancer. *National Cancer Institute: National institute of Health* (2012).at <http://www.cancer.gov/cancertopics/wyntk/lung/>

2. Lung Cancer. *Canadian Cancer Society* (2012).at <https://www.cancer.ca/Canada-wide/About cancer/Cancer statistics/Stats at a glance/Lung cancer.aspx?sc_lang=en>

3. Luo, S. Y. & Lam, D. C. Oncogenic driver mutations in lung cancer. *Translational Respiratory Medicine* **1**, 6 (2013).

4. National Cancer Institute Non-small cell lung cancer treatment. (2014).

5. Canadian Lung Association Lung Cancer. (2012).

6. Bonander, R. Platinum-based cancer treatment. *CancerTreatment.net* (2014).at <http://platinum.cancertreatment.net/>

7. Lovly, C., Horn, L. & Pao, W. Molecular Profiling of Lung Cancer. *My Cancer Genome* (2012).

8. Siegelin, M. D. & Borczuk, A. C. Epidermal growth factor receptor mutations in lung adenocarcinoma. *Laboratory investigation; a journal of technical methods and pathology* **94**, 129–37 (2014).

9. Langer, C. & Soria, J.-C. The role of anti-epidermal growth factor receptor and anti-vascular endothelial growth factor therapies in the treatment of non-small-cell lung cancer. *Clinical lung cancer* **11**, 82–90 (2010).

10. Herbst, R. S. *et al.* Phase I/II trial evaluating the anti-vascular endothelial growth factor monoclonal antibody bevacizumab in combination with the HER-1/epidermal growth factor receptor tyrosine kinase inhibitor erlotinib for patients with recurrent non-small-cell lung canc. *Journal of clinical oncology : official journal of the American Society of Clinical Oncology* **23**, 2544–55 (2005).

11. Herbst, R. S. *et al.* Phase II study of efficacy and safety of bevacizumab in combination with chemotherapy or erlotinib compared with chemotherapy alone for treatment of recurrent or refractory non small-cell lung cancer. *Journal of clinical oncology : official journal of the American Society of Clinical Oncology* **25**, 4743–50 (2007).

12. Camidge, R., Pao, W. & Sequist, L. Acquired Resistance to TKIs in Solid Tumours: learning from lung cancer. *Nature Reviews Clinical Oncology* **11**, 473–481 (2014).

13. Grivennikov, S. I., Greten, F. R. & Karin, M. Immunity, inflammation, and cancer. *Cell* **140**, 883–99 (2010).

14. Balkwill, F. & Mantovani, a Inflammation and cancer: back to Virchow? *Lancet* **357**, 539–45 (2001).

15. Coussens, L. M. & Werb, Z. Inflammation and cancer. *Nature* **420**, 860–7 (2002).

16. Karin, M. Nuclear factor-kappaB in cancer development and progression. *Nature* **441**, 431–6 (2006).

17. Rodier, F. *et al.* Persistent DNA damage signalling triggers senescence-associated inflammatory cytokine secretion. *Nature cell biology* **11**, 973–9 (2009).

18. Murray, P. J. & Wynn, T. a Protective and pathogenic functions of macrophage subsets. *Nature reviews. Immunology* **11**, 723–37 (2011).

19. Sica, A. & Mantovani, A. Macrophage plasticity and polarization: in vivo veritas. *The Journal of clinical investigation* **122**, (2012).

20. Condeelis, J. & Pollard, J. W. Macrophages: obligate partners for tumor cell migration, invasion, and metastasis. *Cell* **124**, 263–6 (2006).

21. Hao, N.-B. *et al.* Macrophages in tumor microenvironments and the progression of tumors. *Clinical & developmental immunology* **2012**, 948098 (2012).

22. Komori, T., Tanaka, M., Senba, E., Miyajima, A. & Morikawa, Y. Lack of oncostatin M receptor β leads to adipose tissue inflammation and insulin resistance by switching macrophage phenotype. *The Journal of biological chemistry* **288**, 21861–75 (2013).

23. Dvorak, H. Tumors: wounds that do not heal. *New England Journal of Medicine* **315**, 1650–59 (1986).

24. Bremnes, R., Dennem, T., Al-Saad, S., Al-Shibli, K. & Andersen, S. The Role of Tumor Stroma in Cancer Progression and Prognosis: Emphasis on carcinoma-associated fibroblasts and non-small cell lung cancer. *Journal of Thoracic Oncology* **6**, 209–217 (2011).

25. Shekhar, M. P. V, Pauley, R. & Heppner, G. Host microenvironment in breast cancer development: extracellular matrix-stromal cell contribution to neoplastic phenotype of epithelial cells in the breast. *Breast cancer research : BCR* **5**, 130–5 (2003).

26. Pietras, K. & Ostman, A. Hallmarks of cancer: interactions with the tumor stroma. *Experimental cell research* **316**, 1324–31 (2010).

27. Shuman Moss, L. & Stetler-Stevenson, W. Influence of Stromal Components on Lung Cancer Carcinogenesis. *J Carcinog. Mutagen.* **13**, (2013).

28. Räsänen, K. & Vaheri, A. Activation of fibroblasts in cancer stroma. *Experimental cell research* **316**, 2713–22 (2010).

29. Olumi, A. F. *et al.* Carcinoma-associated Fibroblasts Direct Tumor Progression of Initiated Human Prostatic Epithelium Carcinoma-associated Fibroblasts Direct Tumor Progression of Initiated Human. *Cancer Research* **59**, 5002–5011 (1999).

30. Akashi, T. *et al.* Basement membrane matrix modifies cytokine interactions between lung cancer cells and fibroblasts. *Pathobiology : journal of immunopathology, molecular and cellular biology* **72**, 250–9 (2005).

31. Elenbaas, B. & Weinberg, R. a Heterotypic signaling between epithelial tumor cells and fibroblasts in carcinoma formation. *Experimental cell research* **264**, 169–84 (2001).

32. Depner, S. *et al.* Cell type specific interleukin-6 induced responses in tumor keratinocytes and stromal fibroblasts are essential for invasive growth. *International journal of cancer. Journal international du cancer* **135**, 551–62 (2014).

33. Silver, J. . & Hunter, C. . gp130 at the nexus of inflammation, autoimmunity, and cancer. *Journal of Leukocyte Biology* **88**, 1145–1156 (2010).

34. Taniguchi, K. & Karin, M. IL-6 and related cytokines as the critical lynchpins between inflammation and cancer. *Seminars in immunology* **26**, 54–74 (2014).

35. Kishimoto, T., Akira, S., Nazaraki, M. & Taga, T. Interleukin-6 Family of Cytokines and gp130. *Blood* **86**, (1995).

36. Richards, C. D. The enigmatic cytokine oncostatin m and roles in disease. *ISRN inflammation* **2013**, 512103 (2013).

37. Xing, Z., Braciak, T., Cauldie, J., Jordana, M. & Croitoru, K. Adenovirus-Mediated Cytokine Gene Transfer at Tissue Sites: Overexpression of IL-6 induces Lymphocytic Hyperplasia in the Lungs. *Journal of Immunology* **153**, 4059–69 (1994).

38. Tamura, T. *et al.* Soluble interleukin-6 receptor triggers osteoclast formation by interleukin 6. *Proceedings of the National Academy of Sciences of the United States of America* **90**, 11924–8 (1993).

39. Tanaka, T., Narazaki, M. & Kishimoto, T. Therapeutic targeting of the interleukin-6 receptor. *Annual review of pharmacology and toxicology* **52**, 199–219 (2012).

40. Yao, X. *et al.* Targeting interleukin-6 in inflammatory autoimmune diseases and cancers. *Pharmacology & therapeutics* **141**, 125–39 (2014).

41. Ernst, M. *et al.* STAT3 and STAT1 mediate IL-11 – dependent and inflammation-associated gastric tumorigenesis in gp130 receptor mutant mice. *Journal of Clinical Investigations* **118**, (2008).

42. Calon, A., Espinet, E. & Battle, E. Dependency of colorectal cancer on a TGF-beta-driven programme in stromal cells for metastasis initiation. *Cancer cell* **22**, 571–584 (2012).

43. Albrengues, J. *et al.* LIF Mediates Proinvasive Activation of Stromal Fibroblasts in Cancer. *Cell reports* **7**, 1664–78 (2014).

44. Tricot, G. New insights into role of microenvironment in multiple myeloma. *Lancet* **355**, 248–50 (2000).

45. Yi, H. *et al.* Blockade of interleukin-6 receptor suppresses the proliferation of H460 lung cancer stem cells. *International journal of oncology* **41**, 310–6 (2012).

46. Tanaka, M. & Miyajima, a Oncostatin M, a multifunctional cytokine. *Reviews of physiology, biochemistry and pharmacology* **149**, 39–52 (2003).

47. West, N. R., Murphy, L. C. & Watson, P. H. Oncostatin M suppresses oestrogen receptor-α expression and is associated with poor outcome in human breast cancer. *Endocrine-related cancer* **19**, 181–95 (2012).

48. Kan, C. E., Cipriano, R. & Jackson, M. W. c-MYC functions as a molecular switch to alter the response of human mammary epithelial cells to oncostatin M. *Cancer research* **71**, 6930–9 (2011).

49. Loewen, G. M. *et al.* Transformation of human bronchial epithelial cells alters responsiveness to inflammatory cytokines. *BMC cancer* **5**, 145 (2005).

50. Weiss, T. W. *et al.* Oncostatin M and IL-6 induce u-PA and VEGF in prostate cancer cells and correlate in vivo. *Anticancer research* **31**, 3273–8 (2011).

51. Johnson, L. *et al.* Somatic activation of the K-ras oncogene causes early onset lung cancer in mice. *Nature* **410**, 1111–6 (2001).

52. Meuwissen, R. & Berns, A. Mouse models for human lung cancer. *Genes & development* **19**, 643–64 (2005).

53. Ji, H. *et al.* K-ras activation generates an inflammatory response in lung tumors. *Oncogene* **25**, 2105–12 (2006).

54. Carpeño, J. D. C. & Belda-iniesta, C. KRAS mutant NSCLC , a new opportunity for the synthetic lethality therapeutic approach. **2**, 142–151 (2013).

55. Rachagani, S. *et al.* Activated $KrasG^{12}D$ is associated with invasion and metastasis of pancreatic cancer cells through inhibition of E-cadherin. *British journal of cancer* **104**, 1038–48 (2011).

56. Sunaga, N. *et al.* Knockdown of oncogenic KRAS in non-small cell lung cancers suppresses tumor growth and sensitizes tumor cells to targeted therapy. *Molecular cancer therapeutics* **10**, 336–46 (2011).

57. Van der Hoeven, D. *et al.* Fendiline inhibits K-Ras plasma membrane localization and blocks K-Ras signal transmission. *Molecular and cellular biology* **33**, 237–51 (2013).

58. Lovly, C., Horn, L. & Pao, W. KRAS Mutations in Non-Small Cell Lung Cancer (NSCLC). *My Cancer Genome* (2012).at <http://www.mycancergenome.org/content/disease/lung-cancer/kras>

59. Jackson, E. L. *et al.* Analysis of lung tumor initiation and progression using conditional expression of oncogenic K-ras. *Genes & development* **15**, 3243–8 (2001).

60. Schubbert, S., Shannon, K. & Bollag, G. Hyperactive Ras in developmental disorders and cancer. *Nature reviews. Cancer* **7**, 295–308 (2007).

61. Pruitt, K. & Der, C. J. Ras and Rho regulation of the cell cycle and oncogenesis. *Cancer letters* **171**, 1–10 (2001).

62. Vivanco, I. & Sawyers, C. L. The phosphatidylinositol 3-Kinase AKT pathway in human cancer. *Nature reviews. Cancer* **2**, 489–501 (2002).

63. Zhang, Z. *et al.* Wildtype Kras2 can inhibit lung carcinogenesis in mice. *Nature genetics* **29**, 25–33 (2001).

64. Patrick, C., Konger, L. & Jeffrey, B. Cancer Growth and Metastasis. **2**, 27–32 (2014).

65. Wang, X. *et al.* Regulation gene expression of miR200c and ZEB1 positively enhances effect of tumor vaccine B16F10/GPI-IL-21 on inhibition of melanoma growth and metastasis. *Journal of translational medicine* **12**, 68 (2014).

66. Chan, I. T. *et al.* Conditional expression of oncogenic K-ras from its endogenous promoter induces a myeloproliferative disease. *Journal of Clinical Investigations* **113**, 528–538 (2004).

67. Tanaka, M. & Hirabayashi, Y. Targeted disruption of oncostatin M receptor results in altered hematopoiesis. *Blood* **102**, 3154–3162 (2003).

68. Yu, C. Targeted Deletion of a High-Affinity GATA-binding Site in the GATA-1 Promoter Leads to Selective Loss of the Eosinophil Lineage In Vivo. *Journal of Experimental Medicine* **195**, 1387–1395 (2002).

69. Lauber, S. Role of il-6 and osm on tumor development in mouse models for lung cancer. 1–155 (2012).

70. Fasbender, a *et al.* Incorporation of adenovirus in calcium phosphate precipitates enhances gene transfer to airway epithelia in vitro and in vivo. *The Journal of clinical investigation* **102**, 184–93 (1998).

71. Wong, S. STAT3 and SMAD Signaling in Mouse Models of Oncostatin M-Induced Lung Extracellular Matrix Remodeling. (2013).

72. Livak, K. J. & Schmittgen, T. D. Analysis of relative gene expression data using real-time quantitative PCR and the 2(-Delta Delta C(T)) Method. *Methods (San Diego, Calif.)* **25**, 402–8 (2001).

73. Lauber S, Wong S, Cutz JC, Tanaka M, Barra N, Lhoták S, Ashkar A, D. R. C. Novel function of Oncostatin M as a potent tumour-promoting agent in lung. *International journal of cancer. Journal international du cancer* **Epub ahead**, (2014).

74. Schmitt, R. & Lanz, U. *Diagnostic Imaging of the Hand*. 64–65 (Thieme Publishing Group: 2011).

75. Bhowmick, N., Neilson, E. & Moses, H. Stromal fibroblasts in cancer initiation and progression. *Nature* **432**, 332–337 (2004).

76. Han, S., Khuri, F. R. & Roman, J. Fibronectin stimulates non-small cell lung carcinoma cell growth through activation of Akt/mammalian target of rapamycin/S6 kinase and inactivation of LKB1/AMP-activated protein kinase signal pathways. *Cancer research* **66**, 315–23 (2006).

77. Hong, L.-Z., Wei, X.-W., Chen, J.-F. & Shi, Y. Overexpression of periostin predicts poor prognosis in non-small cell lung cancer. *Oncology letters* **6**, 1595–1603 (2013).

78. Orecchia, P. *et al.* Identification of a novel cell binding site of periostin involved in tumour growth. *European journal of cancer (Oxford, England : 1990)* **47**, 2221–9 (2011).

79. Wang, Z. & Ouyang, G. Periostin: a bridge between cancer stem cells and their metastatic niche. *Cell stem cell* **10**, 111–2 (2012).

80. Au, A. Von, Vasel, M., Kraft, S., Sens, C. & Hackl, N. Circulating Fibronectin Controls Tumour Growth. *Neoplasia* **15**, 925–938 (2013).

81. Malik, G., Knowles, L., Dhir, R. & Xu, S. Plasma fibronectin promotes lung metastasis by contributions to fibrin clots and tumour cell invasion. *Cancer research* **70**, 4327–4334 (2010).

82. Fritz, D. K. *et al.* A Mouse Model of Airway Disease: Oncostatin M-Induced Pulmonary Eosinophilia, Goblet Cell Hyperplasia, and Airway Hyperresponsiveness Are STAT6 Dependent, and Interstitial Pulmonary Fibrosis Is STAT6 Independent. *The Journal of Immunology* **186**, 1107–1118 (2010).

83. Botelho, F. & Rangel-Moreno, J. Pulmonary expression of Oncostatin M (OSM) promotes inducible-BALT formation independently of IL-6, despite a role for IL-6 in OSM-driven pulmonary inflammation. *The Journal of …* **191**, 1453–1464 (2013).

84. Overwijk, W. & Restifo, N. B16 as a Mouse Model for Human Melanoma. *Curent Protocols in Immunology* 1–33 (2001).doi:10.1002/0471142735.im2001s39

85. Khanna, C. & Hunter, K. Modeling metastasis in vivo. *Carcinogenesis* **26**, 513–23 (2005).

86. Gautam, A., Waldrep, J. & Densmore, C. Growth inhibition of established B16-F10 lung metastases by sequential aerosol delivery of p53 gene and 9-nitrocamptothecin. *Gene therapy* 353–357 (2002).doi:10.1038/sj/gt/3301662

87. Singh, S., Yang, G., Schluns, K. S., Anthony, S. M. & Sastry, K. J. Sublingual vaccination induces mucosal and systemic adaptive immunity for protection against lung tumor challenge. *PloS one* **9**, e90001 (2014).

88. Zarling, J. *et al.* Oncostatin M: A growth regulator produced by differentiated histiocytic lymphoma cells. *Proceedings of the National Academy of Sciences of the United States of America* **83**, 9739–9743 (1986).

89. Li, C., Zhang, F., Lin, M. & Liu, J. Induction of S100A9 gene expression by cytokine oncostatin M in breast cancer cells through the STAT3 signaling cascade. *Breast cancer research and treatment* **87**, 123–34 (2004).

90. Ouyang, L., Shen, L. Y., Li, T. & Liu, J. Inhibition effect of Oncostatin M on metastatic human lung cancer cells 95-D in vitro and on murine melanoma cells B16BL6 in vivo. *Biomedical research (Tokyo, Japan)* **27**, 197–202 (2006).

91. Royuela, M. *et al.* Immunohistochemical analysis of the IL-6 family of cytokines and their receptors in benign, hyperplasic, and malignant human prostate. *The Journal of pathology* **202**, 41–9 (2004).

92. Caffarel, M. M. & Coleman, N. Oncostatin M receptor is a novel therapeutic target in cervical squamous cell carcinoma. *The Journal of pathology* **232**, 386–90 (2014).

93. Queen, M. M., Ryan, R. E., Holzer, R. G., Keller-Peck, C. R. & Jorcyk, C. L. Breast cancer cells stimulate neutrophils to produce oncostatin M: potential implications for tumor progression. *Cancer research* **65**, 8896–904 (2005).

94. Ng, G. *et al.* Gain and overexpression of the oncostatin M receptor occur frequently in cervical squamous cell carcinoma and are associated with adverse clinical outcome. *The Journal of Pathology* **212**, 325–334 (2007).

95. Gurluler, E. *et al.* Oncostatin-M as a novel biomarker in colon cancer patients and its association with clinicopathologic variables. *European review for medical and pharmacological sciences* **18**, 2042–7 (2014).

96. Nagahama, K. Y. *et al.* Oncostatin M modulates fibroblast function via signal transducers and activators of transcription proteins-3. *American journal of respiratory cell and molecular biology* **49**, 582–91 (2013).

97. Vicent, S., Sayles, L., Vaka, D., Khatri, P. & Gevaert, O. Cross-species functional analysis of cancer-associated fibroblasts identifies a critical role for CLCF1 and IL6 in non-small cell lung cancer in vivo. *Cancer Research* **72**, (2012).

98. Liu, F. *et al.* Feedback amplification of fibrosis through matrix stiffening and COX-2 suppression. *The Journal of cell biology* **190**, 693–706 (2010).

99. Tomasek, J. J., Gabbiani, G., Hinz, B., Chaponnier, C. & Brown, R. a Myofibroblasts and mechano-regulation of connective tissue remodelling. *Nature reviews. Molecular cell biology* **3**, 349–63 (2002).

100. Balestrini, J. L., Chaudhry, S., Sarrazy, V., Koehler, A. & Hinz, B. The mechanical memory of lung myofibroblasts. *Integrative biology : quantitative biosciences from nano to macro* **4**, 410–21 (2012).

101. Fu, S. *et al.* Stromal-epithelial crosstalk provides a suitable microenvironment for the progression of ovarian cancer cells in vitro. *Cancer investigation* **31**, 616–24 (2013).

102. Vasse, M. *et al.* Oncostatin M Induces Angiogenesis In Vitro and In Vivo. *Arteriosclerosis, Thrombosis, and Vascular Biology* **19**, 1835–1842 (1999).

103. Modur, V. *et al.* Oncostatin M Is a Proinflammatory Mediator. *Journal of Clinical Investigations* **100**, 158–168 (1997).

104. Winder, D. M. *et al.* Overexpression of the oncostatin M receptor in cervical squamous cell carcinoma cells is associated with a pro-angiogenic phenotype and increased cell motility and invasiveness. *The Journal of pathology* **225**, 448–62 (2011).

105. Rychli, K., Kaun, C., Hohensinner, P., Rega, G. & Pfaffenberger, S. The inflammatory mediator oncostatin M induces angiopoietin 2 expression in endothelial cells in vitro and in vivo. *J Thromb Haemost.* **8**, 596–604 (2010).

106. Fagiani, E. & Christofori, G. Angiopoietins in angiogenesis. *Cancer letters* **328**, 18–26 (2013).

107. Brunckhorst, M. K., Xu, Y., Lu, R. & Yu, Q. Angiopoietins promote ovarian cancer progression by establishing a procancer microenvironment. *The American journal of pathology* **184**, 2285–96 (2014).

108. Ayten, O. *et al.* Angiopoietin 2 levels in serum and bronchial lavage fluids and their relationship with cancer stages in lung cancer patients. *Thoracic Cancer* **4**, 20–26 (2013).

109. Wong, S., Botelho, F. M., Rodrigues, R. M. & Richards, C. D. Oncostatin M overexpression induces matrix deposition, STAT3 activation, and SMAD1 Dysregulation in lungs of fibrosis-resistant BALB/c mice. *Laboratory investigation; a journal of technical methods and pathology* **00**, 1–14 (2014).

110. Tripathi, C. *et al.* Macrophages are recruited to hypoxic tumor areas and acquire a Pro-Angiogenic M2-Polarized phenotype via hypoxic cancer cell derived cytokines Oncostatin M and Eotaxin. *Oncotarget* (2014).at <http://www.ncbi.nlm.nih.gov/pubmed/25051364>

111. Lebrun, J.-J. The Dual Role of TGF β in Human Cancer: From Tumor Suppression to Cancer Metastasis. *ISRN Molecular Biology* **2012**, 1–28 (2012).

112. Jeon, H.-S. & Jen, J. TGF-B Signaling and the Role of Inhibitory Smads in Non-small Cell Lung Cancer. *Journal of Thoracic Oncology* **5**, 417–419 (2010).

113. De Galdeano, A. *et al.* Involvement of interleukin-6 in the biology and metastatic activity of B16F10 melanoma cells. *European Cytokine Network* **9**, 187–92 (1998).

114. Brown, T. J., Rowe, M., Liu, J. & Shoyab, M. Regulation of IL-6 Expression by Oncostatin M. *Journal of Immunology* **147**, 2175–2180 (1991).

115. Kim, M. *et al.* Tumour self-seeding by circulating cancer cells. **139**, 1315–1326 (2010).

116. Ochoa, C. & Mirabolfathinejad, S. Interleukin 6 but not T helper cytokines promotes lung carcinogenesis. *Cancer Prevention …* **4**, 51–64 (2011).

117. Fujiwara, Y., Chang, A. N., Williams, M. & Orkin, S. H. Functional overlap of GATA-1 and GATA-2 in primitive hematopoietic development. *Blood* **103**, 583–585 (2004).

118. Migliaccio, a. R. *et al.* GATA-1 as a Regulator of Mast Cell Differentiation Revealed by the Phenotype of the GATA-1low Mouse Mutant. *Journal of Experimental Medicine* **197**, 281–296 (2003).

119. Huland, E. & Huland, H. Tumor-associated eosinophilia in interleukin-2-treated patients: evidence of toxic eosinophil degranulation on bladder cancer cells. *J Cancer Res Clin Oncol.* **118**, 463–7 (1992).

120. Legrand, F. *et al.* Human eosinophils exert TNF-α and granzyme A-mediated tumoricidal activity toward colon carcinoma cells. *Journal of immunology (Baltimore, Md. : 1950)* **185**, 7443–51 (2010).

121. Pandit, R., Scholnik, A., Wulfekuhler, L. & Dimitrov, N. Non-Small-Cell Lung Cancer Associated With Excessive Eosinophilia and Secretion of Interleukin-5 as a Paraneoplastic Syndrome. *American journal of hematology* **82**, 234–237 (2007).

122. Han, X., Zhang, P., Wang, J. & He, B. Eosinophilic infiltration of lung cancer tissue and its correlation with the expression of interleukin-5. **91**, 956–60 (2011).

123. Zhang, Q., Putheti, P., Zhou, Q., Liu, Q. & Gao, W. Structures and biological functions of IL-31 and IL-31 receptors. *Cytokine & growth factor …* **19**, 347–356 (2008).

124. Perrigoue, J. G. *et al.* IL-31-IL-31R interactions negatively regulate type 2 inflammation in the lung. *The Journal of experimental medicine* **204**, 481–7 (2007).

125. Perrigoue, J., Zaph, C. & Guild, K. IL-31-IL-31R Interactions Limit the Magnitude of Th2 Cytokine-Dependent Immunity and Inflammation following Intestinal Helminth Infection. *The Journal of …* **182**, 6088–6094 (2009).

126. Duan, M.-C., Zhong, X.-N., Liu, G.-N. & Wei, J.-R. The Treg/Th17 paradigm in lung cancer. *Journal of immunology research* **2014**, 730380 (2014).

127. O'Hagan, R. C. & Heyer, J. KRAS Mouse Models: Modeling Cancer Harboring KRAS Mutations. *Genes & cancer* **2**, 335–43 (2011).

128. Wang, P., Henning, S. M. & Heber, D. Limitations of MTT and MTS-based assays for measurement of antiproliferative activity of green tea polyphenols. *PloS one* **5**, e10202 (2010).

129. Wewers, M. D., Rennard, S. I., Hance, a J., Bitterman, P. B. & Crystal, R. G. Normal human alveolar macrophages obtained by bronchoalveolar lavage have a limited capacity to release interleukin-1. *The Journal of clinical investigation* **74**, 2208–18 (1984).

130. Hussell, T. & Bell, T. J. Alveolar macrophages: plasticity in a tissue-specific context. *Nature reviews. Immunology* **14**, 81–93 (2014).

131. Ancrile, B., Lim, K.-H. & Counter, C. M. Oncogenic Ras-induced secretion of IL6 is required for tumorigenesis. *Genes & development* **21**, 1714–9 (2007).